

<https://doi.org/10.15388/vu.thesis.192>

<https://orcid.org/0000-0002-0050-4204>

VILNIUS UNIVERSITY

CENTRE FOR PHYSICAL SCIENCES AND TECHNOLOGY

Aušra

ČIULADIENĖ

# Investigation of paints and binding media of ancient written sources

**DOCTORAL DISSERTATION**

Natural sciences,  
Chemistry (N 003)

---

VILNIUS 2021

This dissertation was written between 2017 and 2021 at Vilnius University.

**Academic supervisors:**

**Prof. Dr. Vida Vičkačkaitė** (Vilnius University, Natural Sciences, Chemistry – N 003) (from 2017-10-01 to 2018-10-02).

**Prof. Habil. Dr. Aivaras Kareiva** (Vilnius University, Natural Sciences, Chemistry – N 003) (from 2018-10-02 to 2021-09-30).

This doctoral dissertation will be defended in a public meeting of the Dissertation Defence Panel:

**Chairman – Prof. Habil. Dr. Albertas Malinauskas** (Centre for Physical Sciences and Technology, Natural Sciences, Chemistry – N 003).

**Members:**

**Prof. Dr. Jurgis Barkauskas** (Vilnius University, Natural Sciences, Chemistry – N 003).

**Assoc. Prof. Dr. Eglė Fataraitė-Urbonienė** (Kaunas University of Technology, Technological Sciences, Materials Engineering – T 008).

**Assoc. Prof. Dr. Tatjana Kochanė** (Vilnius University, Natural Sciences, Chemistry – N 003).

**Prof. Dr. Rasa Pauliukaitė** (Centre for Physical Sciences and Technology, Natural Sciences, Chemistry – N 003).

The dissertation shall be defended at a public meeting of the Dissertation Defence Panel at 14 p.m. on 1 October 2021 in Inorganic Chemistry auditorium 141 of the Institute of Chemistry, Faculty of Chemistry and Geoscience, Vilnius University. Address: Naugarduko g. 24, LT-03225 Vilnius, Lithuania. Tel.: +370 5 2193108. Fax: +370 5 2330987.

The text of this dissertation can be accessed at the libraries of Vilnius University and Center for Physical Sciences and Technology, as well as on the website of Vilnius University:

[www.vu.lt/lt/naujienos/ivykiu-kalendorius](http://www.vu.lt/lt/naujienos/ivykiu-kalendorius)

<https://doi.org/10.15388/vu.thesis.192>

<https://orcid.org/0000-0002-0050-4204>

VILNIAUS UNIVERSITETAS

FIZINIŲ IR TECHNOLOGIJOS MOKSLŲ CENTRAS

Aušra

ČIULADIENĖ

# Senųjų rašytinių šaltinių dažų ir rišiklių tyrimas

**DAKTARO DISERTACIJA**

Gamtos mokslai,  
Chemija (N 003)

---

VILNIUS 2021

Disertacija rengta 2017 – 2021 metais studijuojant doktorantūroje Vilniaus universiteto Chemijos ir geomokslų fakulteto Chemijos institute.

**Moksliniai vadovai:**

**prof. dr. Vida Vičkačkaitė** (Vilniaus universitetas, gamtos mokslai, chemija – N 003) (nuo 2017-10-01 iki 2018-10-01).

**prof. habil. dr. Aivaras Kareiva** (Vilniaus universitetas, gamtos mokslai, chemija – N 003) (nuo 2018-10-02 iki 2021-09-30).

Gynimo taryba:

Pirmininkas – **prof. habil. dr. Albertas Malinauskas** (Fizinių ir technologijos mokslų centras, gamtos mokslai, chemija – N 003).

Nariai:

**prof. dr. Jurgis Barkauskas** (Vilniaus universitetas, gamtos mokslai, chemija – N 003).

**doc. dr. Eglė Fataraitė-Urbonienė** (Kauno technologijos universitetas, technologijos mokslai, medžiagų inžinerija – T 008).

**doc. dr. Tatjana Kochanė** (Vilniaus universitetas, gamtos mokslai, chemija – N 003).

**prof. dr. Rasa Pauliukaitė** (Fizinių ir technologijos mokslų centras, gamtos mokslai, chemija – N 003).

Disertacija ginama viešame Gynimo tarybos posėdyje 2021 m. spalio mėn. 1 d. 14 val. Vilniaus universiteto Chemijos ir geomokslų fakulteto Chemijos instituto Neorganinės chemijos auditorijoje. Adresas: Naugarduko g. 24, LT-03225 Vilnius, Lietuva. Tel.: 2193108. Faksas: 2330987.

Disertaciją galima peržiūrėti Vilniaus universiteto, Fizinių ir technologijos mokslų centro bibliotekose ir VU interneto svetainėje adresu:

<https://www.vu.lt/naujienos/ivykiu-kalendorius>

## CONTENTS

LIST OF ABBREVIATIONS .....	7
INTRODUCTION.....	8
1. LITERATURE SURVEY .....	10
1.1. Brief review of inorganic historical pigments and binding media .....	10
1.2. The red paints in book decor .....	13
1.2.1. Red iron pigments .....	15
1.2.2. Cinnabar .....	17
1.2.3. Realgar .....	20
1.2.4. Red lead.....	24
1.3. Capillary washing method.....	26
2. EXPERIMENTAL SECTION .....	32
2.1. Reagents and materials.....	32
2.2. Paints preparation.....	34
2.3. Artificial photochemical aging.....	34
2.4. Characterization techniques .....	35
3. RESULTS AND DISCUSSION .....	37
3.1. Characterization of analogous to historical red pigments and binding media .....	37
3.1.1. SEM/EDX analysis .....	37
3.1.2. FTIR analysis .....	39
3.1.3. XRD analysis .....	42
3.1.4. TG/DTG/DSC analysis .....	44
3.2. Characterization of reconstructed historical red paints .....	48
3.2.1. Colourimetric measurements.....	48
3.2.2. SEM analysis.....	51
3.2.3. FTIR analysis .....	55
3.2.4. XRD analysis .....	61
3.2.5. TG/DTG/DSC analysis .....	69

3.3. Application of the reconstructed red pain database to the original manuscript .....	75
3.3.1. SEM/EDX analysis .....	76
3.3.2. FTIR analysis .....	77
3.3.3. XRD analysis .....	80
3.3.4. TG/DTG/DSC analysis .....	82
4. Capillary washing of water-sensitive objects .....	84
CONCLUSIONS .....	88
LIST OF PUBLICATIONS .....	90
ACKNOWLEDGEMENTS .....	92
SUMMARY IN LITHUANIAN .....	93
CURRICULUM VITAE .....	116
REFERENCES .....	117
COPIES OF PUBLICATION .....	130

## LIST OF ABBREVIATIONS

CIE(Lab)	Commission Internationale de l'Eclairage
DSC	Differential Scanning Calorimetry
DTG	Derivative Thermogravimetric
EDX	Energy Dispersive X-ray Analysis
FTIR	Fourier-Transform Infrared Spectroscopy
GDL	Grand Duchy of Lithuania
OM	Optical Microscopy
RH	Relative Humidity
SEM	Scanning Electron Microscopy
TG	Thermogravimetry
XRD	X-ray Diffraction Analysis

## INTRODUCTION

Contributing to the growing efforts to preserve cultural heritage, special attention must be paid to historical books. The book is evidence of people's cultural heritage, traveling from generation to generation. Their form has changed throughout the historical period, and the structure is one of the most complex objects [1, 2].

Some of the most impressive objects were created during the medieval and Renaissance periods. Researchers in various fields are interested in the origin of components or elements, the materials they are made off, recipes, degradation processes, etc. It should be noted that in ancient manuscripts, pigments, which are one of the many components, often retained their original colour appearance in the illuminations of medieval and Renaissance manuscripts. Pigments were often better protected in book volumes from external environmental influences: aggressive atmosphere, humidity, temperature fluctuations, light, or other potential factors influencing destruction. Therefore, by studying pigments and paint compositions, we can provide detailed insights into the materials and techniques used by medieval and Renaissance artists, showing geographical changes, their evolution over time, and assessing chemical and physical changes [3–6].

Lithuanian heritage institutions, as all over the world, collect, preserve, investigate, and provide the public with valuable documentary heritage objects. However, the processes of manuscript production, especially for illuminated or rubricated manuscripts have not been sufficiently studied. For a long time, the cultural heritage of Lithuanian books has been studied only from the point of view of book science or art history. As more research opportunities arise, it is important to start researching the manuscripts of the Grand Duchy of Lithuania period. The study of these manuscripts is important not only from the historical or identity point of view, but also in defining their production processes, the structure of the manuscripts, the materials used, and their change during the time of the Grand Duchy of Lithuania [7, 8].

Information on the composition of pigments or paints is especially useful for restorers when they need to choose the right materials and appropriate colour tones for restoration work. The characterization of binders in paints is particularly difficult due to the sample size, the high content of inorganic pigment, the decomposition phenomena that have occurred over time, and at the same time other additives [9, 10]. Discolouration and degradation phenomena are a complex matter, and they are not always easy for scientists and restorers to recognize. Surface impurities, mold, light, and moisture



cause chemical and/or physical changes in the pigments that affect their transformation. It is important to have a good knowledge of paint components and their interactions [11–13].

The ideal way to study these substances is to use non-invasive analytical methods, however, many heritage institutions have techniques that can be classified as micro-destructive, non-invasive analytical techniques have not fully satisfied features and have limitations. For this reason, several test methods are used in most cases [2, 8, 14].

Lithuanian and world restorers have to restore books in which red paint is particularly common: rubrics, miniatures, various footnotes, drawings, etc. These are destroyed or damaged over time or bounce off the surface during paper washing. Therefore, it is important to know the composition of the paint, what kind of pigments or mixtures there were used.

The main scientific novelty of this doctoral dissertation is the development of the database of six historical red pigments and three different binding media and their application to completely unexplored chemical researchers for the collections of books kept in the Wroblewski Library of the Lithuanian Academy of Sciences. In funds: Russian Manuscripts (F19), Vilnius Public library (F22), and Vilnius Belarusians found (F21), are good representatives of the tendencies of book development in the territory of the Grand Duchy of Lithuania [7].

The aim of this PhD thesis was to investigate the six different red pigments (cinnabar, red lead, realgar, red ochre, hematite, and red bole) and three binding media (gum Arabic, parchment glue, fish glue), and to create a short database. For this reason, the tasks of this work were formulated as follows:

1. To explore the possibility of FTIR, SEM/EDX, XRD, and TG/DTG/DSC analysis techniques as standards for the comprehensive characterization of six different red pigments and three binding media.
2. To prepare the analogous to historical red paints with application of accelerated photochemical aging, describing the reconstituted paints before and after artificial aging by FTIR, SEM/EDX, XRD, and TG/DTG/DSC analysis methods.
3. For the first time, to identify and compare red paints and binding media in ancient books using the results summarized as a short database.
4. The further development of capillary washing for water-sensitive objects.

# 1. LITERATURE SURVEY

## 1.1. Brief review of inorganic historical pigments and binding media

Books researcher, conservation scientist, or another person uses different tools to study the technique of artists. The approach of each of them can provide valuable information about the ways in which an individual artist or school performs work, the historical period or the fashion prevailing at the time. But each approach individually leaves something unexplained, something missing in the overall context, including everything from the artist's technique of performance to the preference for certain materials [15].

The first to leave their mark were prehistoric people. Punching on a stone, marking a trail or food source, or perhaps just soaking a hand in a soot and touching the surface noticed that they could leave a mark. It was later observed that some materials worked more effectively when mixed with a medium such as water or saliva, and painting was born. With the discovery of pigments, it was possible to paint various objects, surfaces, or even the body. As can be inferred, prehistoric people used pigments near them – natural colours from minerals on earth (inorganic) or from plants and animals (organic). The colours were yellow, red, brown ochres (iron oxides in various states of hydration) and carbon blacks (soot, charcoal). The first binding agent was water. Some of the oldest surviving drawings in caves were found in Spain, France, and South Africa drawn about 30,000 to 70,000 years ago (Fig. 1).

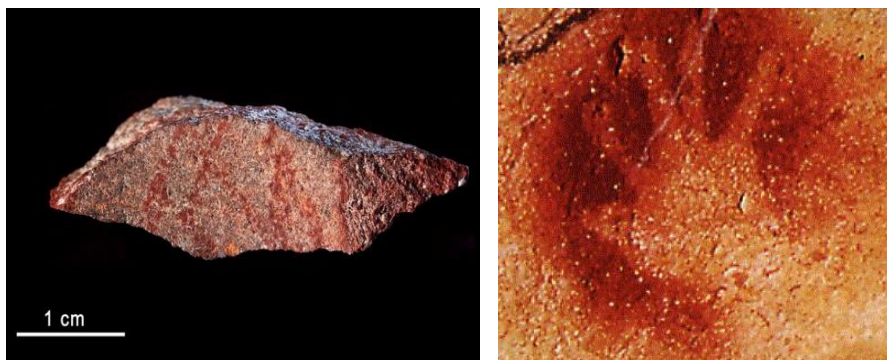


**Figure 1.** The first known drawings on the stone: left in South Africa, right in France [16, 17].

The palette of pigments in early people was limited and only basic technology was used to prepare the paint. By cleverly using what they had,

they created vivid images, although they did not have a large part of the spectrum of colours [16–18].

With the advent of new civilizations began serious colour production. The Egyptians, Mesopotamia and China civilizations started manufacture from about 4000 BC. Their perfected the technologies, introduced new materials: green malachite ( $\text{CuCO}_3 \cdot \text{Cu}(\text{OH})_2$ ), blue azurite ( $2\text{CuCO}_3 \cdot \text{Cu}(\text{OH})_2$ ), red cinnabar ( $\text{HgS}$ ), reddish yellow to orange realgar ( $\text{As}_4\text{S}_4$ ). The most famous in Egypt was Egyptian blue ( $\text{CaCuSi}_4\text{O}_{10}$ ) produced around 3000 BC [19]. The Greek contribution to the production of pigments was also important, a new group of toxic lead pigment: white lead ( $2\text{Pb}(\text{CO}_3)_2 \cdot \text{Pb}(\text{OH})_2$ ), red lead ( $\text{Pb}_3\text{O}_4$ ), and yellow lead ( $\text{PbO}$ ). The Romans used pigments created by the Egyptians and the Greeks. One of the most important colours introduced by the Romans was Tyrian purple (organic one), extracted from molluscs around 1600 BC. The widely used cinnabar was mined in Almaden in Spain [16].

The paint of the Middle Ages and the Renaissance was characterized by a palette of clearly defined and bright colours. In the Middle Ages, bone white, obtained by burning bones and grinding ashes, was used instead of white lead. In the Renaissance, was used umber, sienna, high price pigment ultramarine. Hardly available and expensive cinnabar was replaced by the red lead (*minium*). The confusing name of the minium was used for red lead and cinnabar. Other pigments discovered in the Renaissance were lead tin yellow ( $\text{SnO} \cdot \text{SiO}_2 \cdot \text{PbO}$ ), Naples yellow ( $\text{Pb}(\text{SbO}_3)_2$  or  $\text{PbSbO}_4$ ). Gold substitutes have also been used to reduce the cost of gilding. A popular substitute was tin sulphide, known as mosaic gold and first used in the early 15th century. Other substitutes were a mixture of egg yolk and mercury with various additives [15–17].

The biggest breakthrough in pigment production took place in the 18th – 19th centuries. It was promoted by an industrial manufactory. The first chemical test for the synthesized pigment was made by Diesbach in Germany in 1704. He, using a batch contaminated with animal oil, accidentally made a blue pigment, now known as Prussian blue. Poisonous Scheele's green ( $\text{CuHAsO}_3$ ) was introduced in 1775, cobalt blue ( $\text{CoAl}_2\text{O}_4$ ) was first obtained by Leithner in 1775, cobalt green ( $\text{CoO} \cdot n\text{ZnO}$ ) was developed by Rinmann in 1780, various chromates pigments were used since 1809, synthetic barium sulfate  $\text{BaSO}_4$ , was used since 1830. In the 18th – 19th centuries, synthetic iron oxides, so-called mars pigments, appeared. Only in the 19th century some inorganic pigments began to replace organic pigments, but new inorganic pigments production never stopped [16, 17, 19].

In a similar period, around 1780 an analytical approach to art and its objects began. The ideas of the art historian Johann Wincklemann (1717–1768) were gradually applied in the history of art and technology. Since then, methods of analysis applied to the study of works of art have grown steadily, and among the materials that make up an object of art, organic compounds used as binders or protective coatings have attracted the attention of the conservation specialist [20]. Traditionally, several naturally occurring materials have been used in works of art, given their ability to form uniform and flexible thin films by mixing them with pigments and dyes. The main binders used to illuminate the manuscripts were egg white or glair, gums such as gum Arabic and glue such as fish glue, casein or parchment glue. In most cases the binding media were used alone, but depending on the technique or pigment, the mixtures were also prepared in different proportions. The glair consists mainly of water and protein (with hydrophilic and hydrophobic amino acids), and the strong whipping that produces foam means that the protein is completely denatured, and once the glair has settled, it can be mixed with water to become a binding media. It has been popular since medieval times. The main disadvantages of this binder were the long preparation and the reduced saturation of the natural colours. The medium was better as it got older. Many of these difficulties have been solved with an adhesive mixture. Often, when the glair dried quickly, egg yolk was added and at the same time the intensity and gloss of the egg yolk were combined with the durability of the glair. Egg yolk was the foremost medium for painting in late medieval and early Renaissance Europe, but it was rarely used alone as a binder in manuscript illumination. This resulted in it not having good adhesion and the pigment surface cracked and stains formed. Commonly used in mixtures with other binders. Gum Arabic was one of the most common pigment binding media in illuminated manuscript and the exclusive medium in writing inks. The gum was very easy to prepare and use, has a high water solubility, good adhesion and the fact that the colours become more intense. The disadvantage is its fragility. Glues of animal origin were used since Antiquity in different art techniques. Animal glue is derived from collagen, a protein found in the skin, bones, and connective tissues. Different types of animal glue are available, depending on the animal or part used [21–24].

In addition to natural products, synthetic polymers were introduced. In 1846 by Schönbein was the first synthetic polymer cellulose nitrate introduced. Alexander Parkes exhibited various molded cellulose nitrate objects at an international exhibition in London. In the 20th century, the use of synthetic polymers has become widespread, and these days they are found

not only as materials that make up an art object, but also as adhesives, consolidants, paint varnishes, or fillers for missing parts used in restoration work. Among a wide range of synthetic resins in art and conservation, acrylic, polyvinyl acetate, and polycyclohexanone are widely used as artist's paint media or paint varnishes [20].

Thanks to successful chemical discoveries, the artists' palettes have become much richer than before, customization has become available to almost everyone, however, the harmfulness of some synthetic pigments has further increased. There is no doubt that the last 150 years have been the golden age of pigments, dyes and binding media. Pigments and binding media are still improving, small changes in chemical structure allow to obtain new properties, better absorption, reflective or simply reduce production costs. Art historians can use in-depth knowledge of the artist's technique and its evolution throughout the artist's career in the authentication process, and conservators rely on specific information about pigments, binders, and materials from previous restorations to ensure a safe work strategy, when planning conservation or restoration work. This information can also help to determine the proper chronology of known works by a particular artist [15–17].

## 1.2. The red paints in book decor

The significant artistic and documentary contribution of the manuscripts makes them unique. The culture of manuscripts was inherently diverse, the texts were compiled alongside additional texts throughout the history of the manuscript. The owner, writer, or customer of a book could add something new at any stage in the creation of the book. And if possible, specially decorate the manuscript book [25].

One of the decor or explanatory elements in the book was the rubrics (headings). The word derives from the Latin – rubrica, meaning red colour and was especially prevalent in medieval illuminated manuscripts in the 13th century or earlier. However, it did not lose its popularity in the Renaissance too. When the press appeared, other typographic effects were used to emphasize the text section: italics, bold, or a different font size. Two-colour printing was a more expensive and time-consuming method, so handwritten rubrics survived for a long time. The role of the rubricator in early printed texts is often shortened to that of a book decorator, in red (and sometimes blue, green) ink. It helps the book reader to follow useful links: coloured initials, paragraph marks, instructions. Each person, who assumed the

responsibility of the rubrication, often interpreted their duty differently, leaving researchers with a unique canon of the rubric [26, 27].

The next decor element in the books were miniatures in which red colour paint was used. The artist working with the *minium* (red lead) was called the miniaturist who made the miniature. The term miniature comes from the Italian language for illuminations, originally used to describe the red capital letters used in illuminated manuscripts. But later, the term was eventually applied to any small feature and meant everything that declined. Miniatures or the more common word illuminations are small paintings around the initial capital letters of a paragraph, often found in sacred medieval books in the Middle Ages [16, 17]. An illuminated manuscript adorned with coloured and finely painted miniatures, decorations, letters, and borders, added to the text was to enrich and emphasize the content and value of the book. Miniatures, placed in handwritten pages caused a certain lighting, a luxurious effect. Famous artists were often invited to decorate the manuscripts of the early Renaissance, so such manuscripts have not only great historical and cultural value, but also artistic [4].

Red mercury sulphide (natural or synthetic), or red lead were often prepared with a proteinaceous binding media from the 12th–13th century in medieval monasteries important for the production of miniatures or rubrics. Standard pigment palette was a challenge for the illuminators, they tried to improve the quality of their materials, to extract bright shades, rich tones and surface effects, which were so appreciated by patrons at the beginning of the 15th century. The pigments were mostly used purely in manuscript illumination. The most commonly used red pigments were cinnabar, red lead, different red ochres or realgar. The mixing of the paint was done mainly to obtain secondary colours whose pure form was not satisfactory. To add depth to the form, an organic dye was applied on an opaque middle tone. Today, the technical treatises „*Il libro dell 'arte*“ are well known, author Cennino Cennini (1370–1427) and anonymous „*De arte illuminandi*“. There is also an important Johannes Alcherius (1380–1420) collection of recipes. Unlike these two treatises, Alcherius's set of recipes reflects the latest technical information and insights gathered from master illuminators, painters, and other craftsmen known to him. In addition to these special book decoration elements, red paint was used to decorate the exterior of the books as well: the edge of the block, the cover, using organic dyes for the cover textiles, clasp fragments or other parts [22, 28, 29].

The Middle Ages and the Renaissance have left us beautiful works that we want to grow for centuries. The choice of materials and techniques used by the artists depended on the geographical, cultural and historical context.

There were secret recipes, typical workshops and workshop procedures that were entrusted to produce the book. Fortunately, many of these manuscripts reached us in quite good condition and, most importantly, probably with almost no restorations. Therefore, they provide an opportunity to disclose materials and techniques previously used, also to investigate paint compositions, origins, aging mechanisms, and more [30, 31].

### 1.2.1. Red iron pigments

Iron pigments (*ochres*) are some of the oldest pigments used from prehistoric times until these days. Their use has been associated with the beginning of many people's cultural activities based on the symbolism of colours, such as painting, funeral rituals, or beauty treatments. The vast majority of inorganic pigments are found in the form of natural minerals or these days can be synthesized. Therefore, the researcher must have good skills to describe and distinguish the materials used in a work of art. Iron pigments of various shades are widespread throughout the world (yellow ochres, red earths and boles, dark yellow or brown siennas and umbers). The colour may vary depending on the amount of impurities [19, 32, 33].

The most common iron oxide minerals are magnetite ( $\text{Fe}_3\text{O}_4$ ), maghemite ( $\gamma\text{-Fe}_2\text{O}_3$ ), hematite ( $\alpha\text{-Fe}_2\text{O}_3$ ) and goethite ( $\alpha\text{-FeOOH}$ ), but their red colour is always given by hematite. In most compounds the iron is in the trivalent state, in magnetite the iron contains  $\text{Fe}^{\text{II}}$  and  $\text{Fe}^{\text{III}}$  state [34, 35].

Hematite is the oldest known iron oxide and is widespread in rocks and soils. The name hematite is derived from the Greek word *haimas* meaning blood. It is also known as ferric oxide, iron sesquioxide or red ochre. The colour is blood red if finely crushed, black or gray if coarsely crystalline and is particularly stable in environmental conditions. Hematite has the corundum structure, the unit cell is hexagonal, space group  $R\bar{3}c$ , number 167. The crystal structure is close-packed planes of oxygen anions with iron cations in octahedral or tetrahedral interstitial sites (see Fig. 2). According to its chemical composition, the hematite has about 80% of  $\text{Fe}_2\text{O}_3$  and a small amount of impurities of silicon, aluminium, calcium, potassium, magnesium and other oxides. Hematite powders were used in canvas and wall paintings in the Middle Ages, later adapted for book decoration, ceramics. Depending on the particle size and impurities, the paint has pure and strong shades. They are particularly stable and highly resistant to acids and alkalis [19, 35–39].

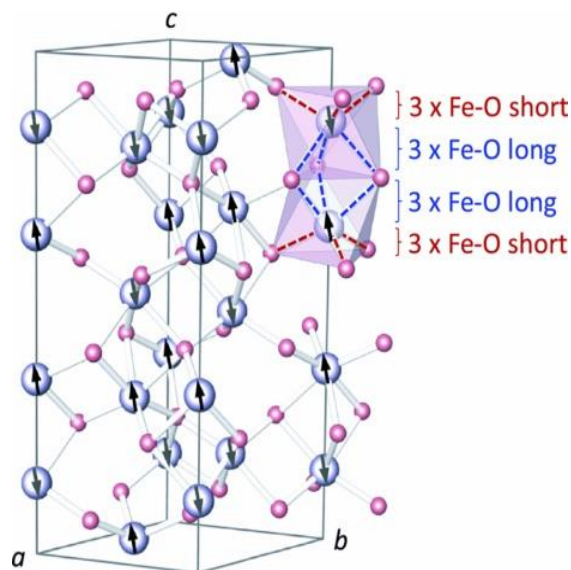


Figure 2. Crystal structure of hematite [40]

Red bolus is a natural, ferruginous aluminium silicate, changing the colour from red to orange. It is similar to ochres in its chemical composition, but is softer and more unctuous. For the first time, the term *bole* (or *bolus*) was used for clays that have healing properties since ancient times. The place of origin of the bolus (formerly Armenia, now probably eastern Turkey) is associated with a specific quality. Therefore, various sources have called *Armenian bolus*. Later, due to its useful properties, Armenian bolus was applied not only in medicine but also in painting technology. The most common mineral found in bolus is kaolinite. This has a neutral charge, which helps to form stable suspensions and facilitates distribution on the surface. Usually, bolus was agglutinated with animal glue (fish, parchment, rabbit), they act as a protective colloid, increasing suspension stability and particle binding. The bolus is capable of receiving a high polish, thus it was used in early medieval times, especially, as a ground for gilding [41, 42].

The use of bolus in Western European art reached its highest point between the 14th and 18th centuries, and it is interesting that the same thing happened in the art of Eastern tradition. In the 17th – 18th centuries, clay mining spread to many parts of Europe, imports of Mediterranean clays gradually decreased and the original Armenian bolus during the first half of the 18th century ceased to be available on the European market. To this day, there is a lack of knowledge about the Armenian bole composition used by artists. Eventually, the term *bole* lost its precision and began to be confused



with terms such as red earth or even red ochre. Historical paints can be found in red earths of various compositions corresponding to different sources and geological origins, and the pigment fillers and paint base used in the early Baroque period bring even more confusion [43].

In general, ochre is a durable pigment, it can be mixed with all pigments, with all binding media, has a good coating, and is resistant to various factors. Its names usually change from location to place, in ancient times the best red ochre was considered from Egypt, later – from Spain. Red ochre is used in all painting techniques to this day [19].

### 1.2.2. Cinnabar

Colour technology has accompanied human history since Neolithic times. Mercury (II) sulphide  $\text{HgS}$ , known as cinnabar, has been a widely used pigment throughout history and played an important role of red colour in many fields of art. It has been mined since the Neolithic age and the earliest use of this pigment dates back to 7000 – 8000 BC, in wall paintings at the Neolithic site of Catalhöyük in Turkey. Other important early decorative uses are known in Chinese civilization, as well as in Mayan Tombs, frescoes in Pompeii, and Nasrid polychrome carpentry in the Alhambra palaces. It has been identified in a wide variety of masterpieces in Egypt, was very appreciated in the Middle Ages, Renaissance, and Baroque [44].

The name cinnabar is from the Greek *kinnabari*, from old Persian sources (about 7th century BC). It was sometimes used to designate dragon's blood or a red resin. Theophrastus wrote that the two kinds of cinnabar were known to the Greeks. One of them was definitely a real cinnabar (mostly from Spain), the other was red lead. The Latin name *miniaria*, used by Pliny, meaning quicksilver (Hg) mine, originated in India, where it referred to minium, which was used to adulterate cinnabar. Three types of mercury sulphide pigment are known: the natural mineral form that is just finely ground cinnabar, and synthetic – vermilion, a form made in the dry or wet process [45, 46]. The name cinnabar was also confused by vermilion from the 17th century, which was previously used interchangeably to describe natural or manufactured products. Cinnabar from China was the best of all, and the vermilion from Spain was known on the markets as a cleaned ground powder ideal for painting. It is not always possible to distinguish analytically natural  $\text{HgS}$  from the synthetic  $\text{HgS}$ . This fact leads to inaccuracies in determining the origin of works of art [47].

Cinnabar was a favorite for its deep red colour, exceptional gloss, good coverage properties, and adhesion to the surface. Due to its low hardness and high density, it was suitable for painting. In addition, it is highly resistant to oxidation, acids and alkalis, and does not react with other pigments or binders. Many of the old artifacts are intact bright red. However, it is light sensitive and its darkening is known when used in binding media such as lime, oil and tempera. There are also specific impurities that can cause the decomposition effects of HgS, catalytic elements (such as halides) to accelerate the darkening process. Degradation processes also depend on where and in what way of preparations cinnabar was obtained [44, 48]. Cinnabar is a red mineral found in nature. The pigment colour is very stable. Shades from light to dark red are observed, depending on the deposit and its crystallization conditions. The darker cinnabar has larger grains; the light red mineral is purer and is excellent for use as a pigment [47].

There are basically four chemico-structural types of cinnabar: red cinnabar  $\alpha$ -HgS is hexagonal at low temperature, black metacinnabar  $\beta$ -HgS is cubic at average temperature, amorphous HgS and black colour with a tinge of violet hypercinnabar  $\gamma$ -HgS is hexagonal at high temperature. Due to the impurities in the composition, the  $\alpha$ -HgS phase converts to cubic metacinnabar  $\beta$ -HgS in the temperature range of 100–362 °C. The metacinnabar  $\beta$ -HgS transforms to hypercinnabar  $\gamma$ -HgS at about 525 °C [45, 48–50].

It is now believed that the knowledge of vermilion production was brought to Europe by the Arabs. They already knew the reaction of sulfur with mercury to form a red compound in the 8th–9th centuries. In addition to the many different ways of preparing the pigment and mixing it with other dyes, two production technologies dry and wet are mainly described. Both methods involve the production of vermilion by converting black  $\beta$ -HgS. In the dry method, mercury is heated with sulfur to give a black phase of  $\beta$ -HgS with lime on an iron pan. The direct reaction leading to the formation of vermilion is complex and the temperature is the crucial parameter to exceed the kinetic barrier of the cubic to hexagonal phase conversion. The colour stability depends on the Hg:S ratio. To remove excess of sulfur, the substance is washed in an alkaline solution (KOH with  $K_2CO_3$ ) and water, and to remove mercury, the pigment is treated with sulfur and soda ( $Na_2CO_3$ ). However, this product is thought to darken easily. The second, the wet method to get vermilion was discovered in 1687 by Gottfried Schulz, and it is easier than dry. This method also starts with  $\beta$ -HgS formed by the reaction of sulfur with mercury or mercury salts in an ammonium or potassium sulphide solution in order to decrease the heating temperature.

Pure Hg or HgO were used for synthesis by cleaning the metal in a solution with sulfur and heating it to 40–60 °C in NaOH solution. Vermilion produced in the wet method darkened faster than in the dry process, and the synthetic forms usually degraded faster than those produced in nature (cinnabar) [46–48, 51]. The darkening of cinnabar induced by light has been noted at various times. The cinnabar is photosensitive, especially in the sun or even in the moonlight. The cause was thought to be related to the continuous exsolution of mercury from the sulphide, even without the influence of oxygen [45].

Several research groups have explored works of art in recent decades and investigated the degradation mechanisms of red mercury sulphide (cinnabar/vermilion) to devise better conservation strategies. Many sources offer different mechanisms to be assigned darkening of cinnabar:

1. Phase transformation of red hexagonal ( $\alpha$ -cinnabar) into black cubic metacinnabar ( $\beta$ -HgS), this case implies that reflectance properties of red cinnabar are altered by light exposure because of the production of dark phase metacinnabar. The effect is accentuated by the original composition of the pigment in addition to its production process (wet or dry synthesis).

2. Reaction with halogens. It is known that chlorine can be incorporated during the formation of natural or synthetic cinnabar. McCormack [52] found that light-sensitive cinnabar contains 0.05-1% chlorine, while non-photosensitive cinnabar contains less than 0.01% chlorine. Halogens play a dominant role in the darkening process of photosensitive coatings that develop on  $\alpha$ -HgS. The region in which cinnabar absorbs exposure to light is from 400 to 570 nm wavelengths.

Vermilion is transformed into the photosensitive  $\alpha$ -Hg<sub>3</sub>S<sub>2</sub>Cl<sub>2</sub> (corderoite), after exposure to humidity and chloride ions. This  $\alpha$ -Hg<sub>3</sub>S<sub>2</sub>Cl<sub>2</sub> degraded into the black  $\beta$ -HgS, white Hg<sub>2</sub>Cl<sub>2</sub> (calomel) and elemental sulfur by a light-induced reaction.

3. Photochemical redox reaction. At high relative humidity in the presence of sunlight elemental Hg<sup>0</sup> and S<sup>0</sup> are obtained after catalysis with halogens. The red pigment turns into a gray pigment with a metallic luster.

4. Thermodynamic effect. Dissociation of  $\alpha$ -HgS to the metallic Hg<sup>0</sup> and  $\beta$ -HgS, due to a transition temperature in the range of 100–400 °C. The transition temperature can decrease drastically in presence of chlorine ions, in the system Hg–S–Cl–H<sub>2</sub>O with prevalence of Hg ions. At 30 °C the effect of pH leads to a simultaneous presence of Hg<sup>0</sup> and  $\alpha$ -HgS with mutual concentration depending on pH. In this condition the presence of  $\beta$ -HgS is not excluded. However, a predominant concentration of chlorine ions,

depending on the pH, implies the formation of Cl-based compounds like calomel or corderoite.

Sometimes, the cleaning with a laser can also cause discolouration. This is due to the energy of the radiation applied. If it is higher than the colour-specific energy of cinnabar, it activates photochemical processes. Mercury readily forms amalgams and reacts with copper to produce Hg–Cu and a patina of CuS at the surface [47].

Cinnabar has been used to colour wooden objects, not only for colouration, but also as a fungicide. Hg has a high adsorption capacity on lignin. HgS is a good wood preservative because reduction to free mercury does not occur and prevents deeper penetration of harmful substances. In an alkaline environment, cinnabar stabilizes colours, especially when it is mixed with lead oxide, red lead, red or yellow iron oxides, and chalk. The red/yellow pigment of arsenic (realgar As<sub>4</sub>S<sub>4</sub> and orpiment As<sub>2</sub>S<sub>3</sub>) with cinnabar is also common in China as well as in India [11, 44, 46–48, 51, 53].

As we can see, cinnabar/vermilion has been used in various arts: painting, polychrome, book decoration, and etc. This pigment can also be found in the manuscript head, fore edge and tail, this form of decoration was initiated by British bookbinders in the mid-seventeenth century. Cinnabar was used for miniatures, rubrics, and inks in the Middle Ages and remained popular until the 20th century, when due to its toxicity was replaced by cadmium red [54, 55].

Sunlight and other lighting systems induce the degradation process of cinnabar. The origin of chlorine, natural (chlorine could as well as in the materials of the works of art themselves, such as varnishes, binders or protein-based adhesives) or sources related to human activities (chlorine compounds in the air), is very important because it determines the way works of art are stored, cleaned and consolidated. All of this is important to evaluate before selecting the right materials for conservation, storage, and exhibition works [56].

### 1.2.3. Realgar

Arsenic sulphide minerals are found naturally and have been used as artists' pigments since prehistoric times until the end of the 19th century, when they were gradually replaced by new pigments such as chromium yellow [57]. Natural orpiment (As<sub>2</sub>S<sub>3</sub>) and pararealgar (As<sub>4</sub>S<sub>4</sub>) are yellow, however, the realgar ( $\alpha$ -As<sub>4</sub>S<sub>4</sub>) is a red mineral. The name realgar comes from the Arabic *rahj al ghar*, powder of the mine. Pliny used the Latin term

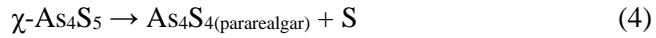
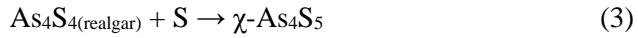
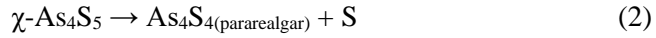
by realgar – *sandarach*, which became the name *sandaraca* used by Agricola [19].

Arsenic sulfide pigments have been used in polychrome works of art, particularly in Egypt and Asia, as well as found in European paintings, monumental decorative panels, illuminated manuscripts, Japanese prints or easel paintings. Both pigments orpiment and the realgar are mentioned in the early bookbinding manuscripts. Orpiment has been identified on Armenian manuscripts in the 11-16th centuries, on Arab – in the 14th century manuscripts, and on Persian miniatures from the early 14th to 16th centuries. Both orpiment and realgar are described in 15th to 18th century recipes from Russia, Armenia, and Azerbaijan. In China, both pigments were known possibly by the 4th century B.C. They later spread to India, Japan and neighbouring regions. In European art, these pigments were not common, but they were used from the 9th century (e. g. Book of Kells) to the late 19th century (e. g. impressionist paintings). Medieval artists used pigment imported from Asia Minor and African-Genoese [58–60].

Realgar contains 70% of As, and is formed under reducing conditions. It is commonly found in low-temperature hydrothermal veins, hot spring deposits and volcanic debris, and is often associated with ores containing gold, silver, or lead. The same terminology was used for the production of artificial orpiment and realgar as for the production of vermilion. Pigment production by heating, with or without sublimation, can be referred to as dry process methods while precipitation methods using substances in solution may be referred to as wet process methods. There are not many historical facts about the production of realgar. The 17th century Paduan manuscript describes melting, cooling, and grinding to obtain a „red orpiment“. There is some knowledge about wet process orpiment production (hydrogen sulfide passing through a hydrochloric acid solution of arsenic trioxide), but there is no evidence that the precipitated material was used as a pigment [58].

Realgar forms different structures depending on temperature and pressure. The structures are generally divided into four types: the monoclinic space group  $P2_{1/n}$  ( $\alpha$ -As<sub>4</sub>S<sub>4</sub>), which is the raw form of As ore, the  $C2_{1/n}$  space group ( $\beta$ -As<sub>4</sub>S<sub>4</sub>), pararealgar, and As<sub>4</sub>S<sub>4</sub> (II). In addition, other allomorphs of As and S also exist, but these are usually intermediates or a mixture of different conformations. The chemical bonds between As and S vary between the different realgar allomorphs. Realgar molecules are held together by Van de Waals forces, it has a very symmetrical structure, and is relatively stable. However, realgar can be easily oxidized to As (III) and As (V) forms, which have higher toxicity [58, 59].

Wind, water and other physical factors can change the physical structure of realgar, while light changes its chemical structure. Light between 500 – 670 nm wavelength transforms realgar (red mineral,  $\text{As}_4\text{S}_4$ ) in arsenolite (white powder,  $\text{As}_2\text{O}_3$ ) and pararealgar (yellow,  $\text{As}_4\text{S}_4$ ), a compound with the same formula of realgar but different structural arrangement of sulphur and arsenic atoms. The highest degradation efficiency is in the part of wavelength between 530–560 nm. The result of the realgar’s reaction with oxygen and light is via a phase ( $\chi\text{-As}_4\text{S}_5$ ) to pararealgar. In  $\chi\text{-As}_4\text{S}_5$  a sulphur atom is inserted between the As atoms in realgar molecules, because the As-As bonds are weaker than the As-S bond. Several authors suggested a reactions to substantiate the result (Eq. 1-4) [60–62]:



The process works cyclically. Pararealgar is formed by releasing a sulfur atom which can be attracted again by other realgar molecules [61]. The transformation of realgar into pararealgar consists of two modes of dynamic reactions: the first stage is the production of arsenolite. It requires photoexcitation (light phase) and the second is a self-accelerated solid-state chain reaction that does not require the effects of light (dark phase). At the end of the process some  $\text{As}_4\text{S}_5$  molecules co-exist with pararealgar, and the red mineral or pigment turns yellow, see Fig. 3 [63–68].

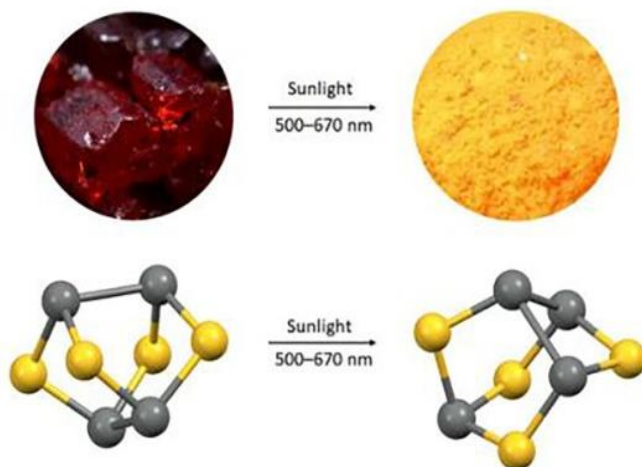


**Figure 3.** Effect of irradiation by light on the transition of red realgar crystals to yellow pararealgar crystals [68]

The oxidation reaction of realgar also takes place in water, where realgar can form oxidized forms of As (III) and As (V). The state of As in water is largely dependent on changes of oxidation/reduction potential and pH. In the oxidizing environment, As exists as As (V) (negative ion), whereas under reduction conditions at  $\text{pH} < 9.2$ , it exists as As (III) and  $\text{As}(\text{OH})_3$ .

The reduction reaction of realgar takes place under hypoxic conditions and an S-rich environment. The resulting product is  $\text{As}_2\text{S}_3$ . This reciprocal transformation of  $\text{As}_2\text{S}_3$ – $\text{As}_4\text{S}_4$  is also influenced by Fe, which has a strong adsorption relationship with As but is also able to precipitate with As, thus further impacting upon its structure and valency. Microorganisms also play an important role in the transformation of realgar. They greatly promote the oxidation of realgar. For example, S- and Fe-oxidizing bacteria act to oxidize realgar to As (III) and As (V). The reducing effects of microorganisms in the Fe–S–As system is also important, As (III) and As (V) can be reduced to  $\text{FeAsS}$  and  $\text{As}_4\text{S}_4$  [59].

Research on multilevel reverse transformations and their processes can help to understand better the structural modifications of realgar molecules and the dynamics of the process. This can be useful in restoring damaged works of art.

#### 1.2.4. Red lead

Red lead was one of the earliest pigments artificially prepared and is still used today. The naturally occurring mineral minium was used as a pigment only at an early date. Pliny the Elder of the first century A.D. applied the name minium to cinnabar, the naturally occurring form of the pigment vermilion and called red lead *minium secundarium*. Cinnabar was often adulterated with red lead and the name minium was used for the mixture. Other writers used a false term *sandarach* for structure, which was attributed to realgar, the term *sandyx* was a mixture of red lead and red ochre; *sy ricum* or *siricum* were synonyms for red lead or litharge. In a Chinese text from 5th century B.C. it was described as „lead cinnabar“ used in the Han Dynasty (2 century B.C. – 2 century A.D.), indicating the pigment was prepared artificially from lead, Vitruvian texts also mention that red lead was inadvertently obtained from lead white in a fire. The earliest objects on which red lead has been found in Egypt were identified on Roman Fayum portraits of the 2 – 4th centuries A.D. Red lead was used in the 5 – 8th centuries in China, India and Turkey for wall painting, on illuminated manuscripts and in miniature painting in Europe from the 8th century, in Byzantine manuscripts beginning in the 7th century. The pigment has been found from the 12th to 15th centuries on polychrome sculpture and panel paintings, and occasionally on mural paintings. Red lead was widely used in medieval manuscripts, mixed with vermilion, white lead or ochre. Often red lead has been used over vermilion to produce a silk effect, or to prevent the oxidation of sulfur and thus stabilizing cinnabar [19, 47, 69].

Red lead and the mineral minium have the same chemical lead tetroxide ( $\text{Pb}_3\text{O}_4$ ) composition and crystallographic structure. It belongs to the tetragonal crystal system (see Fig. 4). It is a brilliant red or orange-red mixed valence compound containing lead atoms both in the Pb (II) and Pb (IV) states. The colour could be related to the amount of unchanged litharge presence and to particle size. This pigment has a high refractive index and good covering properties. Red lead is sometimes confused with the tetragonal form of leady oxide ( $\alpha\text{-PbO}$ ), which also has a red colour, but actually is the raw material for the production of red lead [69, 70].



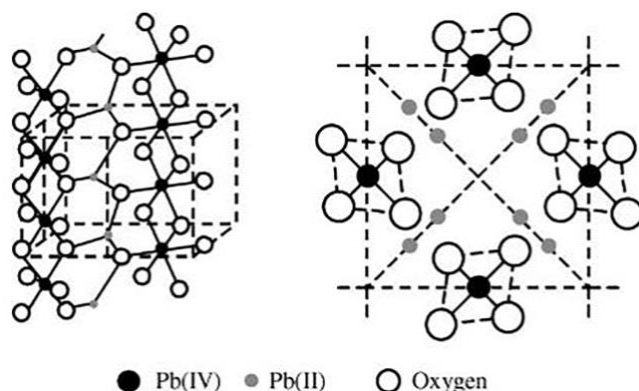


**Figure 4.** Crystal structure of red lead ( $\text{Pb}_3\text{O}_4$ ) [70]

The red pigment preparation from lead white was known in Greek and Roman times. From the Far East, descriptions of the production of red lead using metal have been known much earlier. White lead is obtained from metallic lead. Lead sheets are corroded into lead acetate which is subsequently roasted to form  $2\text{PbCO}_3 \cdot \text{Pb}(\text{OH})_2$ . Further heating allows the production of litharge due to the consistent loss of water and carbonate. At higher temperatures and oxidizing conditions, litharge eventually converted into minium. Another method is when the  $\alpha$ - $\text{PbO}$  is heated at around 450–500 °C. To obtain pure  $\text{Pb}_3\text{O}_4$  the dilute acetic acid can be used to remove  $\text{PbO}$ . The process of converting lead oxide to red lead can be stopped at nearly any percent of oxidation. In the 19th century, industrial processes used an artificial lead monoxide produced by the oxidation of molten lead in reverberatory furnaces. The complete reaction of litharge oxidation into minium occurs after 24 h thermal treatment at 470 °C [69, 71, 72].

The natural aging of lead pigments is often the result of different types of chromatic alterations, associated with the formation of various secondary phases. Both red lead darkening and lightening have been observed on artworks. The unsuitability of red lead as a pigment on frescoes and in watercolor has been noted in the early 15th century by Cennino Cennini. Dark or brown red lead has been reported on medieval manuscripts and miniatures too. These phenomena depend on environmental or internal factors such as pictorial technique or the presence of other pigments. Red lead blackening is strongly influenced by the presence of hydrogen sulfide ( $\text{H}_2\text{S}$ ) in the atmosphere to form lead sulfide  $\text{PbS}$  (galena). This path of degradation is particularly common in manuscripts. The formation of lead sulfide could be caused also by the interaction of the lead pigments with sulfur-based pigments. Other studies show the presence of microorganisms

such as bacteria can accelerate decomposition of white and red lead into plattnerite ( $\alpha$ -PbO<sub>2</sub>) [73, 74]. Red lead can darken in the presence of hydrogen peroxide (H<sub>2</sub>O<sub>2</sub>) caused by the metabolic activity of microorganisms. In addition, some bacteria can convert white lead, red lead, and massicot into PbS. This is caused by the interaction of hydrogen sulfide, produced by bacteria using sulfur-containing amino acids with lead-based pigments. In the case of whitening, red lead may be transformed into lead salts (PbCO<sub>3</sub>, 2PbCO<sub>3</sub>Pb(OH)<sub>2</sub>, PbSO<sub>4</sub>). This phenomenon is thought to be due to the interaction of the pigment with atmospheric pollutants such as SO<sub>2</sub> and CO<sub>2</sub>, which develop into acids under humid conditions (H<sub>2</sub>SO<sub>4</sub> and H<sub>2</sub>CO<sub>3</sub>). Another view is that when plattnerite is formed, it later turns into a more stable anglesite which results in a total loss of colour. Whitening may also be affected by other lead compounds, such as lead monoxides ( $\beta$ -PbO and  $\alpha$ -PbO) identified together with red lead. They may be present as pigments or as impurities in the same red lead [71, 73–76].

Nowadays, red lead is no longer used as a pigment by artists due to its toxicity, poor light stability, and colour changes with aging [54]. Understanding the mechanism of red lead decomposition will allow the development and testing of new conservation strategies that will help preserve the values of art for future generations.

### 1.3. Capillary washing method

One of the most widely used materials for recording and storing information is paper. In cultural heritage institutions, most of the protected heritage consists of paper documents printed or written at various times. Since the emergence of this material, there has also been a problem in how to preserve it for future generations. About one third of the paper items in large libraries are too brittle to handle, with another third in need of attention over the coming century. Chemistry is at the heart of paper preservation, but as a science, paper preservation is a relatively new field. The principal component of paper is cellulose (consisting of  $\beta$ -D-glucose chains and hydrogen bonding between cellulose chains that stick them together). Natural cellulose based materials (wood, hemp, cotton, linen, etc.) have been used by our society as source materials for thousands of years. Raw cellulose fibres are suspended in water, when a grid of the right size is pulled through the suspension, the water drains out, forming an intertwined cellulose fiber – paper. To give the paper better properties (strength, whiteness,

hydrophobicity) were added various additives, sizing materials (gelatin, starch, alum salt), fillers (chalk) [77, 78].

Paper like all other materials ages over time, depending in particular on the technology in which it was produced, the materials used in its manufacture and the quality with which it was written, drawn or otherwise decorated. The durability and survival of the paper are affected by storage conditions (chemical, physical and biological). The most significant and unpleasant method of paper decomposition is the hydrolysis and oxidation reactions of cellulose. The colour of the paper changes with the formation of oxidation and decomposition products. The strength of the paper-forming fibers decreases very rapidly as the cellulose chains shorten, therefore decreases and mechanical strength of paper document becomes fragile, vulnerable, and there is a risk of losing information on the paper (text, drawings, stamps, etc.). Most problems with paper are caused by a change in pH balance. The paper becomes brown, brittle and discoloured as the acidity increases. The problem is compounded when acid pigments and dyes are also used. An effort to stop it is called deacidification [77, 79–87].

During conservation procedures the fibers of papers cannot be renewed, but there are ways to renew a document. Common paper preservation procedures include surface cleaning, wrinkle reduction, tear and hole repair, and reinforcement of paper supports through the lining. Poor quality mounting materials, stains, bad composition glue are removed mechanically and using water or other solvents. Stabilization of paper usually involves reducing the level of acidity and discolouration by washing in deionised water or alkaline solutions. Washing of paper objects is very important in the field of paper preservation and is constantly applied in conservation studies. Since washing is intended to remove water-soluble components, washing of paper objects containing water-sensitive media presents a challenge for paper conservators. The paper may contain media which dissolve immediately after contact with water or change their morphological properties, may contain a binder which becomes soluble in water after prolonged contact with water, but is relatively stable. Heavily deteriorated, or very thin paper is also considered sensitive to water because it is easily vulnerable to mechanical stress and can suffer from water movement when washed by immersion. There are many types of washing methods, involving capillary unit treatment. The capillary unit was developed by Peter Zajicek and Derek Tinwell at the State Library of South Australia and was introduced in 1993. But it became better known when Susanne Kirchner published the results of her final thesis in 2001 in Cologne. In the treatment of a capillary unit, the object is placed on a layer of absorbent material that acts as a reservoir of

water. One end of the material takes clean water from the container, the water travels up the slope, and at the other end dirty water drips down from the material (Fig. 5). In this way, water is constantly moving from one end of the material to the other. Solvents that migrate from the object to the absorbent material are actively removed from the system. The slope of the capillary unit has been found to be an important factor and slope of  $2^\circ$  is recommended. The most suitable material for washing water-sensitive objects is Paraprint OL60, a 0.5 mm thick white viscose nonwoven fabric.

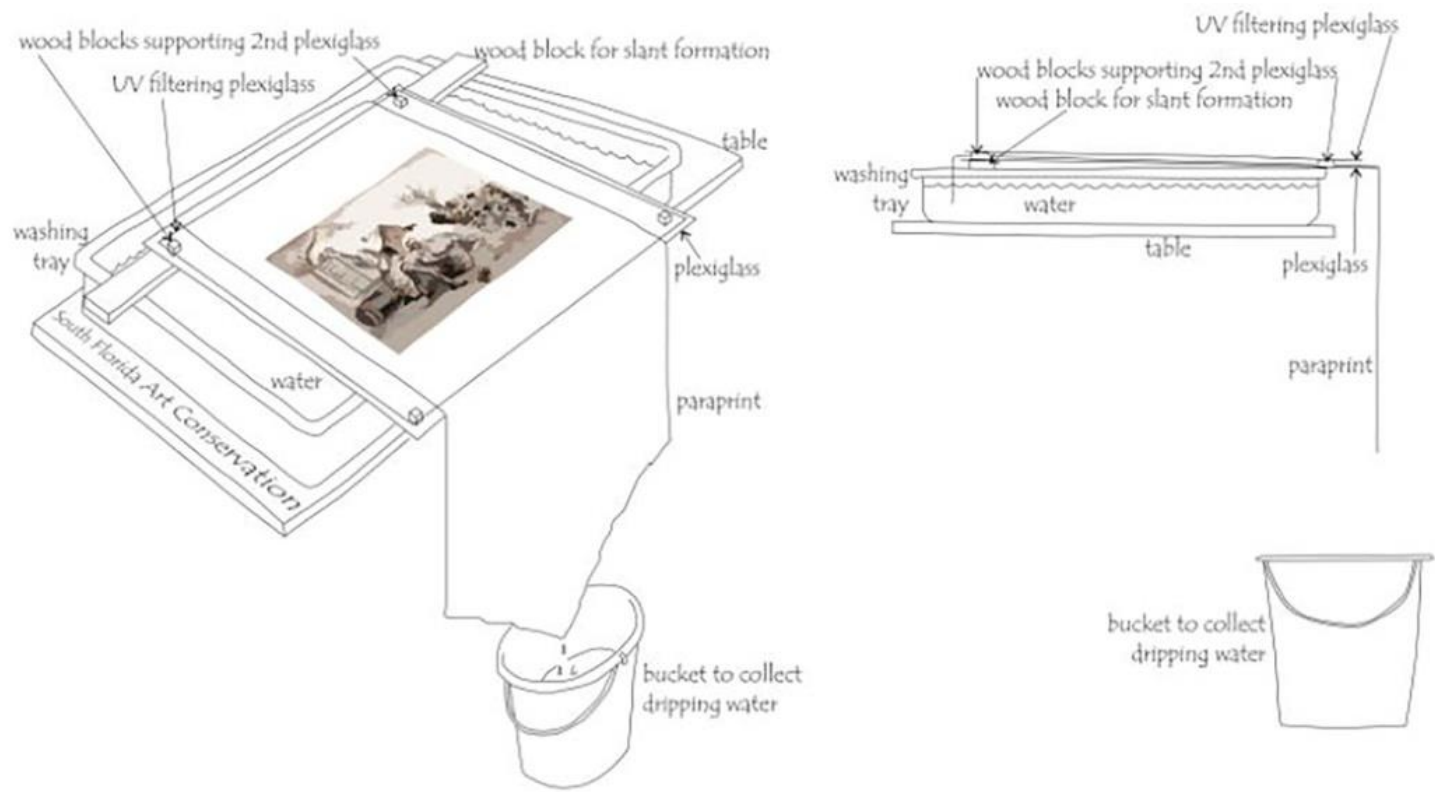


**Figure 5.** Schematic drawing of the modified capillary unit treatment [88]

At the beginning of the wash, the capillaries of the tissue need to be filled with water. This can be done by spraying or immersing Paraprint OL60 in water. Paraprint OL60 absorbs water in a capillary manner. Capillary action is a phenomenon in which fluid travels higher than the surrounding fluid level in thin tubes (capillaries). This is due to the combination of cohesion and grip forces. Saturation of the porous material or reaching a point where gravity is equal to capillary forces creates an equilibrium between capillary forces and gravity. At this point, there is no longer a driving force for further upward movement and water uptake stops. In capillary washing, capillarity allows water to enter the material, but this is not the driving force of the water flow. The water flow is created when one end of the Paraprint OL60 is placed in a container of clean water and the other end is stuck, reaching a lower level than the clean water level. The system acts as a siphon. The driving force of the water flow is the height difference between the two sides, which results in a hydrostatic head or a pressure column. Increasing the height difference, lengthening the hanging end of the fabric, or increasing the water level increases the pressure and speeds up water transport. The purpose of washing is to remove water-soluble discoloration or harmful components from the object. In the treatment of a capillary unit, this transfer occurs due to diffusion. Diffusion transport is determined by the concentration gradient of the solute (Fig. 6) [89].

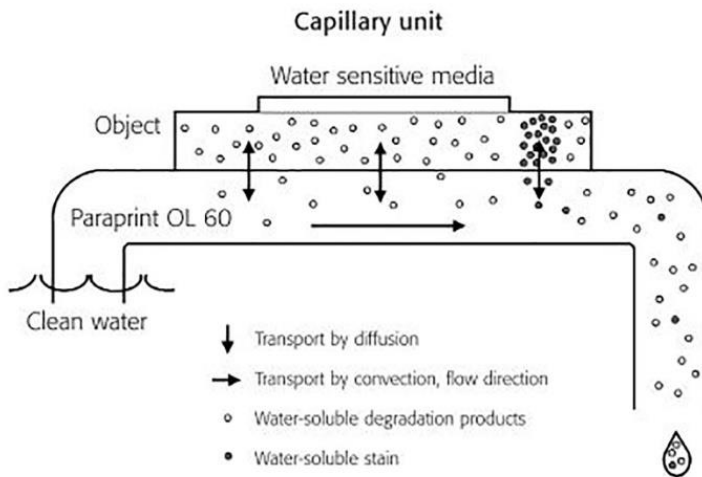


**Figure 6.** Transport in the capillary unit treatment by diffusion and convection [89]

The siphoning action, clean water flowing through the Paraprint OL60 fabric. Solute molecules that pass the interface are transported away from the

object by this water flow, called convection. Transport by convection is much faster than by diffusion. The water that transports the solutes finally leaves the Paraprint OL60 by dripping down into the container for dirty water. Paraprint washing is recommended for aqueous treatment of most water-sensitive paper objects. Using this washing method, alkalizing agents, ink stabilizing additives sizing agents can be added to clean water during the process. This is especially convenient because no additional treatment is required after washing [89–93].

Information collected on medieval inorganic pigments show how it can be difficult to preserve the cultural objects. It is necessary to understand the stability of pigments for specific factors and it is important to know their chemical reactivity. Then it is necessary to consider the study of pigment-binder-additive-base interaction and how they interact with each other. Finally, it is necessary to implement appropriate storage and exhibition conditions to preserve art treasures for future generations.



## 2. EXPERIMENTAL SECTION

### 2.1. Reagents and materials

Six different historical red pigments and three binding media were purchased from Kremer Pigmente as a standard: natural cinnabar Monte Amiata (HgS, 10610), red lead (Pb<sub>3</sub>O<sub>4</sub>, 42500), realgar (As<sub>4</sub>S<sub>4</sub>, 10800), red bolus (Fe<sub>2</sub>O<sub>3</sub>·xSiO<sub>2</sub>·yAl<sub>2</sub>O<sub>3</sub>, 40503), Andalusian red ochre (Fe<sub>2</sub>O<sub>3</sub>, 11274), hematite (Fe<sub>2</sub>O<sub>3</sub>, 48651), gum Arabic (63320), fish glue (63080), and parchment glue (63035). The chemical formulas given in the brackets are as the producer stated. Next, these materials were used for the preparation of analogues to historical red paints. Acetic acid (CH<sub>3</sub>COOH, 99.5% Eurochemicals Reachem) diluted to 9% with distilled water was used to prepare the paint.

The real paint samples were taken from the illuminated and rubricated manuscripts. They are kept in the Manuscript Department of the Wroblewski Library of the Lithuanian Academy of Science, in Vilnius. The basic information about the analyzed manuscript is given in Table 1. Most of the red paint samples were in bad condition or had a thick layer of paint, taken on a cotton swab, or collected with the spatula, using an Olympus SZX16 stereomicroscope. From each sample it was taken approximately 8 mg of paint. One sample was taken per one folio and prepared in powder form.

**Table 1.** Basic information for the analyzed manuscripts

Manuscript	Analyzed folios	Representative details	Abbrev.
<i>Hirmalagionas</i> (1662). Liturgical manuscript on paper written in the Church Slavonic language. Analyzed paint sample represents an initial letter .	170		F19-115
<i>Hirmalagionas</i> (1638-1639). Liturgical manuscript on paper written in the Church	5		F19-116



Continued table.

Slavonic language.  
Analyzed paint  
samples represent a  
headpiece (5 and 260  
folios) and an initial  
letter (154 folio).

154

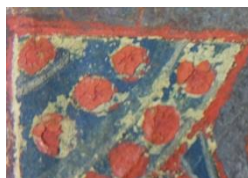


260



*Tetraevangelija.*  
*Mažuju Žuchavičij*  
*evangelija (XVI).*  
Liturgical manuscript  
on paper written in the  
Church Slavonic  
language. Analyzed  
paint sample represents  
illumination.

250



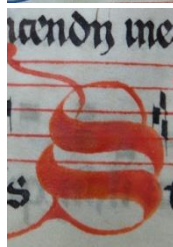
F21-805

6



*Antifonalas* (1469-  
1494, 1607).  
Ecclesiastical  
hymnbook on  
parchment, text in  
latin. Analyzed paint  
samples represent  
initial letters.

81



F22-101

138



## 2.2. Paints preparation

A set of pigment-binding media combinations were prepared according to contemporary medieval recipes. For the preparation of binding media slightly different procedures were used. The parchment and fish glue were washed with distilled water, cut into small pieces and covered with water for 24 h. Next, the glue gently heated (40–50 °C) and stirred for 4 h till it became liquid. Then, a 9% acetic acid solution was added to the prepared binding media with ratio (4:1). Gum Arabic was fine-cut, covered with distilled water and was left to swell. Then it was stirred and filtered through linen fabric. Finally, the glue was mixed with the same concentration solution of acetic acid with ratio (4:1). Small quantities of acetic acid added to animal glues could prevent the formation of a gel at room temperature, to gum Arabic to control pH and the tone of the colour accordingly. Finally it was used to prevent from mould and insects [21].

The red pigments were first ground in an agate mortar with a drop of distilled water and then mixed with the binders resulting in ~ 85 wt% of binding media on a dry-paint composition [28, 94]. Eighteen different analogous to ancient red paints were fabricated using the compositions of each pigment with each binding material. A set of pigment-binding media combinations were coated on microscope glass slides and dried in the dark at room temperature.

## 2.3. Artificial photochemical aging

The prepared red paint samples on the microscope glass slides were artificially aged at intervals of 1, 4, 7, 14, 21, 28 and 35 days in a chamber with a constant intensity of UV irradiation of 14887 mW/m<sup>2</sup>. Measurements were made using a versatile lux-hygrometer ELSEC 764 UV. The UV source in the aging chamber was the 10-luminescent Osram Eversun L40W/79K fluorescent lamp with a power output of 40W (400W total). Lamps disseminated a wavelength of 310–400 nm and were hung 50 cm above the samples. The temperature in the chamber did not exceed 35 °C and the relative humidity (RH) was 21%.

Artificially aged samples were removed at the indicated day intervals and analyzed by the methods described below.

## 2.4. Characterization techniques

**CIE(Lab)\* colour characterisation.** The colour change of the paint was evaluated by the CIELab colourimetric method, which is recommended by the Commission Internationale de l'Eclairage. Artificially aged samples were measured for all the time of aging intervals with a the FLAME-S-VIS-NIR-ES spectrometer with a light source HL-2000-FHSA 20W, resolution ~1.5 nm, measuring time – 2 s, measuring angle – 45 °, measuring range 350–1000 nm, the used standard was WS-1 Reflectance Standard.

Each sample was measured three times and the measurement results were recorded at the CIE(Lab)\* system. The coordinate L\* represents the lightness of the colour (L\* = 0 and L\* = 100 represents black and white, respectively). The negative/positive values of coordinate a\* represent green/red hue, respectively, and the parameter b\* corresponds to blue/yellow hue. The colour difference  $\Delta E$  in the CIE(Lab)\* system of paints was calculated according to equation (Eq. 5) [95]:

$$\Delta E = [(\Delta L^*)^2 + (\Delta a^*)^2 + (\Delta b^*)^2]^{1/2} \quad (5)$$

here  $\Delta L^*$ (lightness – darkness difference) =  $L^*_{\text{aged}} - L^*_{\text{non-aged}}$ ;

$\Delta a^*$ (redness – greenness difference) =  $a^*_{\text{aged}} - a^*_{\text{non-aged}}$ ;

$\Delta b^*$ (yellowness – blueness difference) =  $b^*_{\text{aged}} - b^*_{\text{non-aged}}$ .

**Scanning electron microscopy coupled with energy-dispersive X-ray spectroscopy (SEM/EDX).** The morphological features of samples were investigated using a scanning electron microscope Hitachi SU-70 at different magnifications. The surface morphology of the samples and elemental analysis were studied by the scanning electron microscope coupled with energy dispersive X-ray spectroscopy (SEM/EDX) using Hitachi TM3000. Several micro-crystals of pigment or paint were taken from an initial sample. The analysis was carried out on the surfaces without coating at 15 kV accelerating voltage.

**Fourier-transform infrared spectroscopy (FTIR).** Infrared spectra were recorded on the FTIR spectrophotometer Perkin Elmer Spectrum TWO with ATR accessory in the 4000–450  $\text{cm}^{-1}$  region, with the 24 scans and resolution of 4  $\text{cm}^{-1}$ . A diamond ATR cell was used for measurements of the samples.

***X-ray diffraction analysis (XRD).*** XRD analysis was performed using Benchtop XRD MiniFlex II, Rigaku in the scanning range of 10 to 80° 2 $\theta$ , 5°/min. speed, using CuK $\alpha$   $\lambda$  = 1.541874 Å radiation

***Thermal analysis (TG/DTG/DSC analysis).*** The thermogravimetric and differential scanning calorimetric analysis was performed by the simultaneous thermal analyzer (STA) 6000 PerkinElmer. The heating rate was 10 °C/min in air flow from 30 to 900 °C using Pt crucible.

***Optical microscopy (OM).*** The samples were collected from the manuscripts using an Olympus SZX16 stereomicroscope at different magnifications. The digital images of the pigment, paint and binding media samples were taken using a FUJIFILM X-A2 digital camera. The photographs were processed with Photoshop CC software.

### 3. RESULTS AND DISCUSSION

#### 3.1. Characterization of analogous to historical red pigments and binding media

In this part of the dissertation the results of the characterization of commercial analogous historical red pigments and binding media using SEM/EDX, FTIR, XRD, and TG/DTG/DSC analysis methods are presented.

##### 3.1.1. SEM/EDX analysis

The first aim was to determine the amount of main and trace elements in the commercial red pigments and binding media. For this purpose, the EDX analysis method was applied. The results are given in Tables 2 and 3.

**Table 2.** The EDX analysis results of commercial red pigments

<b>Pigment</b>	<b>Element, wt. %</b>						
Cinnabar	Hg	S	Si	Al			
	77.17	15.68	5.03	2.12			
Red lead	Pb	O					
	84.52	15.48					
Realgar	As	S	C				
	42.80	16.42	40.78				
Red ochre	Fe	O	Si	Al	C		
	48.16	16.80	7.43	2.23	25.38		
Red bolus	Fe	O	Si	Al	C	K	Mg
	12.73	48.67	16.84	8.79	9.90	2.32	0.75
Hematite	Fe	O	Si	Al	C	Ca	
	34.74	45.10	1.39	0.97	17.30	0.50	

**Table 3.** The EDX analysis results of commercial binding media

<b>Binding media</b>	<b>Element, wt. %</b>						
Gum Arabic	C	O	Ca	Al	K		
	49.48	43.85	3.52	2.51	0.64		
Parchment glue	C	O	Al	Ca	S	Na	
	68.16	30.34	0.61	0.31	0.30	0.28	
Fish glue	C	O	Mg	Al	S	Ca	
	35.77	49.43	9.23	4.37	0.94	0.26	

The SEM micrograph (Fig. 7a) shows that cinnabar is composed of plate-like crystals 2–5  $\mu\text{m}$  in size, 77.17 wt.% of mercury and 15.68 wt.% of sulfur. Besides, a small amount of Si (5.03 wt.%) and Al (2.12 wt.%) was also determined. Therefore, it is likely that in addition to HgS there is also a small amount of clay in the commercial cinnabar.

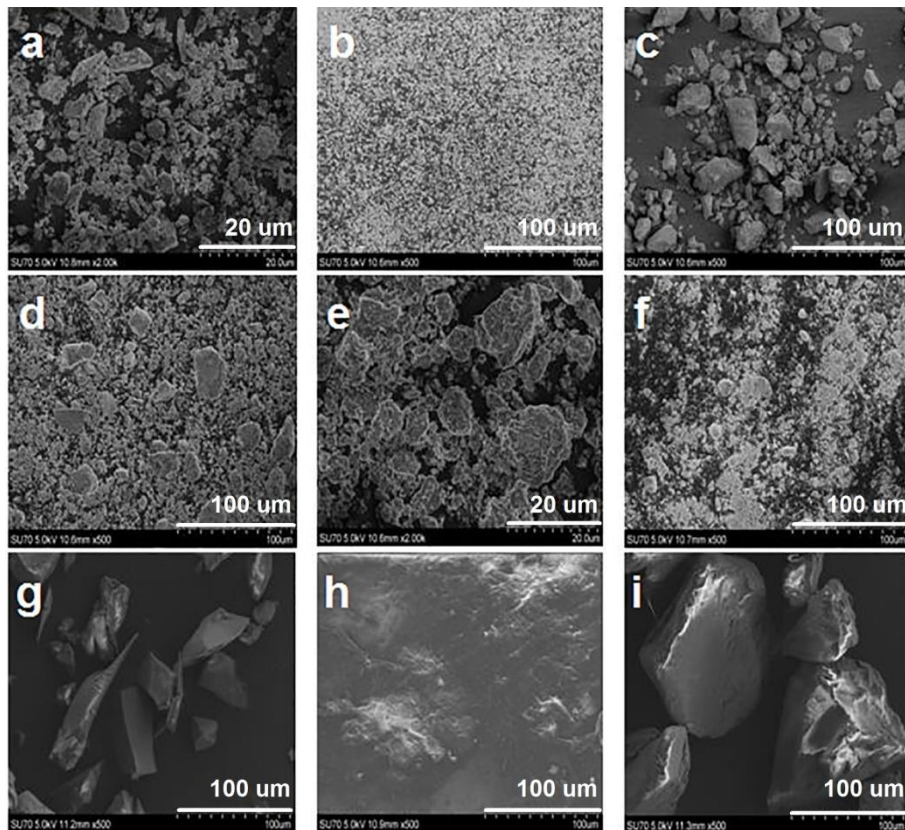


**Figure 7.** SEM micrograph of red pigments and binding media: a – cinnabar, b – red lead, c – realgar, d – red ochre, e – red bolus, f – hematite, g – gum Arabic, h – parchment glue, i – fish glue.

As it seen from the SEM micrograph (Fig. 7b), a narrow particle size distribution is evident for the pigment red lead. Moreover, the spherical particles less than 100 nm are finely distributed within the entire SEM image. The EDX results presented in Table 2 confirm that the material contains only lead (84.52 wt.%) and oxygen (15.49 wt.%). The SEM micrograph of realgar is shown in Fig. 7c. The particles of realgar are differently shaped, varying in size from 5 to 40  $\mu\text{m}$ . The EDX data showed that the amount of arsenic was 42.80 wt.%, sulfur 16.42 wt.% and carbon

40.78 wt.%. The carbon signal visible in the EDX spectrum is from a carbon film used for the sample preparation.

The surface microstructure and elemental composition of the iron pigments are very similar. Red ochre and red bolus (Fig. 7d and e, respectively) shows a plate-like microstructure with a particle size about 2–10  $\mu\text{m}$ . The pigment hematite is composed of nanosized particles, the part of which forms spherical agglomerates (Fig. 7f). The main components are the iron and oxygen in different amounts, and a small amount of impurities Si, Al, Ca, K, Mg. These side elements (Si and Al) can be found in a form of kaolin  $\text{Al}_2\text{Si}_2\text{O}_5(\text{OH})_4$ , iron aluminium silicates,  $\text{CaCO}_3$ , or different oxides.

Gum Arabic is a complex polysaccharide, either neutral or slightly acidic, found as a mixed calcium salt of polysaccharide acid (arabic acid). The backbone of gum Arabic is composed of 1,3-linked  $\beta$ -D-galactopyranosyl units. The side chains are composed of two or five 1,3-linked  $\beta$ -D-galactopyranosyl units, joined to the main chain by 1,6-linkages. Both the main and the side chains contain units of  $\alpha$ -L-arabinofuranosyl,  $\alpha$ -L-rhamnopyranosyl,  $\beta$ -D-glucuronopyranosyl and 4-O-methyl- $\beta$ -D-glucuroopyranosyl, the last two mostly as end units [96]. The SEM micrograph of gum Arabic is presented in Fig. 7g. As seen, the material is composed of lengthened crystals about 15  $\mu\text{m}$  in width and 50–60  $\mu\text{m}$  in length. The EDX elemental analysis shows the highest amount of C (49.48 wt.%) and O (43.85 wt.%) with a smaller amount of Ca (3.52 wt.%), Al (2.51 wt.%) and K (0.64 wt.%).

Parchment glue, like fish glue, is a proteinaceous substance that consists of collagen, whose typical microstructures are presented in Fig. 7h and i. The SEM image of parchment glue presents a monolithic microstructure of this material. According to the EDX analysis, the main elements in the glue are C (68.18 wt.%) and O (30.34 wt.%), and it also contains Al (0.61 wt.%), Ca (0.31 wt.%), S (0.30 wt.%), and Na (0.28 wt.%). The fish glue crystals are about 100  $\mu\text{m}$  in length and 10–20  $\mu\text{m}$  thick. Contains C (35.77 wt.%), O (49.43 wt.%), and small amounts of Mg (9.23 wt.%), Al (4.37 wt.%), S (0.94 wt.%) and Ca (0.26 wt.%). These elements may remain over from glue preparation and processing processes.

### 3.1.2. FTIR analysis

Infrared spectroscopy was applied to test the possibility for the characterisation and determination of analogous to historical red pigments

and binding media. The FTIR spectra of all specimens are represented in Figs. 8–10.

It is known that the red pigment cinnabar does not absorb infrared radiation in the range of  $4000\text{--}350\text{ cm}^{-1}$  [14]. However, in the FTIR spectrum (Fig. 8a) at  $1017\text{ cm}^{-1}$  cinnabar has an intensive absorption band, which is a characteristic vibration of the Si–O bond. The absorption peaks determined at  $773$  and  $692\text{ cm}^{-1}$  could be attributed to the Si–O–Al vibrations. The FTIR spectrum of the pigment red lead presented in Fig. 8b shows the absorption bands in low frequency regions of  $682$  and  $521\text{ cm}^{-1}$  and one band at  $1398\text{ cm}^{-1}$  which are characteristic of lead oxide [14]. No characteristic absorption bands could be seen in the FTIR spectrum of the pigment realgar (Fig. 8c).

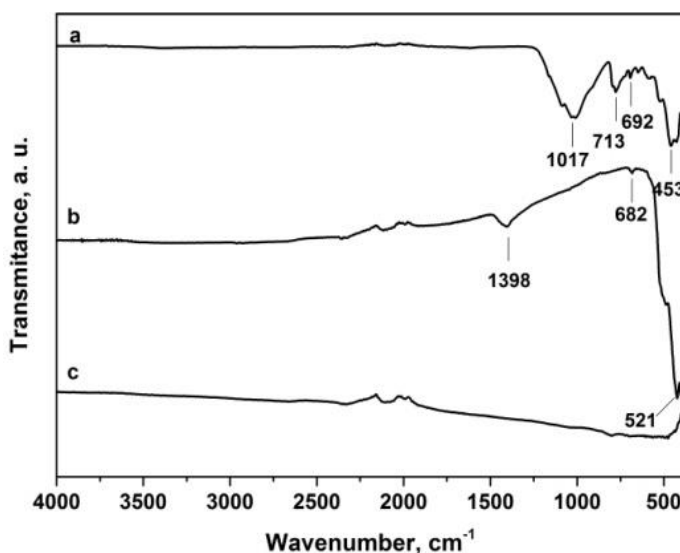


**Figure 8.** FTIR spectra of red pigments: a – cinnabar, b – red lead, c - realgar

The FTIR spectra of three red iron pigments are represented in Fig. 9. Red ochre (Fig. 9d) has an absorption band at  $1030\text{ cm}^{-1}$ , which can be identified as an asymmetric Si–O–Si stretching band. The peak at  $795\text{ cm}^{-1}$  is due to vibrations of Si–O–Al. The absorption bands located at  $531$  and  $431\text{ cm}^{-1}$  could be attributed to the Fe–O vibrations in iron oxide. The spectrum of the pigment red bolus (Fig. 9e) represents the absorption bands characteristic of kaolin ( $\text{Al}_2\text{Si}_2\text{O}_5(\text{OH})_4$ ): the O–H stretching bands are located at  $3689$  and at  $3616\text{ cm}^{-1}$ , an asymmetric Si–O–Si stretching band at  $1001\text{ cm}^{-1}$  and Si–O stretching bands at  $913\text{ cm}^{-1}$ . The absorption peaks visible at  $795$  and  $694\text{ cm}^{-1}$  are due to the Si–O–Al vibrations and at  $526$  and



464  $\text{cm}^{-1}$  are due to the Fe–O vibrations. The FTIR spectrum of the pigment hematite (Fig. 9f) also shows the characteristic absorption bands of asymmetric Si–O–Si stretching band at 1028  $\text{cm}^{-1}$ , and iron oxide at the wavenumbers of 519 and 431  $\text{cm}^{-1}$ . Two intensive absorption peaks visible at 1432 and 876  $\text{cm}^{-1}$  could be attributed to the vibrations in ionic carbonate ( $\text{CO}_3^{2-}$ ) [14].

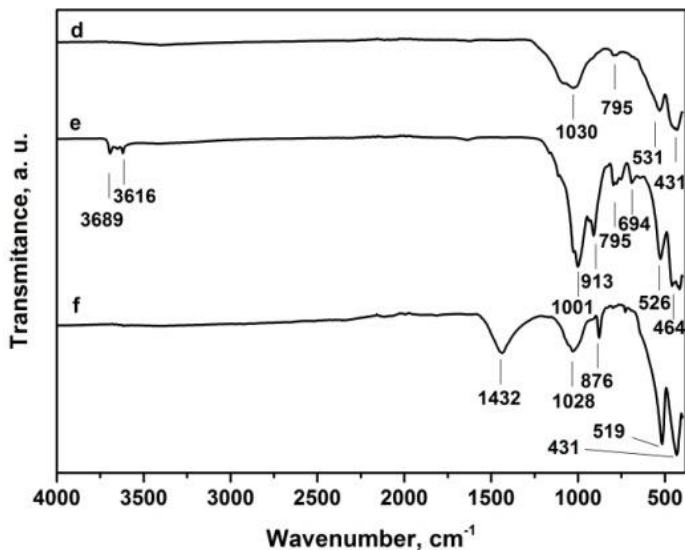


**Figure 9.** FTIR spectra of red pigments: d – red ochre, e – red bolus, f - hematite

The FTIR spectra of three different binding media are represented in Fig. 10. The absorption band specific for gum Arabic (Fig. 10g) is observed at 3300  $\text{cm}^{-1}$  could be attributed to the stretch vibrations of OH group, the band at 2923  $\text{cm}^{-1}$  is due to CH stretch and indicates the presence of sugars, galactose, arabinose, and rhamnose. The other characteristic bands of C=C stretch, amide NH bend,  $\text{NO}_2$  from both aliphatic and aromatic galacto proteins, and amino acids are around 1600  $\text{cm}^{-1}$ . The glucuronic acids have specific vibrations band at 1413 and 1364  $\text{cm}^{-1}$  due to C=O symmetric stretching and OH bending, respectively. A distinct band at 1008  $\text{cm}^{-1}$  represents alkene C-H band from polysaccharides for all gum samples [14, 97].

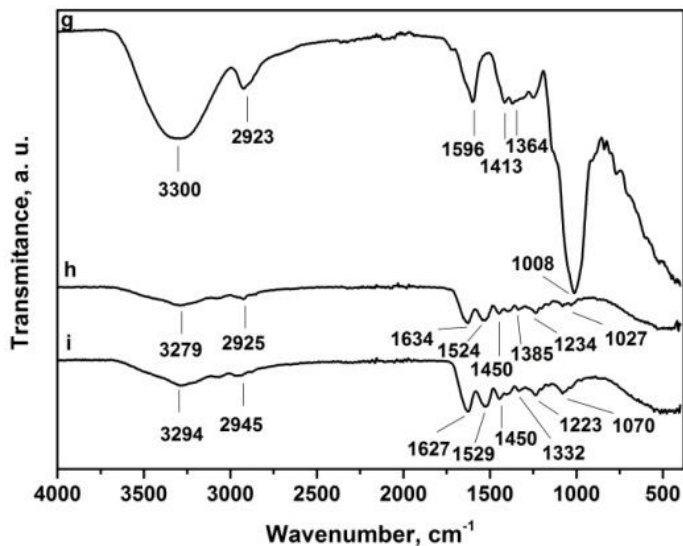


**Figure 10.** FTIR spectra of binding media: g – gum Arabic, h – parchment glue, i – fish glue

The FTIR spectra of parchment and fish glue (Fig. 10h–i) are almost identical, since collagen is the main component of these materials. The typical absorption band in the region of 3500–3400  $\text{cm}^{-1}$  for the amino group is masked by the broad absorption band of the OH group. Protein fingerprints are clearly observed in infrared spectra by the characteristic absorption peaks: amide I (C=O stretching,  $\sim 1630 \text{ cm}^{-1}$ ), amide II (CN stretching and NH bending,  $\sim 1530 \text{ cm}^{-1}$ ), CN bending at  $1450 \text{ cm}^{-1}$ , and amide III at  $\sim 1230 \text{ cm}^{-1}$ . The band at about 1070–1020  $\text{cm}^{-1}$  is attributed to C-O stretching vibration of the carbohydrate residues in collagen [94, 98].

### 3.1.3. XRD analysis

The X-ray diffraction patterns of different red pigments are presented in Fig. 11, and the binding media in Fig. 12. The diffractogram of HgS shows that the purchased pigment cinnabar with the main HgS phase (PDF 96-901-2083) also contains an additional  $\text{SiO}_2$  phase (PDF 00-078-1253) and the crystalline  $\text{Al}_2\text{Si}_2\text{O}_5(\text{OH})_4$  phase (PDF 00-075-1593). These results confirm the results obtained by SEM/EDX and FTIR spectroscopy. The pigment red lead consists only of  $\text{Pb}_3\text{O}_4$  (PDF 00-041-1493), the realgar also consists only of  $\text{As}_4\text{S}_4$  (PDF 00-072-0686).

The diffractograms of the red iron pigments show in all samples the main phase of  $\text{Fe}_2\text{O}_3$  (PDF 00-033-0664).

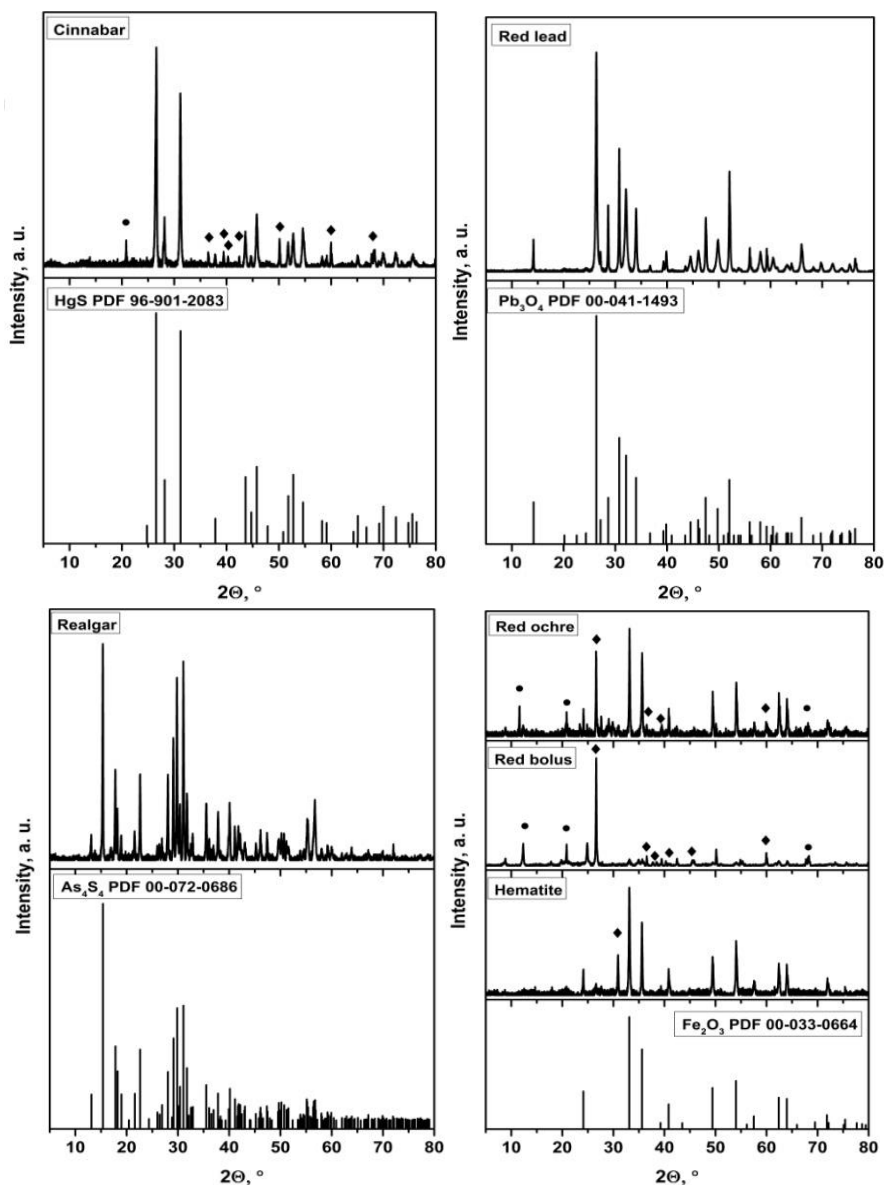


**Figure 11.** XRD patterns of red pigments. The side phases are marked:  $\blacklozenge$   $\text{SiO}_2$   $\bullet$   $\text{Al}_2\text{Si}_2\text{O}_5(\text{OH})_4$

The red ochre and red bolus have an additional  $\text{SiO}_2$  phase (PDF 00-078-1253) and impurity of the crystalline  $\text{Al}_2\text{Si}_2\text{O}_5(\text{OH})_4$  phase (PDF 00-075-1593). The XRD pattern of pigment hematite matches very well correlated with the XRD pattern of standard  $\text{Fe}_2\text{O}_3$  phase, but has an impurity of  $\text{SiO}_2$  phase as well. According to the results of the SEM/EDX, FTIR and XRD analysis the chemical composition of the pigments realgar and red lead

purchased from Kremer Pigmente corresponds to that described in the catalogue. The rest four pigments, however, contain different impurities.

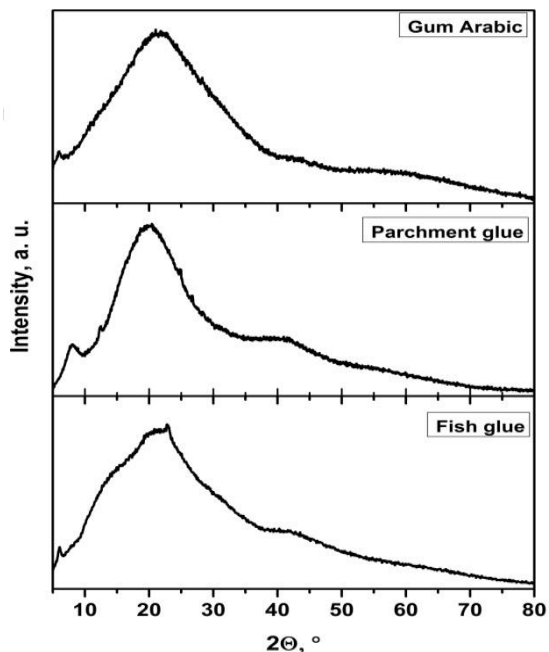


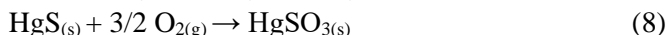
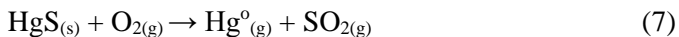
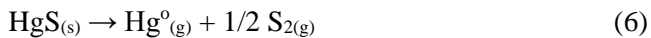
**Figure 12.** XRD patterns of different binding media

Based on literature sources, the main diffraction line in the XRD pattern of pure gum Arabic is located at  $2\theta = 18.9^\circ$  [99]. As mentioned before, the collagen is the main component of parchment and fish glue. Collagen has two diffraction lines. The first one is at  $7^\circ 2\theta$ , which is indicative of the position of the characteristic equatorial peak of collagen and the second one broad peak is at  $20^\circ 2\theta$ , which indicates the position of the characteristic interchain spacing of the collagen triple helix [100, 101]. In our investigated samples (see Fig. 12), the characteristic diffraction peaks are correlated well in parchment glue samples and slightly are shifted of gum Arabic and fish glue samples. It was affected by a small amount of inorganic impurities in the composition of the materials.

#### 3.1.4. TG/DTG/DSC analysis

The TG/DTG/DSC curves of cinnabar are shown in Fig. 13a. The first and the main mass loss (about 45%) is observed at about  $400^\circ\text{C}$ , when the

hexagonal red mercury sulphide  $\alpha$ -HgS rearranges to the cubic black metacinnabar  $\beta$ -HgS in the temperature range of 300–410 °C. These thermal transformations are also related to the presence of O<sub>2</sub> in the chamber. Decomposes of HgS is described by complex reactions (Eq. 6-8) [102, 103]:



The second mass loss ~ 2%, in the temperature range of 510–600 °C is related to the metacinnabar  $\beta$ -HgS transformation to hypercinnabar  $\gamma$ -HgS at about 527 °C, or decomposition of intermediates, such as HgO, HgSO<sub>4</sub> in air condition. This is in good agreement with the DSC curve, which shows a slight endothermic process in this temperature range [28, 45, 48, 102].

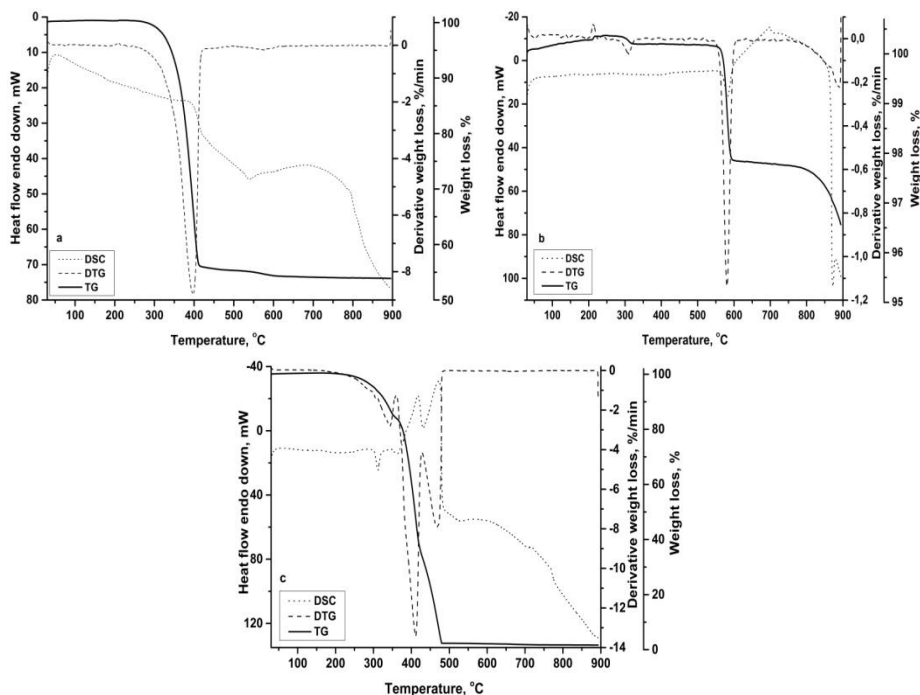


**Figure 13.** TG/DTG/DSC curves of: a – cinnabar, b – red lead, c - realgar

Figure 13b shows the TG/DTG/DSC curves of red lead. Red lead forms through an oxidation process when  $\alpha$ -PbO is heated to around 450–500 °C, but decomposes at atmospheric pressure to yellow litharge ( $\beta$ -PbO, orthorhombic) when temperature exceeds 585 °C [70]. The mass loss during

the decomposition of  $\text{Pb}_3\text{O}_4$  to the  $\beta\text{-PbO}$  process was determined to be about 2%.

As seen from the TG/DTG/DSC curves of the pigment realgar (Fig. 13c), the first mass loss (~ 18%) occurs at 307–370 °C. Red pigment ( $\text{As}_4\text{S}_4$ ) at about 256 °C temperature under normal pressure transforms to the yellow  $\text{As}_4\text{S}_4$  phase, which melts at about 307 °C temperature. The second (~ 45%) mass loss occurs at 370–430 °C, which could be associated with the transformation of the yellow  $\text{As}_4\text{S}_4$  phase to arsenolite. And finally, the third (~ 37%) mass loss starts at 430–500 °C and continuously lasts until 100%, related to the evaporation of material [104].

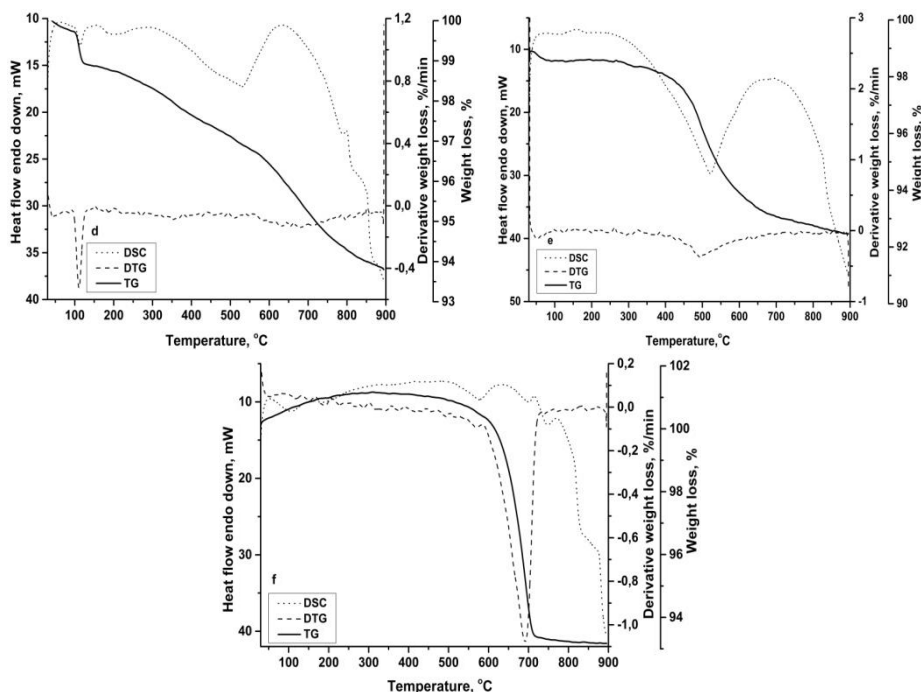


**Figure 14.** TG/DTG/DSC curves of: d – red ochre, e – red bolus, f - hematite

The TG/DTG/DSC curves of red ochre, red bolus and hematite are presented in Fig. 14. Differences in the thermal analysis curves are evident, despite the composition of the materials investigated is very similar. The differences are mainly due to the presence of impurities. The red ochre and red bolus contain the  $\text{Al}_2\text{Si}_2\text{O}_5(\text{OH})_4$  impurity phase which decomposes monotonically by heating the sample up to 700–800 °C. Hematite also contains calcium carbonate according to the FTIR results, which decomposes between 600 and 800 °C [105].

Weight loss of ~ 1% to 145 °C and ~ 1,5% from 145 to 280 °C were due to desorption of physically and chemically adsorbed water, respectively. Endothermic peaks at about 450–650 °C were found in the heating process due to the decomposition of  $\alpha$ -Fe<sub>2</sub>O<sub>3</sub> to  $\gamma$ -Fe<sub>2</sub>O<sub>3</sub>, respectively. The  $\gamma$ -Fe<sub>2</sub>O<sub>3</sub> phase formation temperature is about 500 °C [106, 107]. The mass loss in all cases was found to be about 6–7%.

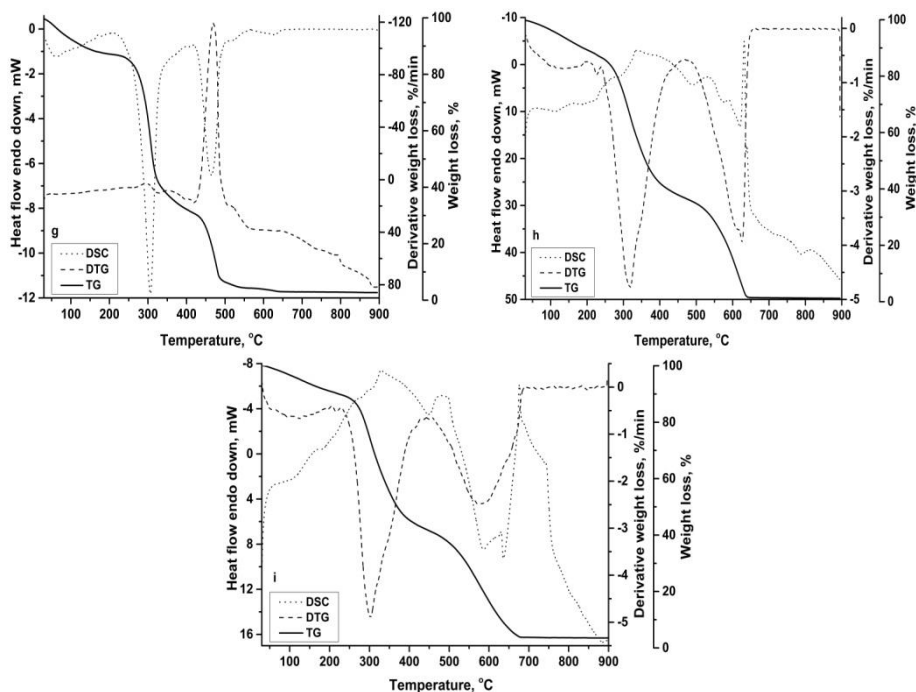


**Figure 15.** TG/DTG/DSC curves of: g – gum Arabic, h – parchment glue, i – fish glue

Fig. 15 shows the TG/DTG/DSC curves of gum Arabic, parchment and fish glue. In Fig. 15g the TG/DTG/DSC curves of gum Arabic are presented. Three main mass losses are visible in the TG curve. The first mass loss (10–15%) is due to the loss of adsorbed and structural water of gums and is observed between 30 and 200 °C. The second mass loss of about 50% at 250–350 °C is related to the decomposition of polysaccharide [97, 108]. The final mass loss (30%) in the temperature range of 400–600 °C could be associated with the thermal decomposition of intermediate residues formed in the carboxymethylated samples with inorganic compounds [109].

The thermal behaviour of parchment and fish glue is very similar during the heating procedure. The main reason for the different behaviour probably

lies in the different preparation methods, the natural aging process, and the presence of impurities.

DSC curve for parchment and fish glue shows a very small fraction of gelatinized collagen, first peak at 40–50 °C, thermal dehydration peak at about 140–200 °C, and a small fraction of crystalline collagen, peak three at 220–270 °C. Conformational changes of the collagen molecules form a triple helix structure to random coil. The broad endothermic peak two is mainly due to the moisture loss and fully overlaps the denaturation endotherm of fibrillar collagen [110, 111]. The mass loss is about 10–12%.

The main DTG peak can be attributed to the thermal decomposition of collagen between 270 and 530 °C. At temperature 300–315 °C are the first stage bulk degradation of dried collagen fibril. The mass loss is about 52%. The second observed peak is between 530–670 °C, which is related to the second stage of gelatin matrix degradation, and the decomposition of intermediate inorganic compounds. The last mass loss is about 36–38% [112–114].

### 3.2. Characterization of reconstructed historical red paints

In this part of the dissertation the results of the characterization of reconstructed analogous historical red pigments before and after artificial photochemical aging using colourimetric, SEM, FTIR, XRD, and TG/DTG/DSC analysis methods are presented.

#### 3.2.1. Colourimetric measurements

To investigate the colour stability, the artificial aging was initially performed on the reconstructed red paints with different binding media [95]. The colour changes are represented in Fig. 16 and Tables 4 and 5.

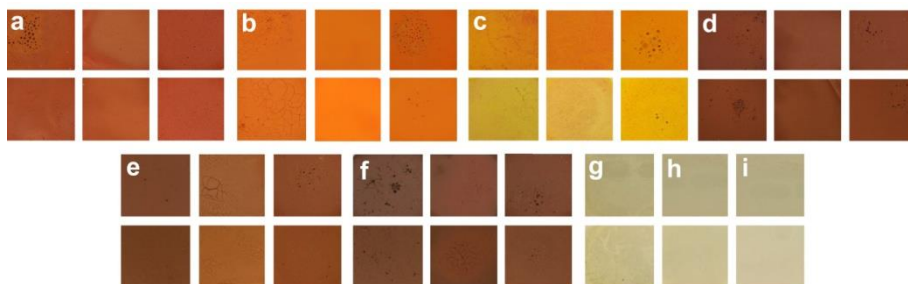


**Figure 16.** The digital images of reconstructed red paints: a – cinnabar, b – red lead, c – realgar, d – red ochre, e – red bolus, f – hematite with gum Arabic, parchment and fish glue (from left to right); and binding medias: g – gum Arabic, h – parchment glue and i – fish glue. Before (top) and after 35 days artificial aging (bottom).



**Table 4.** Determined  $\Delta E$  values for the reconstructed red paints after 35 days aging.

Pigment		Gum Arabic		Parchment glue		Fish glue	
		Before	After	Before	After	Before	After
Cinnabar	L*	52.6	50.7	65.9	65.1	56.1	53.2
	a*	37.8	36.2	39.8	38.7	42.2	38.5
	b*	31.5	30.5	32.9	31.5	32.8	27.7
	$\Delta E$	-	<b>2.7</b>	-	<b>2.0</b>	-	<b>6.9</b>
Red lead	L*	70.9	69.3	78.1	72.9	67.8	65.6
	a*	51.1	48.8	52.4	49.3	50.5	47.3
	b*	54.3	56.7	61.1	56.5	54.9	57.6
	$\Delta E$	-	<b>3.7</b>	-	<b>7.7</b>	-	<b>4.7</b>
Realgar	L*	74.6	75.4	75.5	83.7	72.9	73.5
	a*	42.9	16.1	43.6	15.9	40.7	20.9
	b*	57.8	43.3	55.4	25.5	62.8	59.7
	$\Delta E$	-	<b>30.4</b>	-	<b>41.5</b>	-	<b>20.0</b>
Red ochre	L*	43.0	40.8	50.3	45.4	50.1	43.7
	a*	32.9	30.2	30.7	27.4	32.8	28.9
	b*	22.6	20.8	21.4	20.0	24.1	20.6
	$\Delta E$	-	<b>4.5</b>	-	<b>6.2</b>	-	<b>8.3</b>
Red bolus	L*	39.6	34.8	58.4	52.6	51.6	50.0
	a*	25.1	21.4	28.3	25.3	29.0	24.8
	b*	20.9	15.7	26.0	19.9	24.3	19.2
	$\Delta E$	-	<b>8.0</b>	-	<b>8.9</b>	-	<b>8.7</b>
Hematite	L*	42.2	37.3	48.7	40.7	43.1	39.5
	a*	25.4	23.5	31.0	26.5	27.2	24.9
	b*	16.6	16.3	22.2	16.8	20.3	16.5
	$\Delta E$	-	<b>5.3</b>	-	<b>10.6</b>	-	<b>5.6</b>

**Table 5.** Determined  $\Delta E$  values for the binding media after 35 days aging.

	Gum Arabic		Parchment glue		Fish glue	
	Before	After	Before	After	Before	After
L*	73.1	66.8	75.2	62.3	73.6	69.7
a*	0.2	0.2	-0.2	-0.3	-0.4	-0.8
b*	2.0	4.3	0.0	3.0	-0.6	1.0
$\Delta E$	-	<b>6.7</b>	-	<b>13.2</b>	-	<b>4.2</b>

The colour difference  $\Delta E$  in the CIE(Lab)\* system of paints was calculated according to the formula (see Para. 2.4., Eq. 5). Each sample was photographed under the same lighting and at the same height from the sample to capture the appropriate colour. Since the binding media are transparent their photos were made using a white sheet of the paper base.

From the digital images, as we can see, the deep red colour change was observed in cinnabar (Fig. 16a). The colour difference is  $\leq 3$ , except for the cinnabar with the fish glue  $\Delta E$  value is 6.9 and the paint looks a bit brighter. Red lead pigment produced the paint with red-orange colour (Fig. 16b). A visual assessment of the colour of the pigment with different binders shows that the colours are very close with gum Arabic and fish glue. The more intensive colour before aging was of the paint obtained from red lead with parchment glue. After accelerated aging, the colour changed considerably. The colour difference  $\Delta E$  was 3.7 with gum Arabic, 4.7 with fish glue and 7.7 with parchment glue. The paint with gum Arabic was cracked after accelerated aging also showing a low adhesion of the paint to the surface. The same effect (lower adhesion and pigment „dusting“) was observed with the remaining binders. The colour of red lead with parchment glue has changed from red-orange to orange after accelerated aging. The biggest colour change determined from the digital images of paints was observed for realgar pigment based paints (Fig. 16c). The colour with different binders before aging was bright red-orange, and the paint did not crack. After accelerated aging the paint with gum Arabic was cracked, and the colour faded to a greenish tint with a colour difference of 30.4. The biggest colour change to beige was observed for the paint with parchment glue, and  $\Delta E$  was 41.5. The paint had a poor adhesion to the surface. The paint with fish glue changed the colour to brightly yellow. There was the pigment „dusting“ process, and the  $\Delta E$  was 20.0.

Visually, the paints fabricated using red ochre (Fig. 16d) exhibit deep red colour independent of the used binding media. After accelerated aging, the colour changed slightly,  $\Delta E$  was 4.5 with gum Arabic, 6.2 with parchment glue and a little bit more 8.3 with fish glue. However, the paints produced from red bolus (Fig. 16e) and parchment or fish glue have a slightly yellowish tint. The colour difference  $\Delta E$  was 8.0 with gum Arabic, 8.9 with parchment glue and 8.7 with fish glue. Red-brownish colour was observed for the paints prepared using hematite pigment (Fig. 16f). The colour difference  $\Delta E$  was almost the same with gum Arabic – 5.3 and the fish glue – 5.6. The biggest colour change was observed for the paint with parchment glue,  $\Delta E$  was 10.6.

Evidently, the colours of most of the paints have changed after artificial aging. The dependence of colour difference  $\Delta E$  on accelerated aging time for the parchment glue was mostly affected by artificial aging, while determined  $\Delta E$  for the fish glue and gum Arabic are negligible. The results of dependencies of colour differences  $\Delta E$  for different reconstructed paints on accelerated aging time, however, were distributed very widely. The results show that the colour changes during artificial aging are not distributed evenly and are dependent very much on individual composition. Note that a colour difference of  $\Delta E \leq 3$  is invisible to the human eye [115].

### 3.2.2. SEM analysis

SEM analysis was performed to evaluate the morphologic changes of the paint before and after accelerated aging. The SEM micrographs for different paints are presented in Fig. 17–22. The surface morphology of cinnabar paints is very similar independent of the binding media used. The surface is mostly composed of plate-like particles (see Fig. 17).

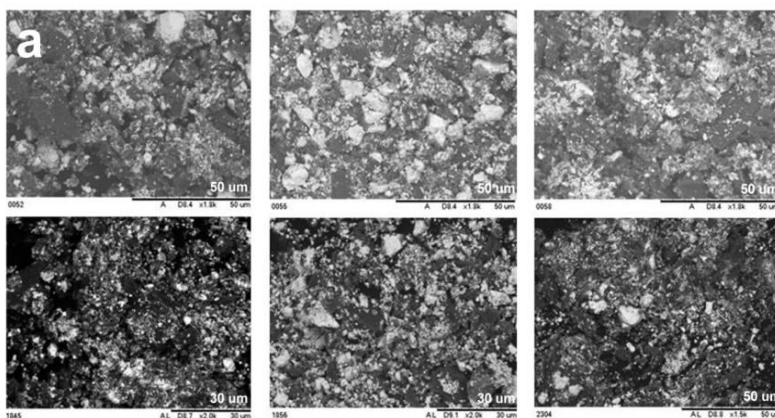


**Figure 17.** SEM micrographs of different paint composition of cinnabar (a) with (from left to right) gum Arabic, parchment and fish glue before (top) and after 35 days of accelerated aging (bottom)

The particle size of paint with gum Arabic and fish glue was almost unaffected by accelerated aging (1–15  $\mu\text{m}$  before and 1–10  $\mu\text{m}$  after aging with gum Arabic and 1–5  $\mu\text{m}$  before and after aging with fish glue). The biggest changes in particle size were determined by the paint of the cinnabar with parchment glue. The particle size varied from 1 to 15  $\mu\text{m}$  before aging and from 1 to 3  $\mu\text{m}$  after artificial aging.

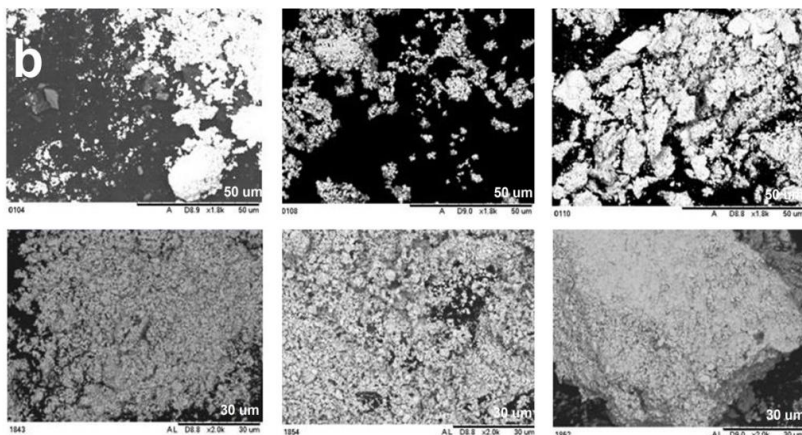


**Figure 18.** SEM micrographs of different paint composition of red lead (b) with (from left to right) gum Arabic, parchment and fish glue before (top) and after 35 days of accelerated aging (bottom)

The biggest changes of surface morphology before and after artificial aging were observed for the paints fabricated with red lead pigment (Fig. 18). The paints were composed of differently shaped particles with a size of 1–10 μm before aging. However, the particle size decreased significantly after accelerated aging. Moreover, these mostly spherically shaped particles showed a tendency to form hard agglomerates.

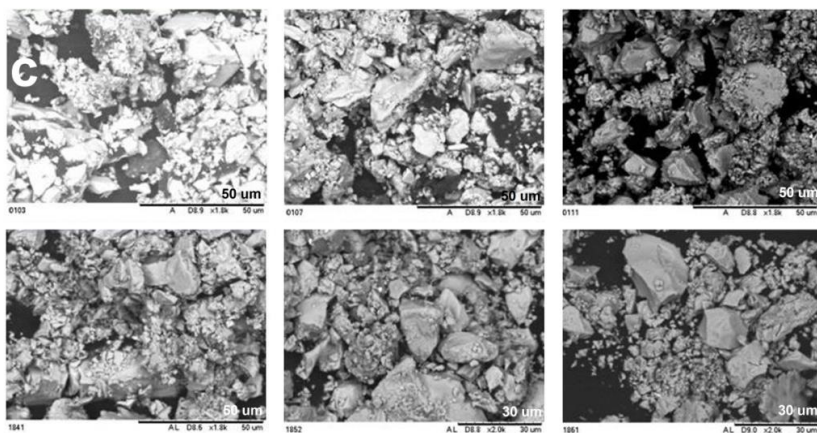


**Figure 19.** SEM micrographs of different paint composition of realgar (c) with (from left to right) gum Arabic, parchment and fish glue before (top) and after 35 days of accelerated aging (bottom)

The morphological features determined for the realgar paints were almost identical as for the case of cinnabar (see Fig. 19). Volumetric rectangular particles of 5–40  $\mu\text{m}$  in size have formed and no specific changes after aging were observed.

According to the SEM images (Fig. 20–22), the surface morphology of the red iron paints has changed significantly after 35 days of accelerated aging. The microstructure of three red paints containing the gum Arabic is quite different. Red bolus and hematite paints with gum Arabic are composed of different shape particles of about 10–20  $\mu\text{m}$  in size. However, the particles of red bolus show evident tendency to form agglomerates. On the other hand red ochre paint with gum Arabic is composed of smaller mostly spherical particles. It is clear that the particle size of all red paints with gum Arabic decreased to 3–10  $\mu\text{m}$  after aging for 35 days.

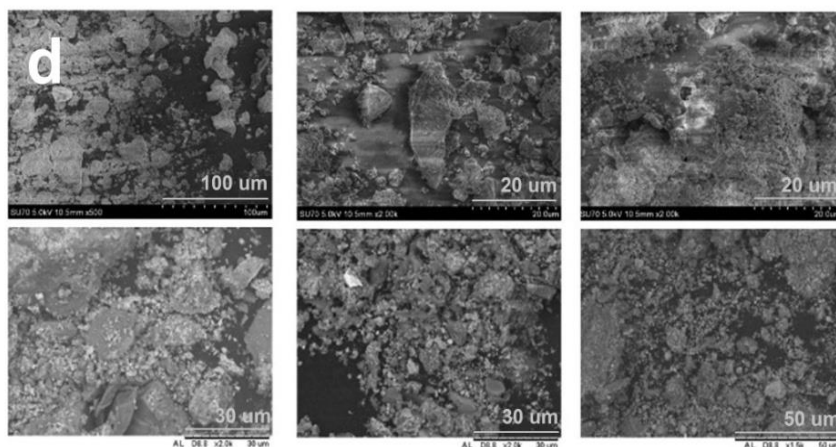


**Figure 20.** SEM micrographs of different paint composition of red ochre (d) with (from left to right) gum Arabic, parchment and fish glue before (top) and after 35 days of accelerated aging (bottom)

The microstructure of red paints fabricated with fish glue is also mostly determined by used pigment but not by binding media, which like parchment glue is a proteinaceous substance consisting of collagen. The SEM micrograph of composition of hematite and fish glue shows the presence of large microsized particles. When red bolus was used for the preparation of red paints with fish glue the distribution of smaller particles around the large ones is clearly seen. Again, the red ochre paint with fish glue is composed of smaller mostly spherical particles. After artificial aging the particle sizes reduced to approximately 10  $\mu\text{m}$  for all red iron paints obtained with fish glue.

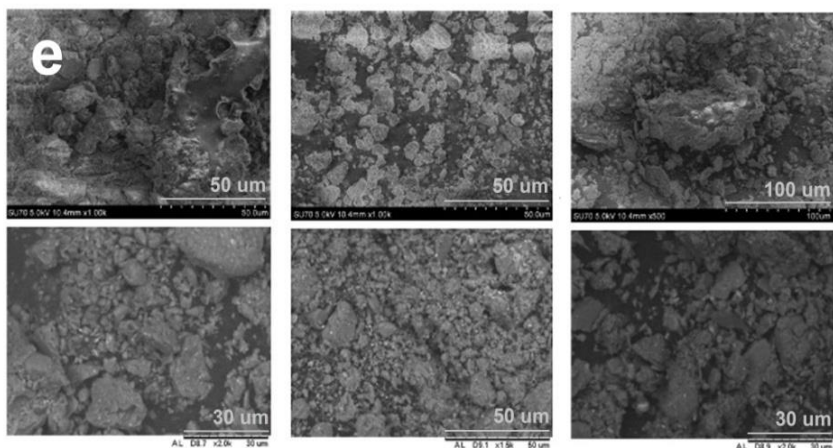


**Figure 21.** SEM micrographs of different paint composition of red bolus (e) with (from left to right) gum Arabic, parchment and fish glue before (top) and after 35 days of accelerated aging (bottom)

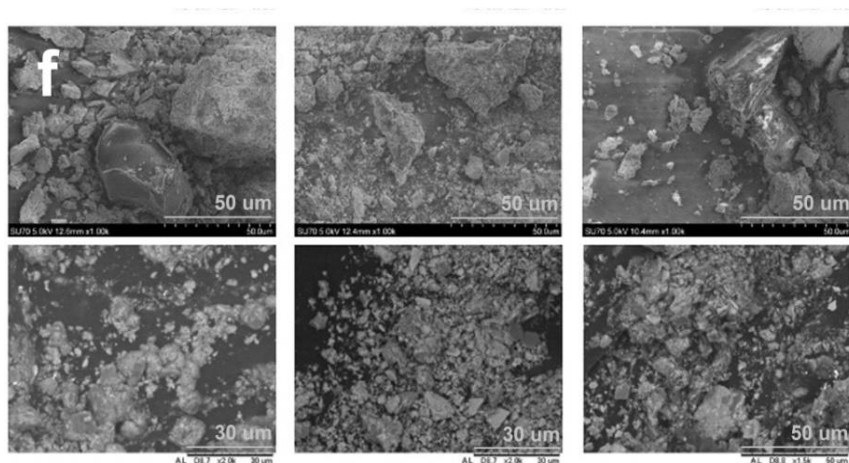


**Figure 22.** SEM micrographs of different paint composition of hematite (f) with (from left to right) gum Arabic, parchment and fish glue before (top) and after 35 days of accelerated aging (bottom)

The similar microstructure before and after aging was observed for the red iron paint samples fabricated with parchment glue.

In conclusion, the microstructure of red paints is mostly influenced by the nature of red pigment. In most of the cases the decrease of particle size of paint components was observed during the artificial aging.

### 3.2.3. FTIR analysis

FTIR spectroscopy has been used to understand better the colour change of paint during accelerated aging, providing additional information. The FTIR spectra of binding media before and after accelerated aging did not change, or changes were insignificant, so these results confirm that artificial aging does not destroy the chemical composition of gum Arabic, parchment and fish glue. The main vibrations could be attributable to the functional groups of binding media and acetic acid (see Fig. 23) [14, 18, 21].

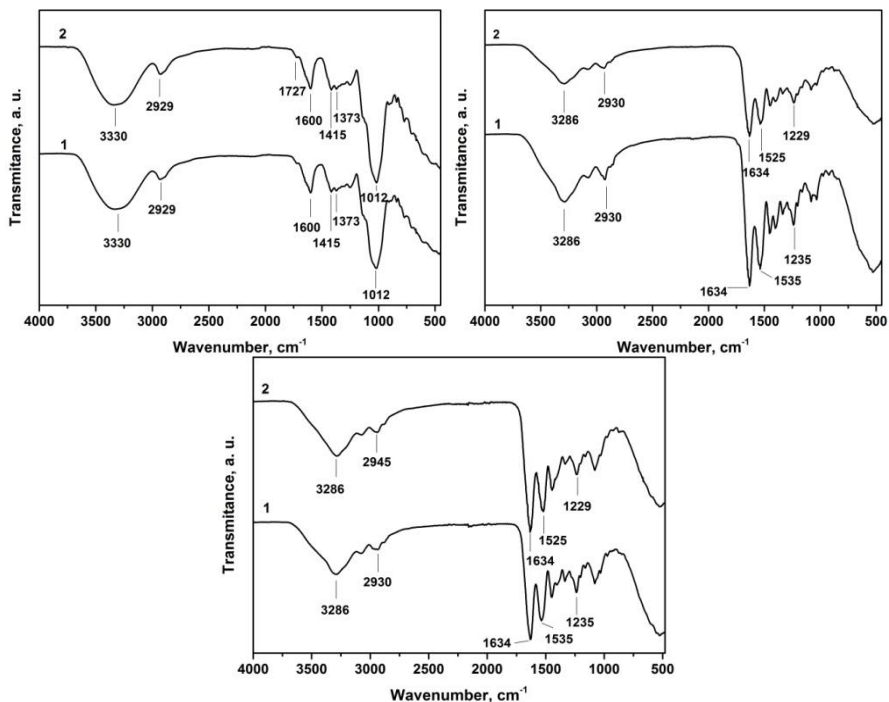


**Figure 23.** FTIR spectra of binding media with acetic acid before (1) and after (2) 35 days of accelerated aging: g – gum Arabic, h – parchment glue, i – fish glue

In the FTIR spectrum of gum Arabic, the intensive absorption bands at  $3300\text{ cm}^{-1}$  and  $1012\text{ cm}^{-1}$  are characteristic stretching vibrations of the O–H bond [116]. The band at  $2929\text{ cm}^{-1}$  is due to characteristic vibrations of C–H, indicating the presence of sugars, galactose, arabinose, and rhamnose. The absorption band at  $1600\text{ cm}^{-1}$  could be attributed to vibration of the characteristic bands of C=C stretch, amide NH bend,  $\text{NO}_2$  from both aliphatic and aromatic galacto proteins, and amino acids. The glucuronic acids have specific vibrations band at  $1415$  and  $1373\text{ cm}^{-1}$  due to C=O symmetric stretching and OH bending, respectively. The new absorption

band of low intensity was observed at  $1727\text{ cm}^{-1}$  after aging, which could be attributed to C=O stretching vibrations and representative of a partial hydrolysis of the polysaccharide units [97].

The FTIR spectra of parchment and fish glue are almost identical since the collagen is the main component of these materials. The assignment of absorption band visible at  $3286\text{ cm}^{-1}$  is the same as for gum Arabic. The bands detected at  $2930$  and  $2945\text{ cm}^{-1}$ , from  $1480$  to  $1300\text{ cm}^{-1}$  could be attributed to C–H vibrations. Absorption bands of amides coupled to C=O are seen at  $1634\text{ cm}^{-1}$  (amide I), at  $1535$  and  $1525\text{ cm}^{-1}$  (amide II) and at  $1235$ ,  $1229\text{ cm}^{-1}$  (amide III) [117]. Thus, the FTIR spectra of binding media samples qualitatively are the same before and after artificial aging. Just the intensity of some absorption bands is slightly different upon the aging of the specimens.

The representative absorption bands observed in the FTIR spectra of red paints with various compositions are represented in Fig. 24–29.

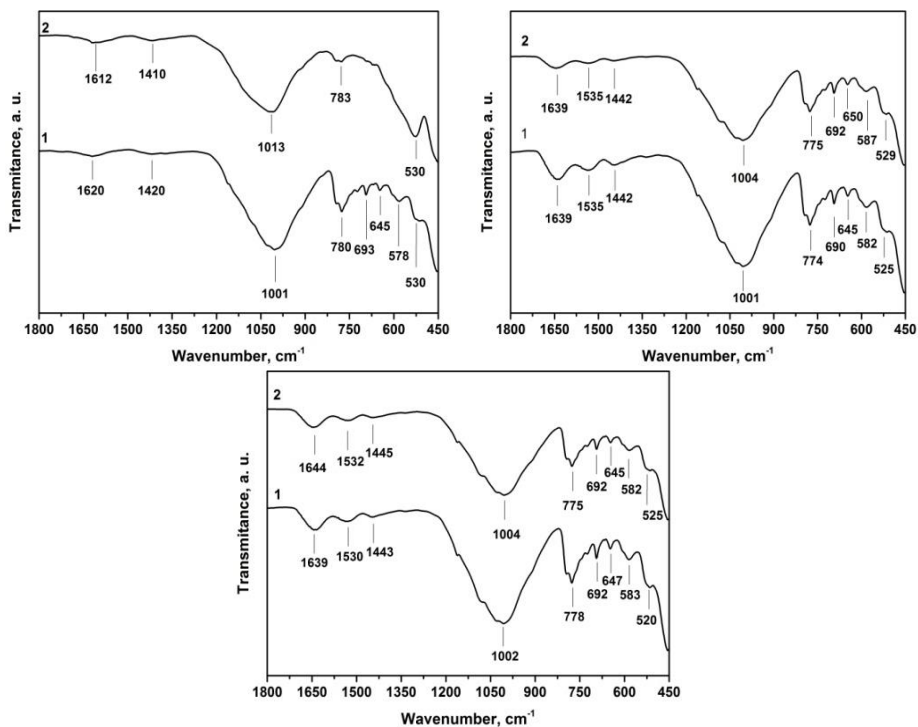


**Figure 24.** FTIR spectra of cinnabar with gum Arabic (top, left), parchment glue (top, right), and fish glue (bottom). Before (1) and after (2) 35 days of accelerated aging

The red pigment cinnabar does not absorb infrared radiation in a range of  $4000\text{--}350\text{ cm}^{-1}$  [14], however, an intensive absorption band at



1100–500  $\text{cm}^{-1}$  are presented in our investigated red paint: cinnabar fabricated with different binding media (Fig. 24). This band could be attributed to the characteristic vibration of Si–O bond confirming the presence of silica impurity in commercial cinnabar pigment. The absorption peaks determined at about 780–530  $\text{cm}^{-1}$  could be attributed to the Si–O–Al, Al–O, Al–O–Al vibrations. The binding media had no changes in the FTIR spectra.

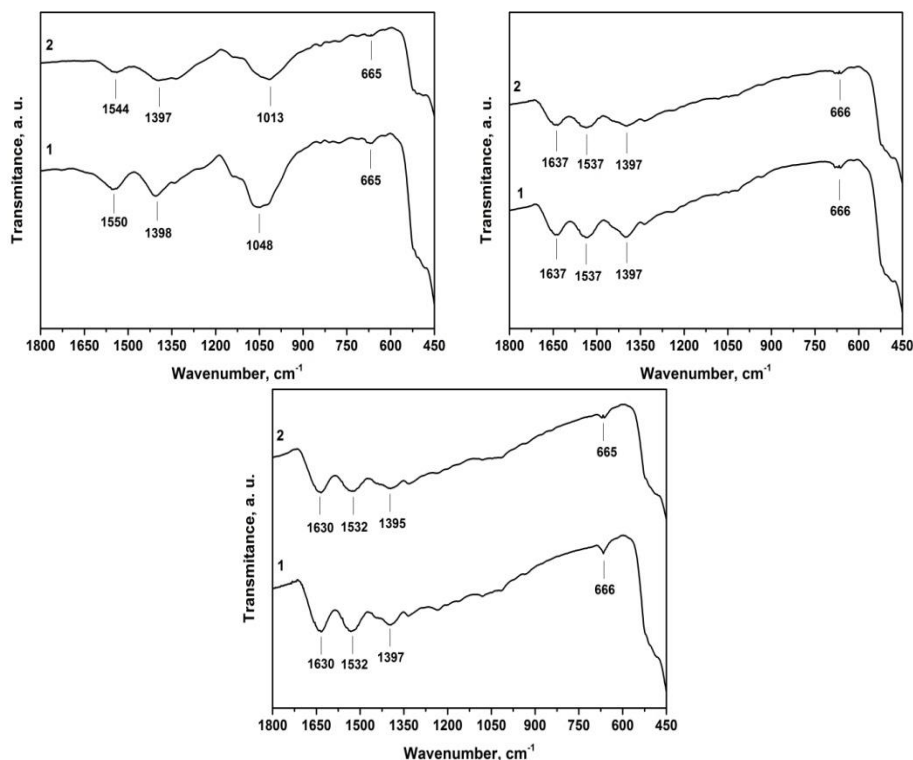


**Figure 25.** FTIR spectra of red lead with gum Arabic (top, left), parchment glue (top, right), and fish glue (bottom). Before (1) and after (2) 35 days of accelerated aging

Red lead has infrared absorption bands in low frequency regions of 680–531  $\text{cm}^{-1}$  and one band at 1398–1390  $\text{cm}^{-1}$  which is characteristic of lead oxide [14]. New peaks in the red lead paint with different binders (Fig. 25) are not seen after accelerated aging, only small shifts in the paint with gum Arabic, which is related to displacement of C–H band from polysaccharides at 1050–1010  $\text{cm}^{-1}$ .

Before accelerated aging, no bands other than the binding media were detected in the FTIR spectra of realgar paint (Fig. 26). After accelerated aging, the realgar paint with gum Arabic showed a new peaks at 1724  $\text{cm}^{-1}$

and very insignificant at about 790 and 480  $\text{cm}^{-1}$ . The new absorption band at 1724  $\text{cm}^{-1}$  could be attributed to C=O stretching vibrations and representative of a partial hydrolysis of the polysaccharide units [118, 119].

Three new peaks were noticed in the paint with parchment and fish glue at about 1040, 790 and 480  $\text{cm}^{-1}$ . The first peak is attributed to C-O stretching vibration of the carbohydrate residues in collagen and the second group to a specific As-O vibration band, which could be linked to the paint discolouration. Arsenic trioxide and various sulphate compounds are expected to be formed as degradation products for all the arsenic sulphide pigments. Aging of arsenic sulphide containing painting systems often leads to whitening or increased transparency due to the formation of water-soluble white arsenic trioxide and/or arsenate species plane movements [120]. The origin of the main band detected at 478  $\text{cm}^{-1}$  is related to the As-S vibration [121, 122].

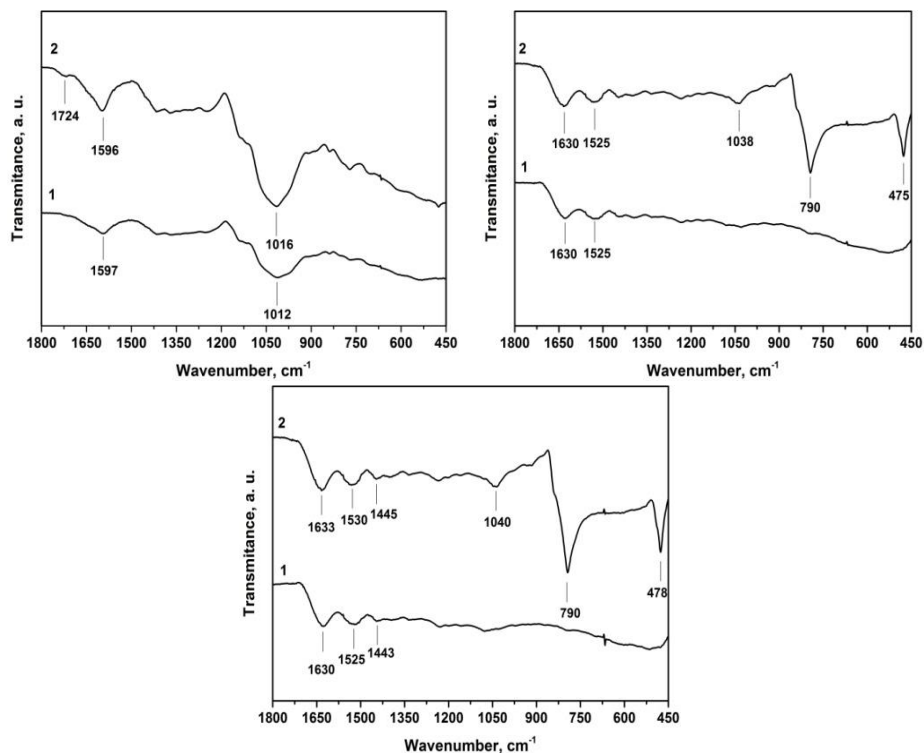


**Figure 26.** FTIR spectra of realgar with gum Arabic (top, left), parchment glue (top, right), and fish glue (bottom). Before (1) and after (2) 35 days of accelerated aging

Figure 27 shows the FTIR spectra of red ochre with different binding media. Before and after accelerated aging, no bands other than the binding

media, Si–O–Al at about  $790\text{ cm}^{-1}$ , and the Fe–O vibrations in iron oxide at  $531\text{ cm}^{-1}$  were detected in the FTIR spectra.

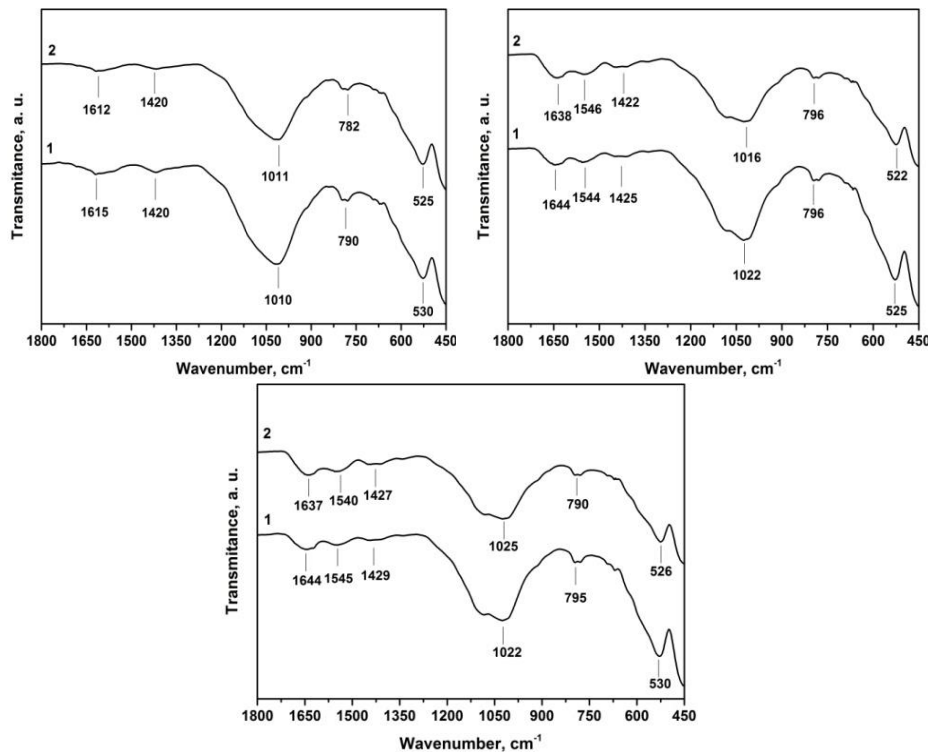


**Figure 27.** FTIR spectra of red ochre with gum Arabic (top, left), parchment glue (top, right), and fish glue (bottom). Before (1) and after (2) 35 days of accelerated aging

The FTIR spectrum of the red paint fabricated from pigment red bolus with different binding media represents all absorption bands characteristic to gum Arabic, parchment and fish glue (Fig. 28). Additional bands for kaolin ( $\text{Al}_2\text{Si}_2\text{O}_5(\text{OH})_4$ ) are observed too.

The asymmetric Si–O–Si stretching band and Si–O stretching bands are visible at  $1000\text{ cm}^{-1}$  and  $908\text{ cm}^{-1}$ , respectively. The absorption bands determined at  $795$  and  $690\text{ cm}^{-1}$  are due to Si–O–Al vibrations, and the origin of absorption at  $525\text{ cm}^{-1}$  is Fe–O vibrations.

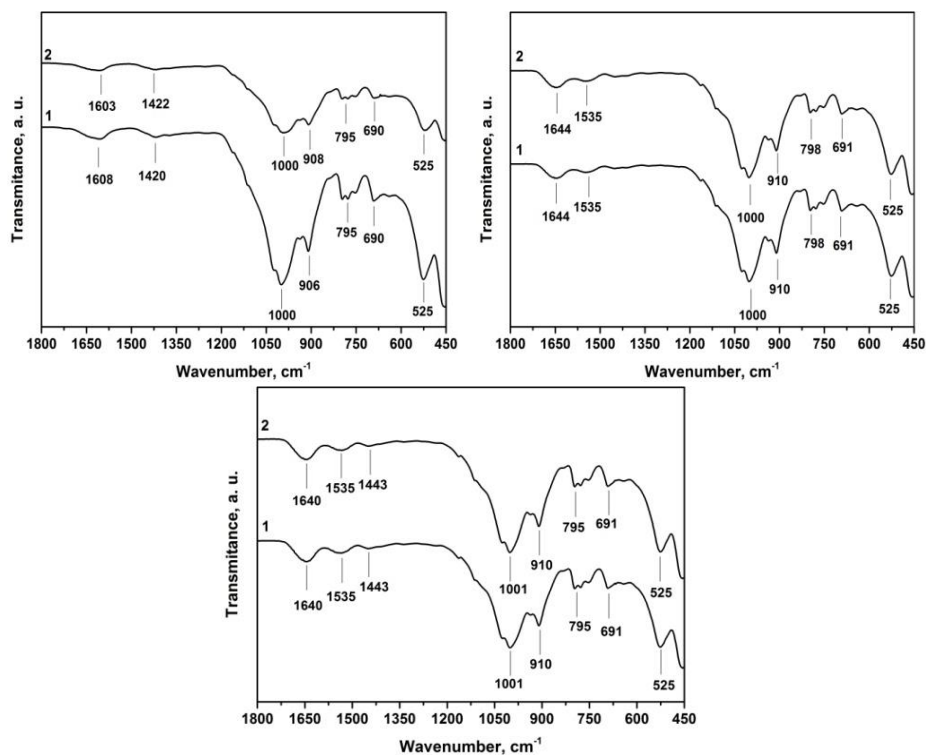


**Figure 28.** FTIR spectra of red bolus with gum Arabic (top, left), parchment glue (top, right), and fish glue (bottom). Before (1) and after (2) 35 days of accelerated aging

The FTIR spectrum of the hematite paints (Fig. 29) with different binding media also shows the characteristic absorption bands of iron oxide at about  $520\text{ cm}^{-1}$ . The absorption bands at  $1435\text{ cm}^{-1}$  and  $872\text{ cm}^{-1}$  are due to vibrations in ionic carbonate ( $\text{CO}_3^{2-}$ ). Again, the absorption band at  $1017\text{ cm}^{-1}$  could be identified as asymmetric Si–O–Si stretching band, at  $795\text{ cm}^{-1}$  are due to Si–O–Al vibrations [14]. Other absorption bands are due to binding media.

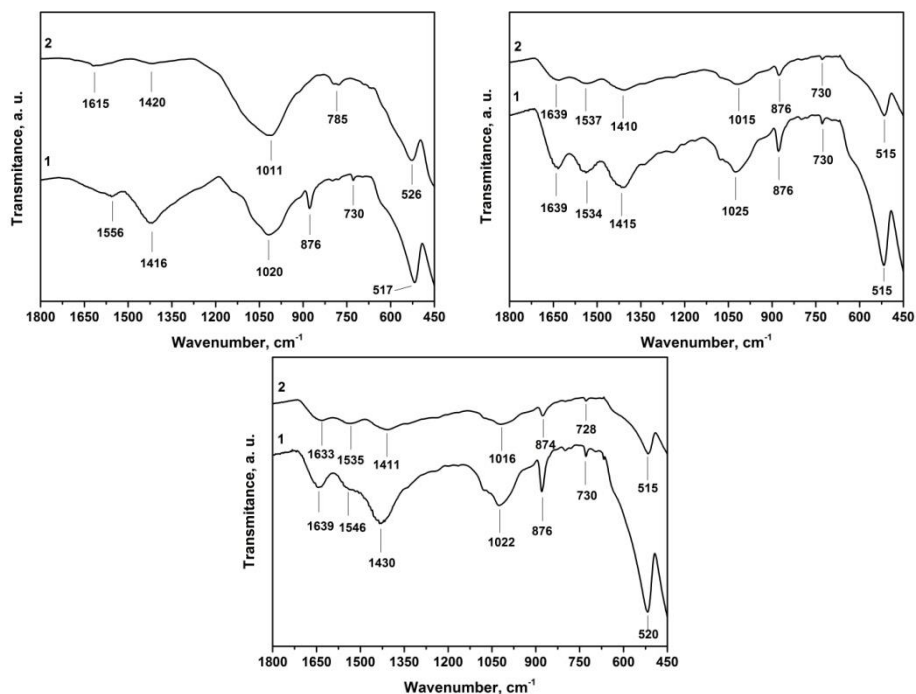


**Figure 29.** FTIR spectra of hematite with gum Arabic (top, left), parchment glue (top, right), and fish glue (bottom). Before (1) and after (2) 35 days of accelerated aging

According to the FTIR spectroscopy results, artificial aging had no deleterious effect on the fabricated red iron paints. The biggest changes are visible at realgar paint with all binding media, and insignificant at cinnabar and red lead paint.

### 3.2.4. XRD analysis

The XRD analysis of reconstructed red paints and binding media before and after artificial aging was also performed. XRD patterns of gum Arabic, parchment glue, and fish glue with acetic acid as was expected, these materials are mostly amorphous but crystalline phases could be detected (Fig. 30) [99–101].

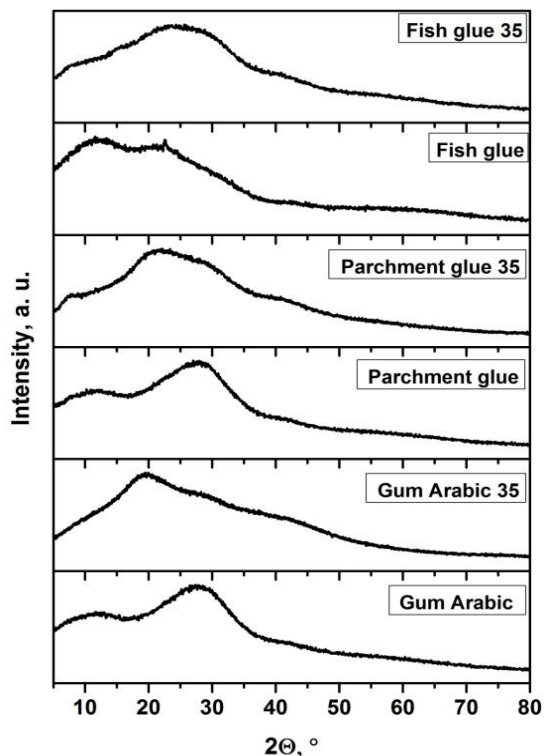


**Figure 30.** XRD patterns of gum Arabic, parchment glue and fish glue with acetic acid before and after accelerated aging for 35 days

The only one diffraction peak of low intensity at around  $2\theta = 23.5^\circ$  could be detected in the XRD pattern of fish glue. The exact origin of this diffraction line is unknown. Interestingly, this peak disappeared after artificial aging of material for 35 days. The XRD patterns of binding media samples before and after 35 days of accelerated aging are just slightly different with small shifts of amorphous bumps to various directions.

The XRD patterns of all compositions of red paints are represented in Fig. 31–36.

The XRD patterns of cinnabar with different binders (Fig. 31) showed the diffraction peaks attributable to the main HgS crystalline phase (PDF 96-901-2083). Also, the XRD patterns contain an additional SiO<sub>2</sub> phase (PDF 00-078-1253) at  $2\theta = 26.60^\circ$ ,  $36.55^\circ$ ,  $37.68^\circ$ ,  $45.68^\circ$  and  $59.84^\circ$  and the crystalline Al<sub>2</sub>Si<sub>2</sub>O<sub>5</sub>(OH)<sub>4</sub> phase (PDF 00-075-1593) at  $2\theta = 20.34^\circ$ . The characteristic peaks of gum Arabic were not detected in the XRD patterns before and after 35 days of accelerated aging. In the cinnabar paints with parchment and fish glue were detected at small peaks at  $2\theta = 7^\circ$  before aging

and only in fish glue after 35 days accelerating aging, which belongs to the equatorial peak of collagen [100, 101].

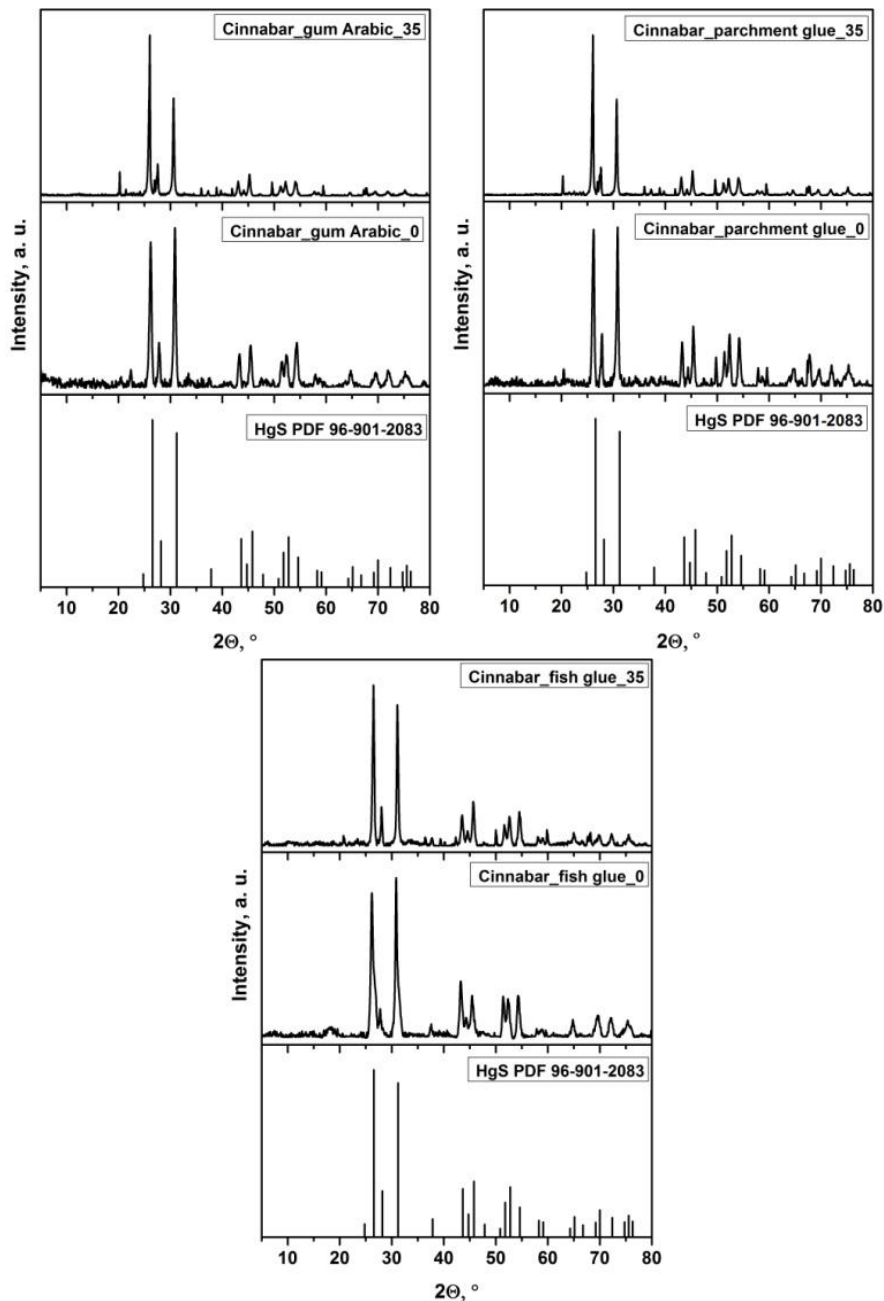


**Figure 31.** XRD patterns of cinnabar with gum Arabic (top left), parchment glue (top right) and fish glue (bottom) before and after accelerated aging for 35 days

According to the XRD analysis data, the paint of red lead with different binding media consists only of  $\text{Pb}_3\text{O}_4$  (PDF 00-041-1493) (see Fig. 32). However, in the XRD patterns of red lead with fish glue and parchment glue diffraction lines at  $2\theta = 17.69^\circ$  and at  $2\theta = 50$  to  $60^\circ$  were determined showing the possible formation of  $\text{PbO}$  after aging.

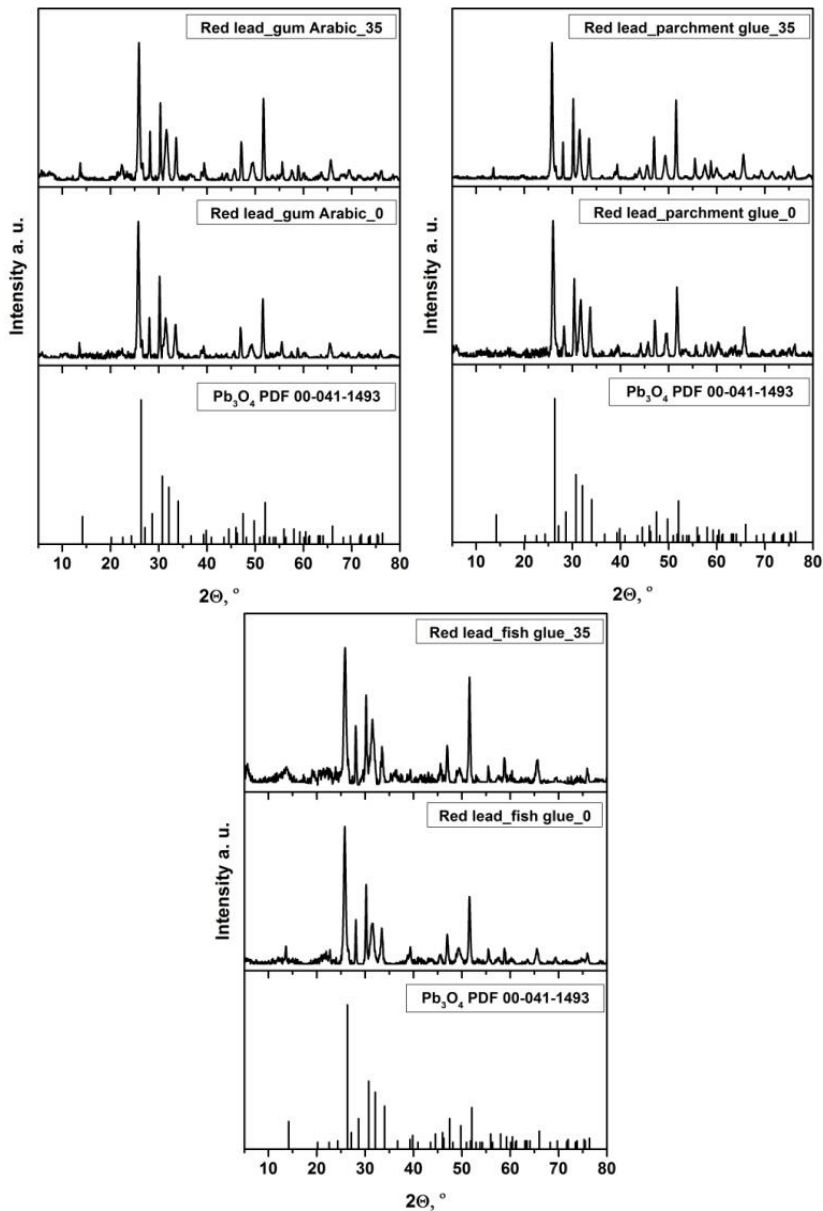


**Figure 32.** XRD patterns of red lead with gum Arabic (top left), parchment glue (top right) and fish glue (bottom) before and after accelerated aging for 35 days



The characteristic diffraction peaks of collagen were observed only in the XRD patterns of red lead paints with fish glue. The characteristic peaks of other binders were not detected in the XRD patterns of these paints.

The XRD patterns of red paints with realgar were quite different before and after artificial aging (see Fig. 33). Realgar, which is a red mineral,  $\text{As}_4\text{S}_4$ , partially transforms in arsenolite (white powder,  $\text{As}_2\text{O}_3$ ) and pararealgar (yellow,  $\text{As}_4\text{S}_4$ ) and the  $\chi$ -phase ( $\text{As}_4\text{S}_5$ ) when exposed to light. Pararealgar has the same formula as realgar, and is characterized as having a different structural arrangement of sulphur and arsenic atoms. At the end of the process,  $\text{As}_4\text{S}_5$  coexists with pararealgar, and the colour of pigment turns from red-orange to yellow [66].

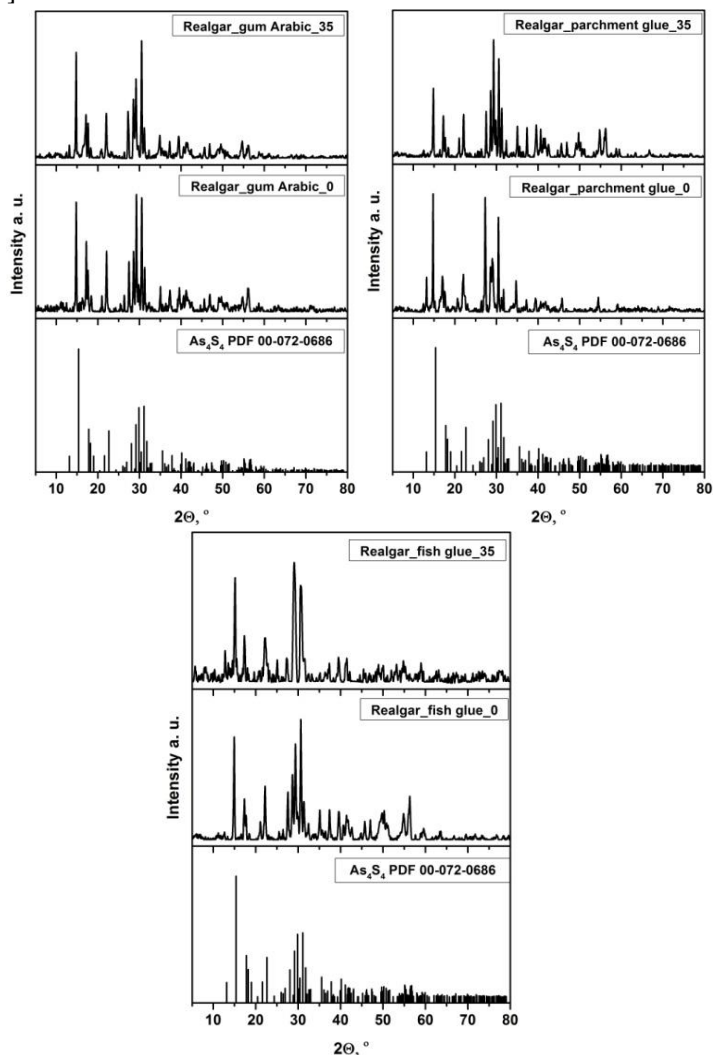


**Figure 33.** XRD patterns of realgar with gum Arabic (top left), parchment glue (top right) and fish glue (bottom) before and after accelerated aging for 35 days

In the XRD pattern of realgar paints, after aging the diffraction peaks attributed to arsenolite and pararealgar were detected. The XRD patterns of realgar paints with gum Arabic and with fish glue have diffraction lines at  $2\theta = 8.99$  and  $12.85^\circ$  from pararealgar, and  $2\theta = 13.62$  and  $25.13^\circ$  from arsenolite. The XRD patterns of realgar paint with parchment glue also have diffraction lines attributable to the pararealgar and arsenolite phase. The binding media diffraction peaks were detected only in realgar paint with fish glue, at  $2\theta = 7$  and  $23^\circ$  after aging [100, 101].

The XRD patterns of all compositions of red iron paints were without any big differences after aging. The red ochre paint with different binding media was shown in Fig. 34.

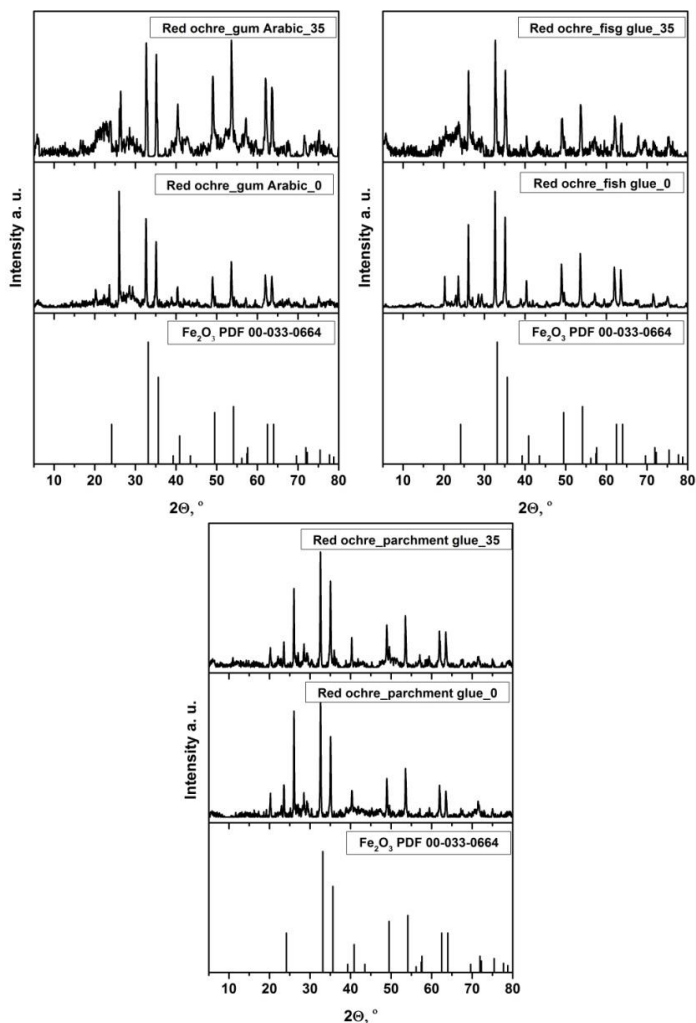


**Figure 34.** XRD patterns of red ochre with gum Arabic (top left), parchment glue (top right) and fish glue (bottom) before and after accelerated aging for 35 days

The main crystalline phase of the red ochre paint is  $\text{Fe}_2\text{O}_3$  (PDF 00-033-0664), but additional crystalline  $\text{Al}_2\text{Si}_2\text{O}_5(\text{OH})_4$  phase at  $2\theta = 12.33^\circ$ ,  $20.98^\circ$ ,  $68.29^\circ$  and an impurity of  $\text{SiO}_2$  phase at  $2\theta = 26.60^\circ$ ,  $36.37^\circ$ ,  $37.68^\circ$ ,  $45.68^\circ$ ,  $59.84^\circ$  are also present in the paint. The binding media diffraction peaks were detected in all paints before and after aging at  $2\theta = 18^\circ$  with gum Arabic,  $2\theta = 7^\circ$  with parchment glue, and  $2\theta = 7$  and  $\sim 23^\circ$  with fish glue.

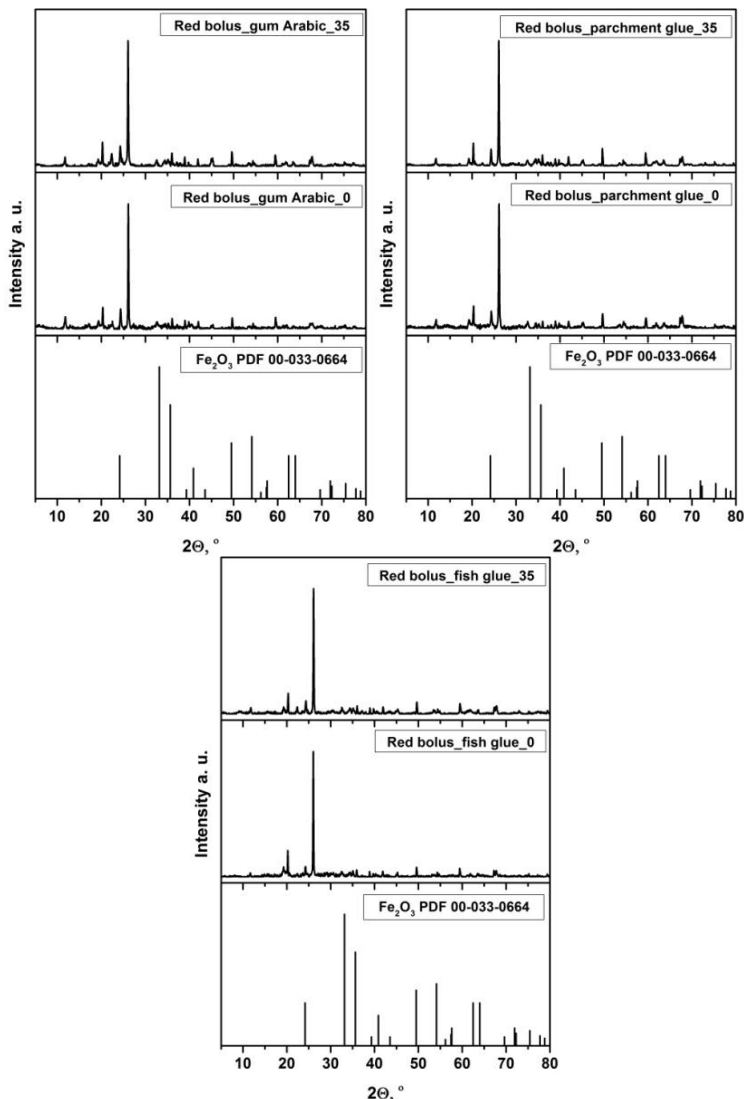


**Figure 35.** XRD patterns of red bolus with gum Arabic (top left), parchment glue (top right) and fish glue (bottom) before and after accelerated aging for 35 days

The XRD patterns of all compositions of red bolus paints were also almost identical before and after aging (Fig. 35). Additionally, the paints of red bolus contain three  $\text{Fe}_2\text{O}_3$ ,  $\text{SiO}_2$ , and  $\text{Al}_2\text{Si}_2\text{O}_5(\text{OH})_4$  crystalline phases.

The XRD patterns recorded for the hematite paint with parchment glue before and after aging were almost identical. However, the phase compositions of hematite with fish glue and gum Arabic were slightly different after artificial aging (see Fig. 36).

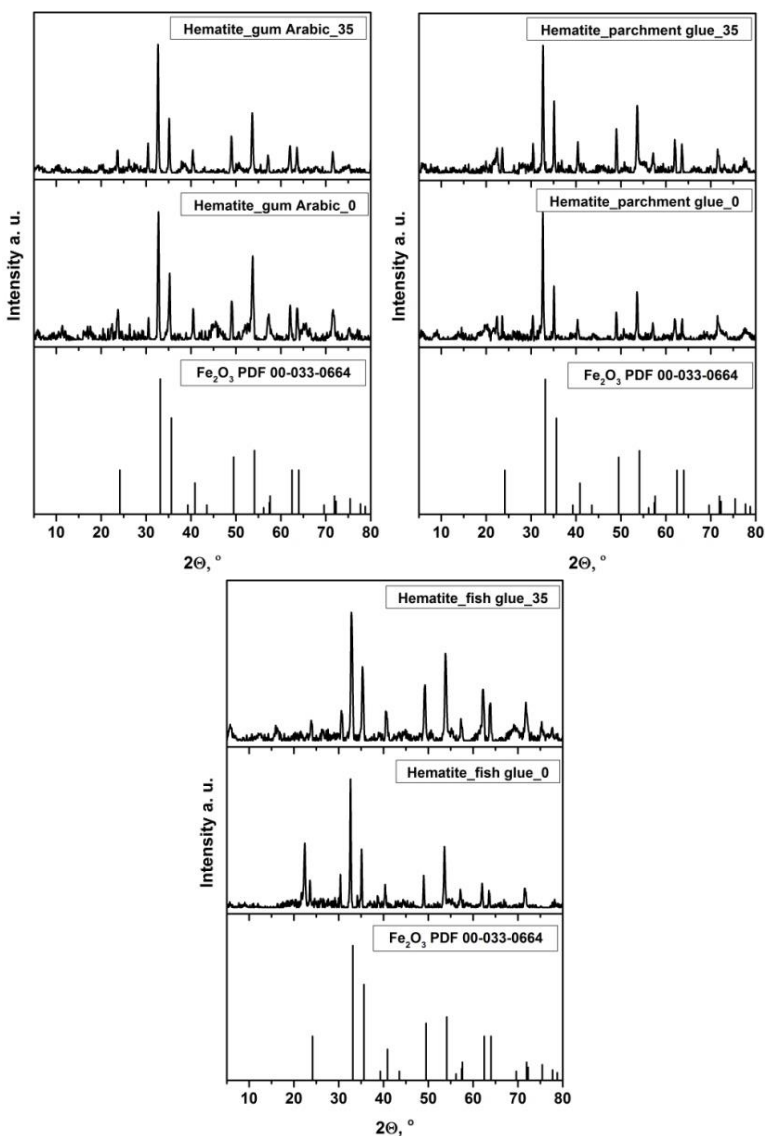


**Figure 36.** XRD patterns of hematite with gum Arabic (top left), parchment glue (top right) and fish glue (bottom) before and after accelerated aging for 35 days

As seen, the paints of hematite also contain diffraction peaks attributable to the impurity of  $\text{SiO}_2$  phase at  $2\theta = 30.74^\circ$  and to  $\text{CaCO}_3$  phase at  $2\theta = 29.64^\circ$ .  $\text{CaCO}_3$  phase is lower after aging. Moreover, the diffraction peak at around  $2\theta = 23.5^\circ$  visible in the XRD pattern of hematite paint with fish glue is not detectable already after artificial aging. This peak probably originates from fish glue. Also, a small diffraction line located at about  $2\theta = 34.5^\circ$  in the XRD pattern of hematite paint with fish glue is not visible anymore after aging. Small changes in the XRD patterns upon aging could be determined in the range of  $2\theta = 44\text{--}46^\circ$  for the hematite and gum Arabic system.

### 3.2.5. TG/DTG/DSC analysis

Thermal analysis is suitable for the investigation of stability of biological macromolecules presented with gum Arabic, parchment and fish glue (polysaccharide and collagen). It was reported that this method is useful to detect the changes in the biomaterials, such as protein denaturation and aggregation, and degradation during thermal treatment [123]. Fig. 37 shows the TG/DTG/DSC curves of binding media before and after artificial aging of 35 days.

Multistep decomposition with several mass losses could be determined from the TG curve of the gum Arabic. The first mass loss ( $\sim 11\%$ ) observed in the temperature range of  $30\text{--}250^\circ\text{C}$  is due to the loss of adsorbed and structural water of gums. The next mass losses of about  $89\%$  at the temperatures  $250\text{--}450^\circ\text{C}$ ,  $450\text{--}480^\circ\text{C}$ ,  $480\text{--}560^\circ\text{C}$ ,  $560\text{--}660^\circ\text{C}$  is related to the decomposition of polysaccharide and could be also associated with thermal decomposition of intermediate residues formed in carboxymethylated samples with inorganic compounds [97, 108, 109]. As seen, the total mass loss for gum Arabic aged for 35 days is also about  $100\%$ . TG/DTG/DSC curves are relevant and without major changes before and after artificial aging.

The thermal behaviour of parchment and fish glues is very similar and proceeds via three main decomposition steps. The total mass loss of  $100\%$  was determined for both specimens, however, the full combustion of the fish glue reaches at about  $680^\circ\text{C}$  and the full decomposition of parchment glue could be achieved at a lower temperature ( $\sim 630^\circ\text{C}$ ). The initial mass loss of these glues (up to  $200^\circ\text{C}$ ) is associated with broad endotherms and could be attributed to the evaporation of moisture, so-called structurally bound water, and decomposition of hydroxyl groups present in the collagen molecule.

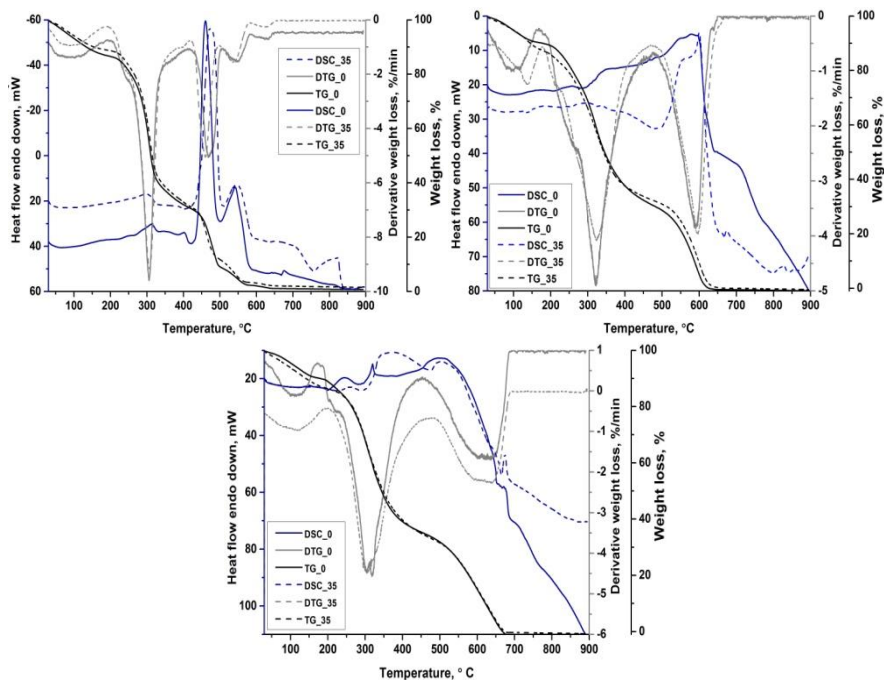


**Figure 37.** TG/DTG/DSC curves of binding media before and after artificial aging of 35 days: gum Arabic (top left), parchment glue (top right) and fish glue (bottom)

Conformational changes of the collagen molecules form a triple helix structure to a random coil [110, 111]. The mass loss is about 10%. The main DTG peak can be attributed to the thermal decomposition of collagen between 200 and 470 °C, this is a lower temperature range, compared with the single material [113]. At temperatures, 300–310 °C are the first stage bulk degradation of the dried collagen fibril. The mass loss is about 60%. The second observed peaks are between 500–670 °C in parchment glue and between 450–680 °C in fish glue, which is related to the second stage of gelatin matrix degradation, and the decomposition of intermediate inorganic compounds. The last mass loss is about 30% [112–114]. As in the gum Arabic samples, these also did not show changes before and after artificial aging.

The TG/DTG/DSC curves of cinnabar paints in all compositions are very similar (Fig. 38). The first mass loss (~ 3 and ~ 1% before and after aging, respectively) observed in a temperature range of 30–250 °C is due to the loss of adsorbed and structural water of gums. The second mass loss of about 12% before and 14% after aging observed at 260–350 °C is related to the decomposition of polysaccharide. The third mass loss before aging is 24%, and after aging 22% is related to structural changes of cinnabar in a

temperature range of 350–410 °C. The hexagonal red mercury sulphide  $\alpha$ -HgS rearranges to the black mercury sulphide  $\beta$ -HgS having a cubic crystal structure in this temperature interval. Also, thermal transformation are related to the presence of O<sub>2</sub> in the chamber, where HgS decomposes to HgO, SO<sub>2</sub> and HgSO<sub>3</sub> [102, 103].

The fourth mass loss ~ 1%, in the temperature range of 500–600 °C is related to the metacinnabar  $\beta$ -HgS transformation to hypercinnabar  $\gamma$ -HgS, or decomposition of intermediates, such as HgO, HgSO<sub>4</sub> in air [28, 45, 48, 102].

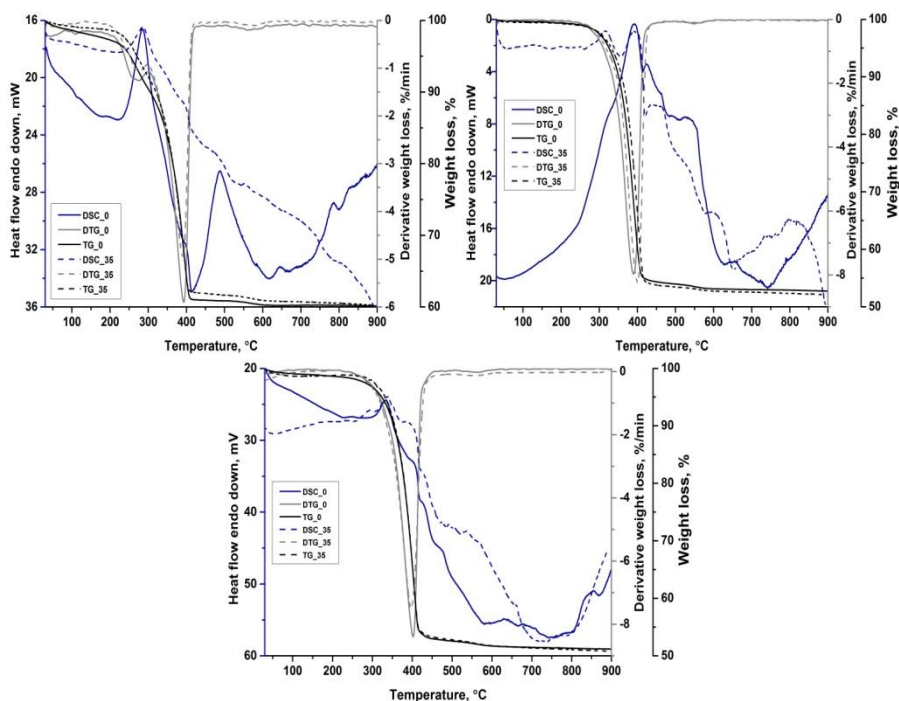


**Figure 38.** TG/DTG/DSC curves of cinnabar before and after artificial aging of 35 days: with gum Arabic (top left), parchment glue (top right) and fish glue (bottom)

Cinnabar with parchment and fish glues before and after artificial aging are very similar and have three decomposition steps. The first one is very insignificant, from 30 to 250 °C, and total mass loss is about 1%. The second one and the main are from 280 to 450 °C, total mass loss is about 45–47%, and the last, ~ 1% mass loss in the temperature range of 450–570 °C. The main TG/DTG/DSC curves are related to HgS transformation and thermal behaviour of parchment and fish glues are not seen.

Figure 39 shows the TG/DTG/DSC curves of red lead paints reconstructed with the gum Arabic, parchment and fish glues. The main weight losses could be explained in the same manner as in the case of cinnabar paint. However, for the red lead paints a negligible weight gain is seen in a temperature range of 450–550°C. This is related to the reversible oxidation–reduction process.

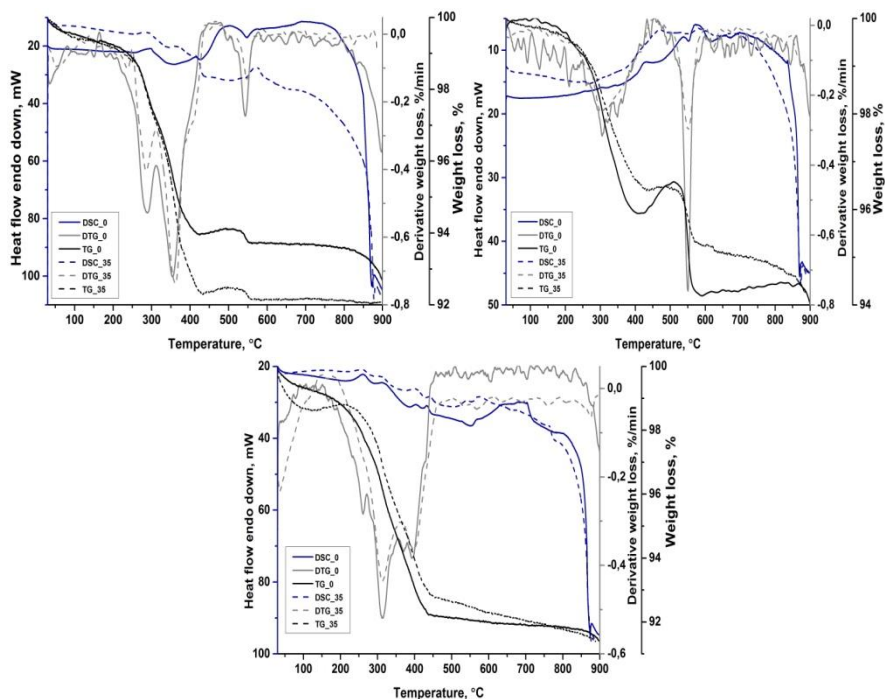


**Figure 39.** TG/DTG/DSC curves of red lead before and after artificial aging of 35 days: with gum Arabic (top left), parchment glue (top right) and fish glue (bottom)

Red lead forms through an oxidation process when  $\alpha$ -PbO is heated to around 450–500 °C, but decomposes at atmospheric pressure to yellow litharge ( $\beta$ -PbO, orthorhombic) when temperature exceeds 585 °C [70]. The mass loss during the decomposition of  $\text{Pb}_3\text{O}_4$  to the PbO process was determined about 1–2% in gum Arabic and parchment glue. The sample with fish glue shows a very weak DSC peak at 560 °C. In all cases, total mass loss is about 6–8%.

The realgar paint with different binding media is shown in Fig. 40. At about 250 °C temperature, under normal pressure, realgar transforms to the pararealgar ( $\text{As}_4\text{S}_4$ ) phase, which was detected in the paints after aging by XRD analysis. Pararealgar melts at about 310 °C temperature, which is



supported by endotherms visible in the DSC curves. Next, in a range of about 350–430 °C the transformation of pararealgar to arsenolite takes place. And finally, the material formed starts to evaporate in a temperature range of 430–530 °C as an endothermic process [104].

The DTG curves in realgar paint with parchment and fish glue after aging are shifted toward lower temperatures at about 20–50 °C, which are good correlates with other analysis methods, where the most noticeable degradation process was confirmed.

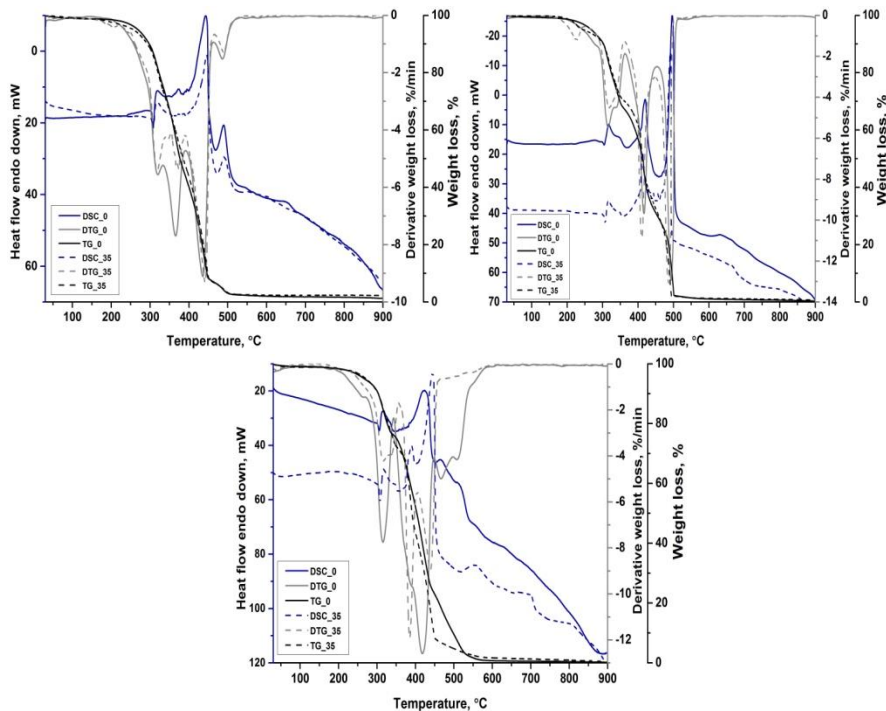


**Figure 40.** TG/DTG/DSC curves of realgar before and after artificial aging of 35 days: with gum Arabic (top left), parchment glue (top right) and fish glue (bottom)

The TG/DTG/DSC curves of fabricated red ochre, red bolus and hematite paints with selected binding media are presented in Fig. 41–43. Differences in the thermal analysis curves are insignificant. The differences are mainly due to the presence of impurities. The red ochre and red bolus contain the  $\text{Al}_2\text{Si}_2\text{O}_5(\text{OH})_4$  impurity phase which decomposes monotonically by heating the sample up to 650–800 °C. Hematite also contains calcium carbonate according to the FTIR results, which decomposes between 600 and 750 °C [105].

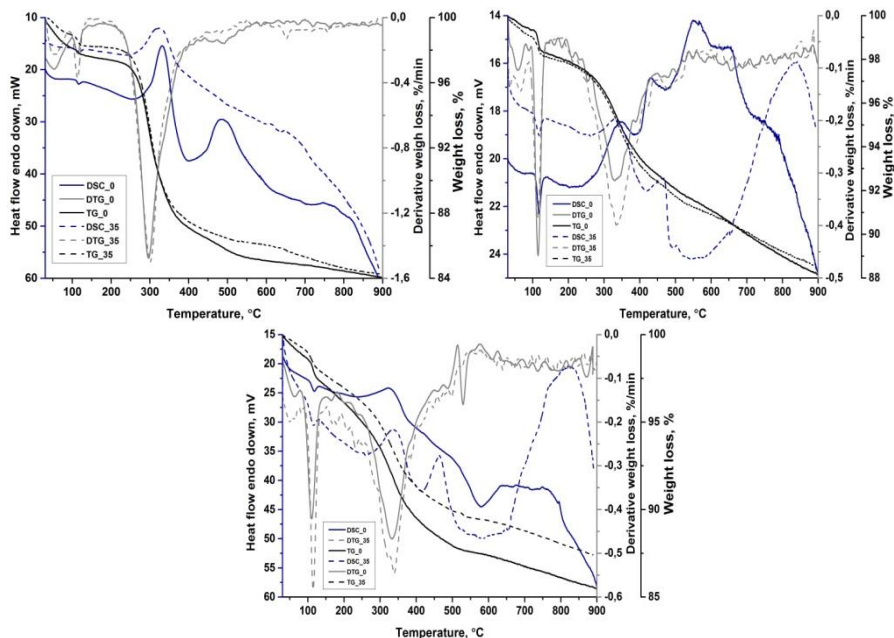


**Figure 41.** TG/DTG/DSC curves of red ochre before and after artificial aging of 35 days: with gum Arabic (top left), parchment glue (top right) and fish glue (bottom)

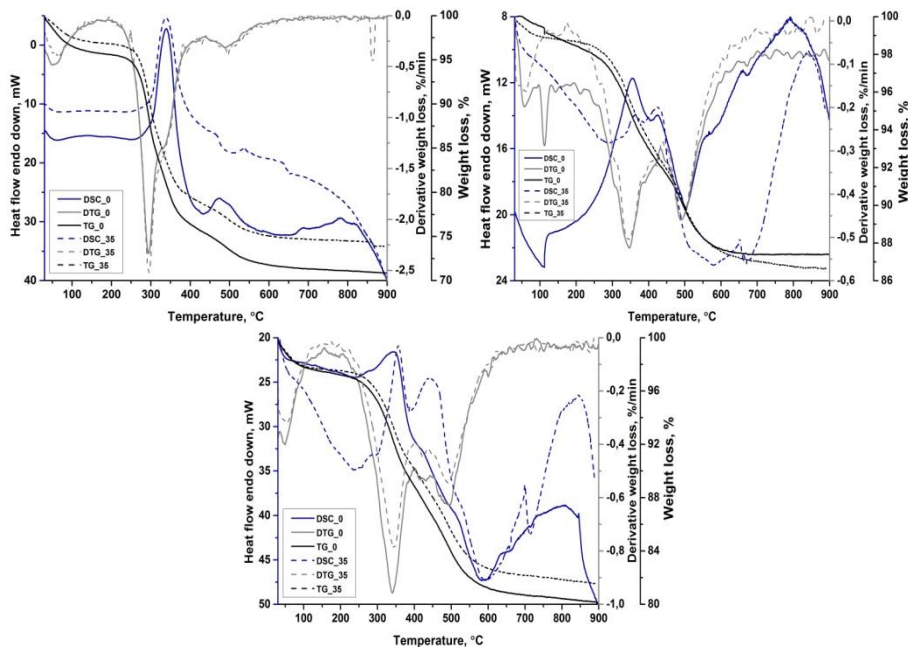


**Figure 42.** TG/DTG/DSC curves of red bolus before and after artificial aging of 35 days: with gum Arabic (top left), parchment glue (top right) and fish glue (bottom)

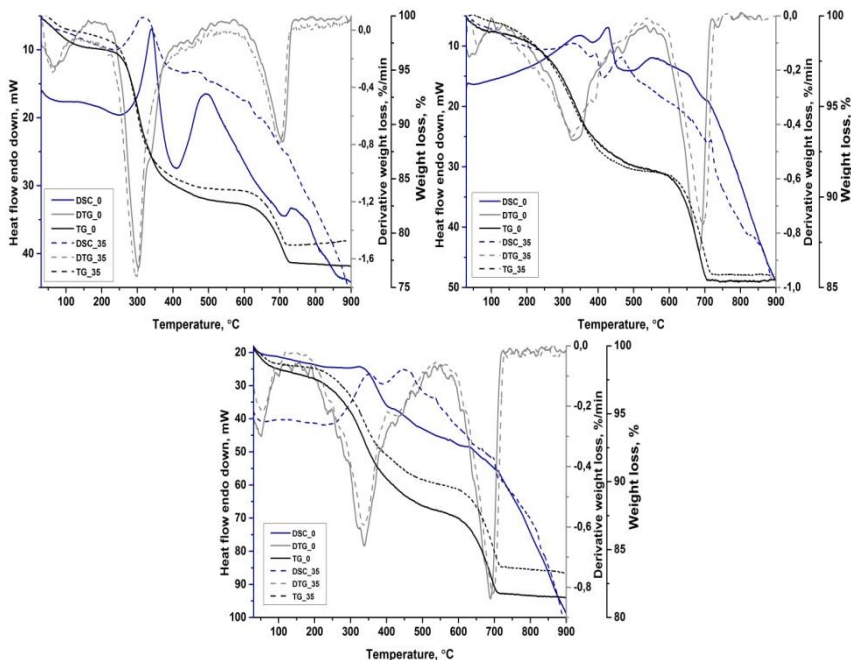


**Figure 43.** TG/DTG/DSC curves of hematite before and after artificial aging of 35 days: with gum Arabic (top left), parchment glue (top right) and fish glue (bottom)

Weight loss of ~ 1–3% to 150 °C due to desorption of physically and chemically adsorbed water, respectively. The mass loss ~ 10–20% from 150 to 400 °C is related to the decomposition of polysaccharide in samples with gum Arabic. The mass loss ~ 5–10% from 150–450 °C is related to the thermal decomposition of collagen in parchment and fish glue. Endothermic peaks at about 450–650 °C were found in the heating process due to the phase transition of  $\alpha$ -Fe<sub>2</sub>O<sub>3</sub> to  $\gamma$ -Fe<sub>2</sub>O<sub>3</sub>, respectively. The  $\gamma$ -Fe<sub>2</sub>O<sub>3</sub> phase formation temperature is about 500 °C [106, 107]. The mass loss in all cases was found to be about 12–23%.

### 3.3. Application of the reconstructed red pain database to the original manuscript

In this part of the dissertation the previously created red paints database has been applied to investigate and characterize the manuscripts from the time of the Grand Duchy of Lithuania. Most of the manuscripts studied belonged to the F19 collection, but with the predominance of one type of red pigment (cinnabar), the F21 and F22 collections were studied to find and

adapt a database of other red pigments. The original samples were analyzed using SEM/EDX, FTIR, XRD, and TG/DTG/DSC analysis methods.

The basic information about the analyzed manuscripts (which are kept in the Manuscript Department of the Wroblewski Library of the Lithuanian Academy of Science, in Vilnius), dating, the number of analyzed folios, and the place of each manuscript are given in Para. 2.1., Table 1.

### 3.3.1. SEM/EDX analysis

The red colour is a dominant colour in the illuminations and rubrications of all investigated four books (see Table 1.). Shades of pigments vary widely, ranging from orange-red, bright red, red, and deep-red. Mixtures of red pigments, especially cinnabar with red lead are very common in old manuscripts [124, 125], however, were not found in the study of the collection F19, F21, and F22. The cinnabar (HgS) was identified in all investigated manuscripts. Exceptionally, the red lead ( $Pb_3O_4$ ) was detected only in one manuscript. The morphology of cinnabar paints in the same book but different pages were very similar. The representative SEM micrographs of different samples are presented in Fig. 44.

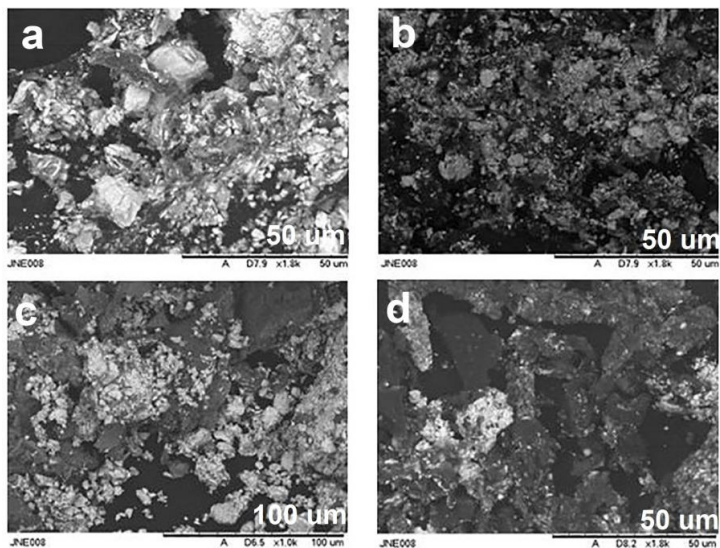


**Figure 44.** SEM micrograph of red paint samples from analyzed manuscripts: F19-115, f. 170 (a); F19-116, f. 154 (b); F22-805, f. 250 (c) and F21-101, f. 6 (d)

The red paint in book F19-115 was composed of differently shaped particles with size of 1 to 20  $\mu\text{m}$ . For the determination of the amount of

main and trace elements in the paints the SEM/EDX analysis method was applied. The EDX elemental analysis of these books showed that the amount of lead in the sample was 63.5 wt.%, which was in a good agreement with red lead. Carbon (26.3 wt.%), oxygen (6.8 wt.%), and aluminium (3.4 wt.%) determined in the sample probably come from paper or binding media.

The red paints in the remaining books are composed of cinnabar and different kinds of binding media. In the F19-116 the pigment is evenly distributed on the surface of the binding media, the surface composed of plate-like particles from 1 to 10  $\mu\text{m}$  sizes. The EDX elemental analysis showed that red paints are composed of mercury (62.3 wt.%), sulphur (11.4 wt.%), and impurities of paper or binding media elements, such as carbon (19.5 wt.%), oxygen (6.1 wt.%) and aluminium (0.7 wt.%).

The paint from book F21-805 is composed of different size sharp agglomerates from 1 to 20  $\mu\text{m}$  in size. The EDX elemental analysis showed that mercury (72.1 wt.%) and sulphur (14.5 wt.%) are the main elements of the paints, and oxygen (10.8 wt.%) and aluminium (2.6 wt.%) are as impurities. The pigment is well mixed with binding media in the last book F22-101. The particle size of the paints varied from 1 to 5  $\mu\text{m}$ . The EDX elemental analysis again showed the presence of cinnabar (mercury – 67.3 wt.%, sulphur – 13.7 wt.%) and impurities (carbon – 15.7 wt.%, oxygen 2.5 wt.% and aluminium 0.6 wt.%). It is not surprising that slightly different morphological features were observed for different red paints. For example, the microstructure of red iron (III) oxide pigment depends on the synthesis temperature influencing the particle size and shade of the pigment [39].

Thus, the red paints studied in these books were sufficiently pure. Interestingly, the halogens which could play a dominant role in the darkening process of cinnabar, or sulphur compounds that cause darkening of the  $\text{Pb}_3\text{O}_4$  were not detected in the paints. It can be assumed that the pigments have been particularly thoroughly cleaned and used only of the highest quality.

### 3.3.2. FTIR analysis

The FTIR analysis was an excellent tool for the identification of binding media. The FTIR spectra of original red paint samples taken from the manuscripts were successfully compared with the recorded ones for the reconstructed and artificially aged red paints containing different binding media. Red pigments were also investigated using the FTIR spectroscopy. The obtained FTIR spectra showed high similarity with FTIR spectra of

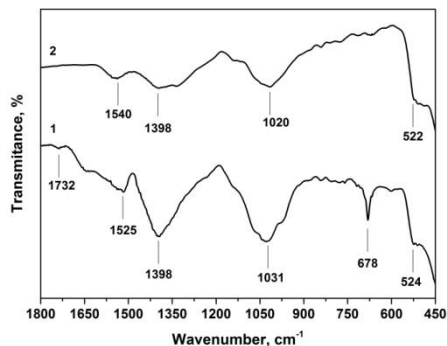
commercial ones. The representative FTIR spectra are presented in Figs. 45–48.

It can be seen from the spectra presented from our database they coincide well with the original red paints spectra. The absorption bands specific for gum Arabic are observed at 3400–3200  $\text{cm}^{-1}$  could be attributed to the stretch vibrations of OH group, the bands at 2930–2900  $\text{cm}^{-1}$  are due to C-H stretch and indicate the presence of sugars, galactose, arabinose, and rhamnose. The other characteristic bands of C=C stretch, amide NH bend,  $\text{NO}_2$  from both aliphatic and aromatic galacto proteins, and amino acids are around 1600  $\text{cm}^{-1}$ . The glucuronic acids have specific vibrations band at about 1410 and 1360  $\text{cm}^{-1}$  due to C=O symmetric stretching and OH bending, respectively. A distinct band at around 1030  $\text{cm}^{-1}$  represents alkene C-H band from polysaccharides for all gum samples [97].

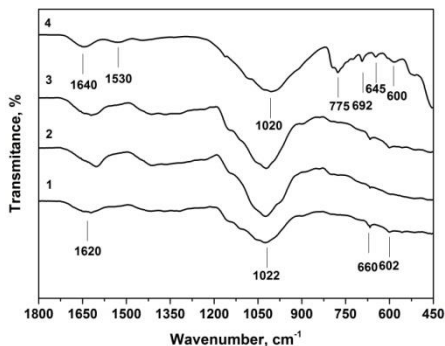
Animal glues (parchment, fish or other) are natural polymers derived from animal collagen. These adhesives can have a variety of physical, chemical, and mechanical properties depending on their origin and method of preparation. The FTIR spectra of parchment glue and fish glue are almost identical. The assignment of absorption bands at 3400 and 3200  $\text{cm}^{-1}$  is the same as for gum Arabic. The typical absorption band in the region of 3500–3400  $\text{cm}^{-1}$  for the amino group is masked by the broad absorption band of the OH group. Protein fingerprints are clearly observed in infrared spectra by the characteristic absorption peaks: amide I (C=O stretching,  $\sim 1650 \text{ cm}^{-1}$ ), amide II (CN stretching and NH bending,  $\sim 1550 \text{ cm}^{-1}$ ), CN bending at 1450  $\text{cm}^{-1}$ , and amide III at  $\sim 1230 \text{ cm}^{-1}$  [94]. Typical bands assigned to cellulose are observed in the region of 1630–900  $\text{cm}^{-1}$ . The peaks located at about 1630  $\text{cm}^{-1}$  correspond to the vibration of water molecules absorbed in cellulose. The absorption bands at 1420, 1360, 1330, 1020  $\text{cm}^{-1}$  and 890  $\text{cm}^{-1}$  belong to stretching and bending vibrations of  $\text{CH}_2$  and CH, OH and C-O bonds in cellulose [126].

Figure 45 shows the red lead with gum Arabic in the original sample. The paint adhered poorly to the surface of the paper and crumbled. The absorption bands in low frequency regions of 680–520  $\text{cm}^{-1}$  and one band at 1398  $\text{cm}^{-1}$  are attributed to lead oxide. A more intense band in the original sample than in an artificially aged reconstructed paint sample at 678  $\text{cm}^{-1}$  can be associated with lead (II) oxide formation or as impurities in the same red lead, which affects the colour change of the pigment. The new absorption band at 1732  $\text{cm}^{-1}$  could be attributed to C=O stretching vibrations and representative of a partial hydrolysis of the polysaccharide units [118, 119]. The FTIR spectra of gum Arabic also showed the characteristic bands of C=C stretch, amide NH bend,  $\text{NO}_2$  from both aliphatic and aromatic galacto

proteins, and amino acids at around  $1600\text{ cm}^{-1}$ , but in the original sample spectra, the absorption bands are shifted towards the shorter waves at  $1525\text{ cm}^{-1}$ . A distinct band at  $1031\text{ cm}^{-1}$  represents alkene C-H band from polysaccharides for all gum samples [14].



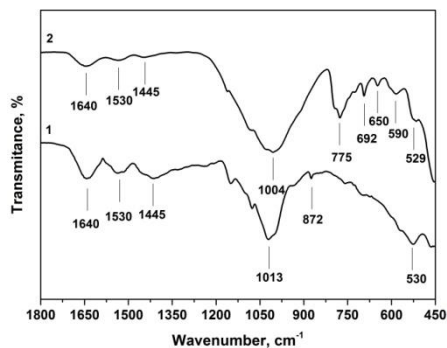
**Figure 45.** FTIR spectra of original sample from book F19-115, f. 170 (1) and reconstructed paint: red lead with gum Arabic after accelerating aging (2)



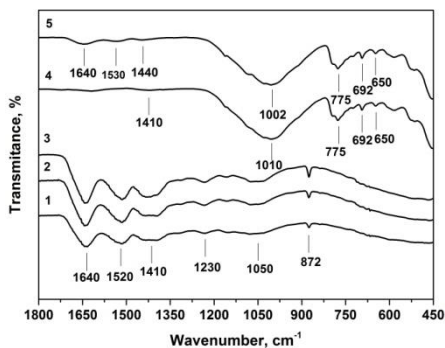
**Figure 46.** FTIR spectra of original sample from book F19-116, f. 5 (3), 154 (2), 260 (1) and reconstructed paint: cinnabar with fish glue after accelerating aging (4)

Figure 46 represents cinnabar with fish glue in the original sample. Aged reconstructed red paint (4) and original samples (1, 2, 3) spectra showed different absorption bands of the amides group. In the book F19-116 the absorption band of amides coupled to C=O is seen at  $1620\text{ cm}^{-1}$  (amide I), and in the aged reconstructed paint spectra at  $1640\text{ cm}^{-1}$ . In the original spectra, there are not seen the absorption band of amide II at  $1530\text{ cm}^{-1}$ . The main band at  $1022\text{ cm}^{-1}$  is attributed to C-O stretching vibration of the carbohydrate residues in collagen. The absorption peaks determined at  $780\text{--}600\text{ cm}^{-1}$  could be attributed to the Al-O and Al-O-Al vibrations.

Figure 47 shows cinnabar with parchment glue in the original sample. The spectra are almost identical. The main protein absorption bands of amides coupled to C=O are seen at  $1640\text{ cm}^{-1}$  (amide I), at  $1530\text{ cm}^{-1}$  (amide II) and at  $1445\text{ cm}^{-1}$  very weak  $\text{CH}_2$  asymmetric bending vibration in collagen or overlapping with ionic carbonate ( $\text{CO}_3^{2-}$ ). The main band at  $1013\text{ cm}^{-1}$  is attributed to C-O stretching vibration of the carbohydrate residues in collagen. The absorption band visible in the original sample at  $872\text{ cm}^{-1}$  is due to the vibrations in ionic carbonate ( $\text{CO}_3^{2-}$ ), peaks from  $780\text{--}530\text{ cm}^{-1}$  could be attributed to the Al-O and Al-O-Al vibrations. These paint and binding media are in good condition, there are no signs of degradation.



**Figure 47.** FTIR spectra of original sample from book F21-805, f. 250 (1) and reconstructed paint: cinnabar with parchment glue after accelerating aging (2)



**Figure 48.** FTIR spectra of original sample from book F22-101, f. 6 (3), 81 (2), 138 (1) and reconstructed paint: cinnabar with parchment glue (5) and with gum Arabic (4) after accelerating aging

The FTIR spectrum of the last sample F22-101 presented in Fig. 48 contains absorption bands characteristic to parchment glue and gum Arabic. This could have happened by the base of the manuscript was parchment. In the IR spectra of the original samples there are no signs of parchment or gum Arabic degradation. Only a new peak at  $872\text{ cm}^{-1}$  from ionic carbonate is observed.

In summary, the first two samples showed signs of paint degradation: gum Arabic acidified and hydrolysis of polysaccharide chains took place, which could have caused poor adhesion of the paint to the surface. The intense peak of lead (II) oxide also indicates aging of the pigment and causes discolouration of the paint. The second sample with fish glue media lost structure in the amide II. This is because the collagen in the paint binders is partially hydrolysed. The presence of the pigment in paint composition induces a conformation and even more in aged paint. The shift of peaks in gum Arabic and fish glue may also have been influenced by the metal center with the oxygen atoms of proteins [127]. Calcium carbonate peaks in the last two samples were observed from the binding media or substrate. This material is used in the process of making parchment glue or parchment itself. The rest features were stable and unchanged [117, 120, 128–131].

### 3.3.3. XRD analysis

By the XRD analysis, based on the reconstructed red paint database, original materials were tried to identify and compare the crystalline forms of the components determined in our original sample. The XRD patterns of red



paint collected from the same book from different pages were very similar and the results correlate well with the results obtained by EDX and FTIR analysis.

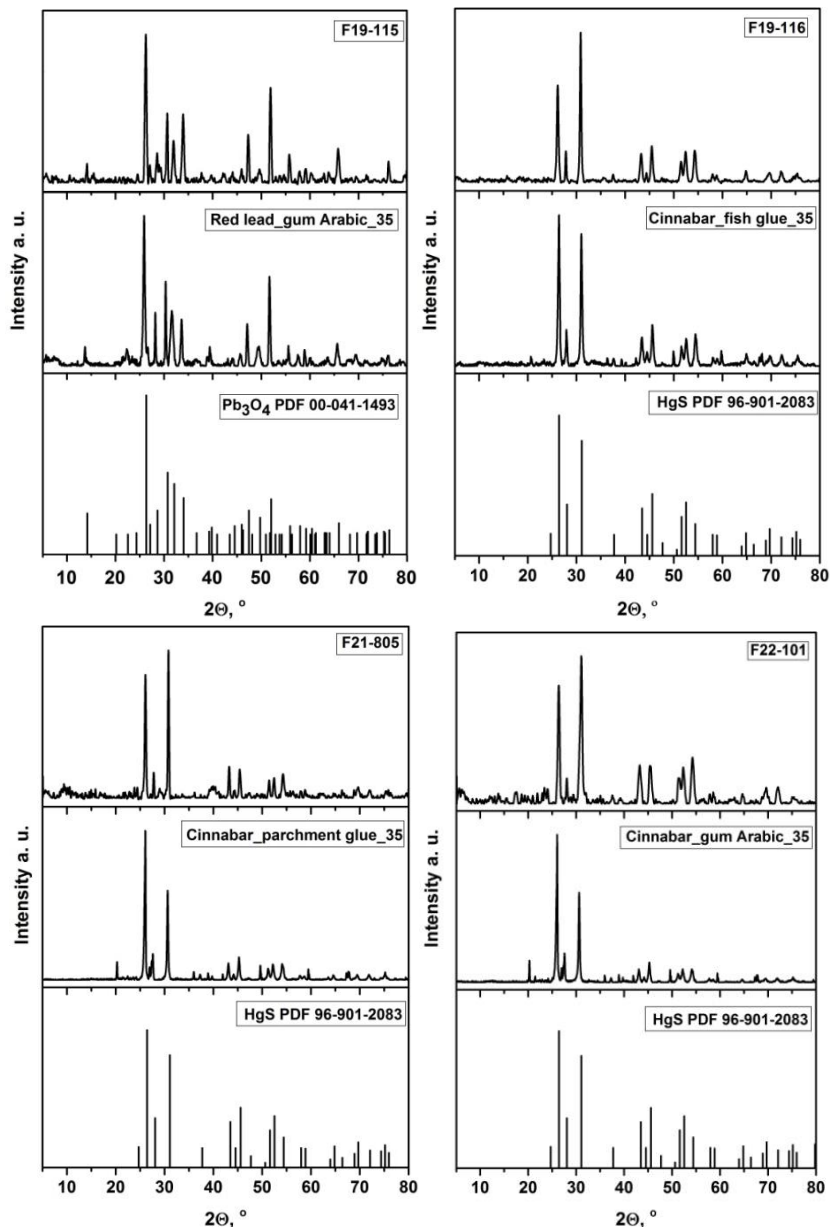


**Figure 49.** XRD patterns of different book red paint: F19-115, f. 170 (top left), F19-116, f. 154 (top right), F21-805, f. 250 (bottom left) and F22-101, f. 6 (bottom right) – top, middle – reconstructed red paint with different binding media after accelerated aging and bottom – standard XRD patterns

The first sample F19-115 (see Fig. 49) consists of red lead ( $\text{Pb}_3\text{O}_4$  PDF 00-041-1493). No significant differences were observed in comparison with library data, only small fluctuations in the intensity of side PbO phase at  $2\theta = 50^\circ$  to  $60^\circ$  were observed. The diffraction lines of binding media are not observed in our sample. The next samples F19-116, F21-805, F22-101 (Fig. 49) consist of HgS crystalline phase (PDF 96-901-2083). Again, the diffraction lines of binding media (fish glue, parchment glue and gum Arabic) are not observed in the XRD patterns. The XRD patterns of reconstructed HgS paint show additional reflections attributable to  $\text{SiO}_2$  phase (PDF 00-078-1253) at  $2\theta = 20.86^\circ, 26.60^\circ, 36.37^\circ, 37.68^\circ, 45.68^\circ, 59.84^\circ$ , but these diffraction lines are not visible in the XRD patterns of original sample.

The standard XRD patterns coincide well with those of the original samples. However, in the F21-805 and F22-101 samples new diffraction lines at  $2\theta = 29.64^\circ$  are visible, which could be attributed to  $\text{CaCO}_3$  phase. Moreover, the diffraction line at  $2\theta = 7^\circ$  seen in the XRD pattern of F21-805 sample could be attributed to the collagen from parchment glue [99–101, 132].

#### 3.3.4. TG/DTG/DSC analysis

The original samples were characterized by thermogravimetric (TG) analysis method under air flow. The obtained results were compared with the artificially aged reconstructed red paint TG/DTG/DSC analysis data (Fig. 50).

The sample of red lead with gum Arabic from book F19-115 showed the first decomposition step between  $30\text{--}150^\circ\text{C}$  with mass loss  $\sim 2,5\%$  due to the evolution of adsorbed and structural water of gum Arabic. The second mass loss of about 12% at about  $200\text{--}370^\circ\text{C}$  is related to the decomposition of polysaccharides, and the third mass loss of about 8% at about  $370\text{--}500^\circ\text{C}$  is associated with thermal decomposition of intermediate residues formed in carboxymethylated samples. The mass loss of about 2% from  $480\text{--}600^\circ\text{C}$  is related to the red lead reversible oxidation-reduction process when PbO is forming. And the last mass loss of about 1,5% is related to the other inorganic components (aluminium or other) which could have entered in to the sample from the surface of the paper [70, 133, 134]. The thermal events of the original sample compared with reconstructed red paint are shifted toward lower temperatures about  $50\text{--}70^\circ\text{C}$ . This could be related to the partial hydrolysis of gum Arabic.

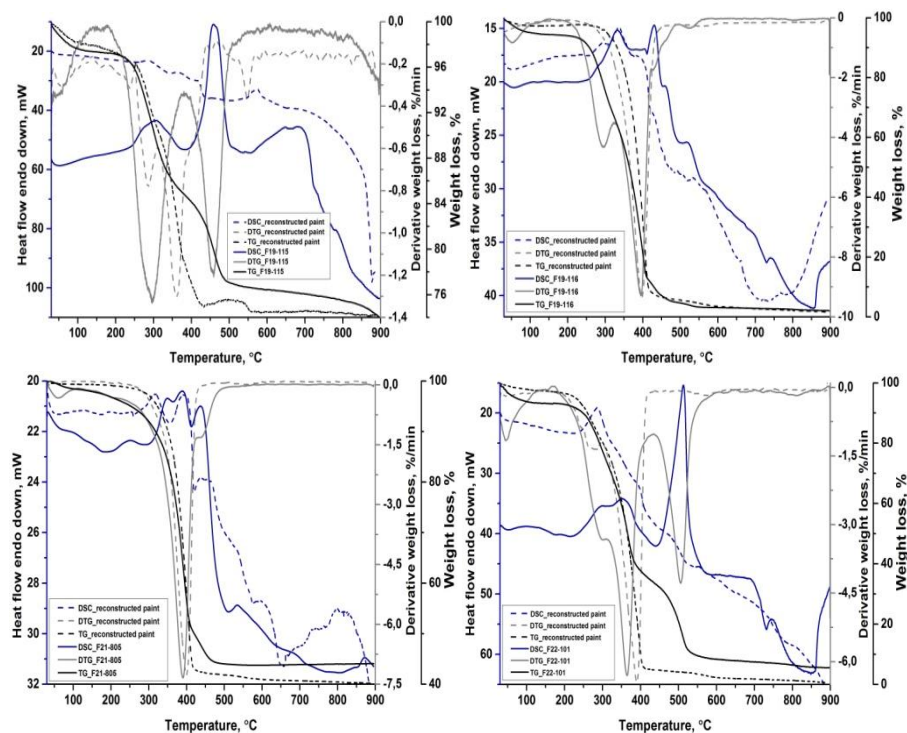


**Figure 50.** TG/DTG/DSC curves of original samples from the book and reconstructed red paint: F19-115, f. 170 compared to  $\text{Pb}_3\text{O}_4$  with gum Arabic (top left), F19-116, f. 154 compared to  $\text{HgS}$  with fish glue (top right), F21-805, f. 250 compared to  $\text{HgS}$  with parchment glue, (bottom left) and F22-101, f. 6 compared to  $\text{HgS}$  with gum Arabic (bottom right)

Similar binding media processes occur in the last sample F22-101, where cinnabar with gum Arabic was identified. First mass loss in the original sample about 10% was observed between 30–150 °C, the second mass loss about 30% was detected in the range of 200–320 °C, the third mass loss ~30% is seen at 350–450 °C, the fourth mass loss 20% is seen at 450–550 °C and the last mass loss 3% is visible from 600 °C. The structural changes of  $\text{HgS}$  occur in the third step. The hexagonal red mercury sulphide  $\alpha\text{-HgS}$  rearranges to the black mercury sulphide  $\beta\text{-HgS}$  [28, 69]. Also, the  $\text{HgS}$  decomposes to  $\text{HgO}$ ,  $\text{HgSO}_3$ ,  $\text{HgSO}_4$  and  $\text{SO}_2$  in air [102, 103].

The last two samples (F19-116 and F21-805) have the proteinaceous materials and the same inorganic pigment  $\text{HgS}$ . The decomposition of proteinaceous substances via two main stages of decomposition always takes place. The first proceeds at about 300 °C, which is characteristic of the thermal oxidative cleavage of the polypeptide chain, and the second one at about 500 °C, which is due to the entire combustion process [9, 135]. In our

case, the binding media are almost identical (fish and parchment glue), but only in one case (F19-116) thermal decomposition is clearly visible. However in the second case (F21-805) the observed thermal behaviour is very insignificant. The structural changes of HgS from the hexagonal red mercury sulphide  $\alpha$ -HgS to the black mercury sulphide  $\beta$ -HgS, and decomposition in air occurs at almost identical temperatures.

#### 4. Capillary washing of water-sensitive objects

Although the viscose non-woven fabric Paraprint OL60 was introduced into conservation in 2001 by S. Kirchner for the wet cleaning of water-sensitive paper objects carrying coloured media [89], there was no knowledge of its use in the workshops of Lithuanian restorers. Using the paraprint fabric, these objects were exposed only on their reverse to streaming water passing through a capillary unit. Paraprint OL60 is a 100% alkaline-resist, which is particularly convenient for introducing alkaline agents, binding media or other into the paper medium after washing. This non-woven fabric is also interesting for conservation due to its strong capillary action, high diffusion rate and wet strength, as well as its physical stability. The high rate of diffusion is due to the pore size. By the capillary action on thin viscose fibers, discolouration products are removed from the object in contact with the fabric. This prevents the dissolved compounds from migrating back into the paper. Due to the good wet strength of the material, it is an ideal intermediate support for aqueous procedures [91].

With water-sensitive paper objects, the challenge is to remove water-soluble degradation products, while keeping the water-sensitive medium in its place. In this work, the washing method on Paraprint OL60 fabric was tested. Initially, samples of different reconstructed paint compositions were prepared on filter paper (5 cm x 10 cm) sheets. The paraprint fabric was placed over the organic glass and wetted thoroughly. The prepared samples were gently wetted in a *GoreTex*<sup>®</sup> system (many restorers agreed that *GoreTex*<sup>®</sup> was most suitable for slow and controlled humidification of very reactive paper-based artefacts). The upper edge of the paraprint is placed in the reservoir with clean water, the lower edge is hanging over a second reservoir placed underneath it to collect the dirty water. The edge was cut into a blunt v-shape of 145°, to make it easier for the water to collect and drip down. The samples were placed on the Paraprint OL60 (Fig. 51). The capillary unit was then covered with a second sheet of organic glass, resting

on supports to maintain enough distance from the samples and to diminish the evaporation of the water along the surface of the paper.



**Figure 51.** Paraprint OL60 washing of prepared sample

In our case, the washing process took about 1 h. Dripping water was collected for further investigation. Washing the real object stops the process when water comes out of it completely clear. The process also should be monitored at every moment in case inks or colours start to bleed or move through the paper.

The samples after washing were photographed with an optical microscope to observe the changes. The collected water was evaporated to dryness and examined with FTIR and SEM/EDX analysis methods. The paint contour lines after washing on Paraprint OL60 capillary fabric did not show any changes in the samples with parchment and fish glue binders, except gum Arabic (see Fig. 52). The micrographs show the removal of paint colour in the direction of washing. The lowest paint flow was observed in paint gum Arabic with red lead. The paint is spread on the paper surface at a distance of about 1–2 mm from the contour line.

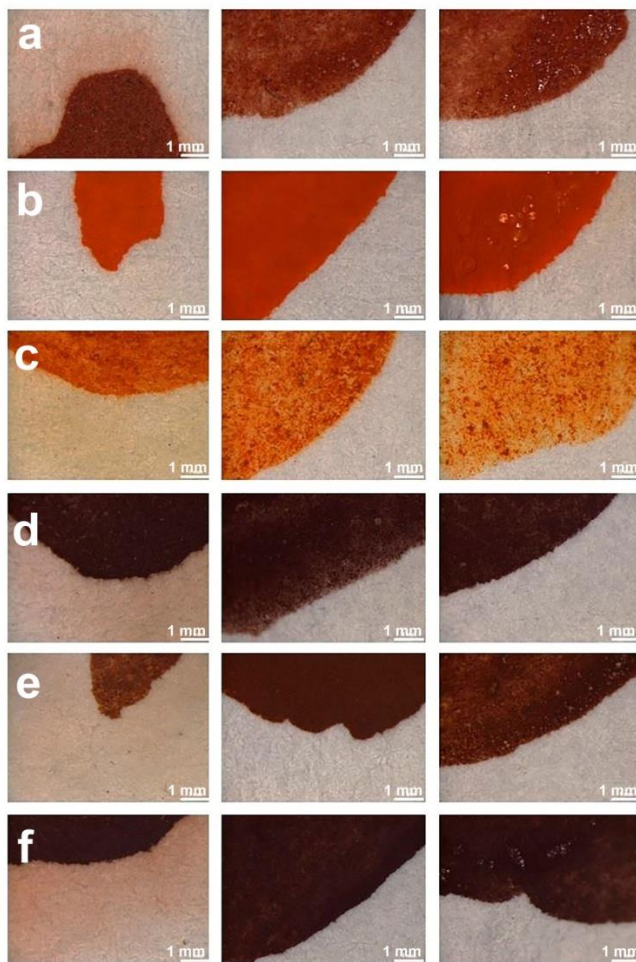


**Figure 52.** Paint samples micrographs after washing on Paraprint OL60 capillary fabric. Left – gum Arabic, middle – parchment glue, right – fish glue. A – cinnabar, b – red lead, c – realgar, d – red ochre, e – red bolus, f – hematite

FTIR analysis of the dried washes showed mainly the binding media (Fig. 53). All samples more or less have acetic acid characteristic absorption bands in the region from  $1780\text{--}1720\text{ cm}^{-1}$ , C=O stretching and from  $700\text{--}500\text{ cm}^{-1}$ , C=O op-bend and C–O torsion [136]. The paint with parchment and fish glue did not show the band at  $\sim 1630\text{ cm}^{-1}$  (amide I, C=O stretching), and the amide II band  $\sim 1545\text{ cm}^{-1}$  were shifted or overlapped in the region  $1590\text{--}1575\text{ cm}^{-1}$  with the acetic acid absorption band. No specific pigment absorption bands were found in any FTIR spectra.

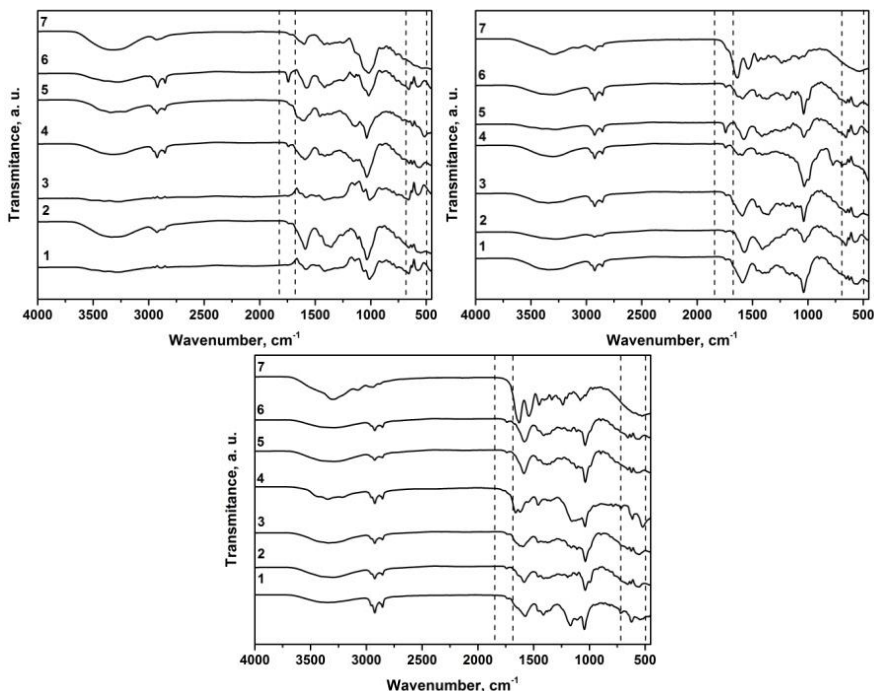


**Figure 53.** FTIR analysis of different dried washes: 1 – cinnabar, 2 – red lead, 3 – realgar, 4 – red ochre, 5 – red bolus, 6 – hematite with: top left – gum Arabic with acetic a. (7), top right – parchment glue with (7), bottom – fish glue (7).

SEM/EDX analysis of the dried washes showed the same elements in all samples. The main elements were C (~ 50–60 wt.%) and O (~ 20–30 wt.%), the remaining elements were Na, Mg, Al, Si, P, S, Cl, K, Ca and Cu. Only samples of gum Arabic with cinnabar, realgar and hematite had a small amount of pigment impurities (~ 0.4–0.7 wt.%). SEM/EDX analysis of the filter paper before washing showed C (61.17 wt.%), O (36.51 wt.%), Al (1.77 wt.%), Si (0.20 wt.%), Ca (0.20 wt.%), Cu (0.15 wt.%) elements, after washing – C (59.13 wt.%), O (38.81 wt.%), Al (1.85 wt.%), Si (0.07 wt.%), Cu (0.14 wt.%).

The capillary washing method was suitable and safe for the samples with parchment and fish glue, however, the samples with gum Arabic were sensitive. Migration of paint was observed, as well as a paint uptake on the other side of the paper sheet was determined. However, this method also has its advantages: a convenient, easily controlled process, it is possible to stop washing at any time, a safe top layer of paint during washing, economical.

## CONCLUSIONS

1. In this study, six different historical red pigments, as a standard (natural cinnabar Monte Amiata ( $\text{HgS}$ ), red lead ( $\text{Pb}_3\text{O}_4$ ), realgar ( $\text{As}_4\text{S}_4$ ), red bolus ( $\text{Fe}_2\text{O}_3 \cdot x\text{SiO}_2 \cdot y\text{Al}_2\text{O}_3$ ), Andalusian red ochre ( $\text{Fe}_2\text{O}_3$ ), hematite ( $\text{Fe}_2\text{O}_3$ )) and three binding media (gum Arabic, parchment glue and fish glue) were investigated using SEM/EDX, FTIR, XRD, and TG/DTG/DSC analysis techniques. Eighteen different analogous paint compositions were prepared for historical red paints. The obtained models of the red paints before and after accelerating aging for 35 days have been characterized by SEM/EDX, FTIR, XRD, and TG/DTG/DSC analysis methods. The short data library of red pigments, paint and binding media was created.
2. The SEM micrographs of single materials showed that the surface microstructure of pigments and binding media depend very much on the nature of materials. The EDX results demonstrated the presence of side chemical elements in the investigated specimens, while the FTIR spectra showed additional absorption bands. Finally, the XRD results were in good agreement with the SEM/EDX and FTIR analyses results confirming that the chemical composition of realgar and red lead pigments purchased from Kremer Pigmente corresponded to that one described in the catalogue. The rest of the four pigments, however, contained different impurities. The main peaks of the single materials were determined from the TG/DTG/DSC curves.
3. The fabricated paints with cinnabar exhibited deep red colour, red lead and realgar were red-orange, red ochre was deep red colour independent of the used binding media. However, the paints produced from red bolus and parchment or fish glue had a slightly yellowish tint. Red-brownish colour was observed for the paints prepared using hematite pigment. After accelerated aging, the biggest colour change and colour difference  $\Delta E$  was observed for the realgar paints. These paints have brightened and turned to greenish, yellowish colour. The red lead paints changed the colour negligibly, and the paints fabricated with cinnabar sustained colour almost without any changes. Red iron paints have changed slightly after artificial aging.
4. According to the SEM micrographs, the surface morphology of red paints has not changed significantly after 35 days of artificial aging. However, the particle size in most of the cases decreased significantly after accelerated aging. FTIR spectroscopy results let us to conclude that the artificial aging had some deleterious effect. The biggest changes and



new absorption bands at 790 and 480  $\text{cm}^{-1}$  were visible at realgar paint with all binding media spectra. The XRD analysis results confirmed the FTIR spectroscopy data. In the XRD patterns of red lead with fish glue and parchment glue after aging, the diffraction lines attributable to the PbO were detected. The XRD patterns of red paints with realgar showed the formation of white arsenolite ( $\text{As}_2\text{O}_3$ ) and yellow pararealgar ( $\text{As}_4\text{S}_4$ ) during the artificial aging. The TG/DTG/DSC curves after artificial aging are slightly shifted toward a lower temperature range.

5. For the first time, a short database of red paints was applied to investigate and characterize the manuscripts from the time of the Grand Duchy of Lithuania. SEM/EDX and XRD analysis data showed that the cinnabar pigment was predominated in the F19 collection during the studied period, however, the red lead was also detected. The red paint was sufficiently pure without a large amount of impurities, only in the book F19-115, PbO which causes the colour change in the paint was identified.
6. The FTIR spectra of the samples F19-115 and F19-116 showed binding media degradation. The formation of acid groups has been identified in the gum Arabic, which affects the hydrolysis of the polysaccharide chain and poor adhesion of the paint to the surface. The FTIR spectrum of the fish glue binder did not show an amide II group. This may be related to the collagen partial hydrolysis in the paint.
7. Capillary washing of water-sensitive objects on Paraprint OL60 non-woven fabric were applied to the reconstructed red paint samples, which have not been used by Lithuanian restorers yet. This washing method was suitable and safe for the samples with parchment and fish glue, however, samples with gum Arabic were sensitive. In any case, in order to apply this washing method to original cultural heritage objects, it would be necessary to know the exact composition of the paint and to assess the possible consequences.
8. This work once again demonstrated the role of several methods providing very important information for the characterization of cultural heritage materials. The non-invasive methods of characterization of cultural heritage objects always could be more advantageous. However, having a sufficient amount of sample the combination of SEM/EDX, FTIR, XRD, and TG/DTG/DSC analysis methods could be successfully employed instead of non-invasive methods to avoid the possible influence of the constituents on the reliability of obtained results.

## LIST OF PUBLICATIONS

### Articles in journals

1. Čiuladienė, Aušra, Kareiva, Aivaras. (2021). Application of red paint data library for the characterization of the manuscript from Grand Duchy of Lithuania. *Microchemical Journal*, 164, 105961. <https://doi.org/10.1016/j.microc.2021.105961>

2. Čiuladienė, Aušra, Beganskienė, Aldona, Senvaitienė, Jūratė, Kareiva, Aivaras. (2021). Study of the red iron paints for rubrics and miniatures: accelerated aging and analytical data. *Materials Science (Medžiagotyra)*, 27(1), 77–83. <https://doi.org/10.5755/j02.ms.25190>

3. Čiuladienė, Aušra, Kareiva, Aivaras, Raudonis, Rimantas. (2020). From model to artefact: Versatile characterization of cinnabar, red lead and realgar red paints for rubrics and miniatures. *Chemija*, 31(4), 238–246. <https://doi.org/10.6001/chemija.v31i4.4320>

4. Čiuladienė, Aušra, Luckutė, Austėja, Kiuberis, Jonas, Kareiva, Aivaras. (2018). Investigation of the chemical composition of red pigments and binding media. *Chemija*, 29(4), 243–256. <https://doi.org/10.6001/chemija.v29i4.3840>

### Published contributions to academic conference

1. Čiuladienė, Aušra, Kareiva, Aivaras. (2021). Identifying an illuminated and rubricated manuscript using red paint database. *Meetings of conservators and restorers of archival and library materials and art on paper, May 26-28, 2021, Dubrovnik, Croatia*.

2. Čiuladienė, Aušra, Kareiva, Aivaras. (2020). Determination of red paint using the database of analysis of red pigments. *Research. Dilemmas. Solutions: The 12-Th Baltic States Triennial Conservators' Meeting, Vilnius, Lithuania, 2020: Preprints*, 399–400.

3. Čiuladienė, Aušra, Kareiva, Aivaras. (2019). Painting the page – the red paint analysis an illuminated and rubricated manuscript. *4th*

*International Student Conference of Conservation and Restoration of Works of Art, November 6-8, 2019, Cracow, Poland.*

4. Čiuladienė, Aušra, Luckutė, Austėja, Kareiva, Aivaras. (2018). Investigation of red ballpoint pen inks. *EcoBalt 2018: The International Conference Proceedings Book, October 25-27, 2018, Vilnius, Lithuania. p. 45.*

5. Čiuladienė, Aušra, Luckutė, Austėja, Kareiva, Aivaras. (2018). On the chemical composition of red pigments and binding medium. *Advanced Materials and Technologies 2018: Book of Abstracts of 20th International Conference-School, August 27-31, 2018, Palanga, Lithuania, Kaunas: Technologija. p. 100.*

## ACKNOWLEDGEMENTS

I would like to start my gratitude with compliments for dr. Monika Skruodienė. Thank you Monika for the encouragement to start this study and inspiration to learn.

I am thankful to my research supervisors, prof. dr. Vida Vičkačkaitė and I am especially grateful to prof. habil. dr. Aivaras Kareiva, for all the knowledge, guidance, investment of his precious time passing down the knowledge, and comprehension during these past years.

Besides that, I would also like to thank all the team of Sol-Gel Chemistry Group and colleagues from the Faculty of Chemistry and Geoscience for practical help, their valued opinions and explanations.

I really appreciate the comprehension, encouragement, and constant motivation, provided by my colleagues from the Wroblewski Library of the Lithuanian Academy of Sciences.

Finally, I would like to acknowledge the support, care, and love from my family and friends during all the challenging moments. My deepest gratitude goes to my beloved husband Paulius, sons Arnas and Joris, my Brother, Mom, Dad and my Mother-in law. Their help provided me opportunities to develop as a person and a young scientist.

Thank you to everyone I did not mention here.

## SUMMARY IN LITHUANIAN

### ĮVADAS

Prisidedant prie vis didesnių pastangų išsaugoti kultūros paveldą, ypatingas dėmesys turi būti skiriamas istorinėms knygoms. Knyga yra žmonių kultūros paveldo, keliaujanti iš kartos į kartą, įrodymas. Jos forma keitėsi per visą istorinį laikotarpį, o struktūra yra viena iš sudėtingiausių ir daugialypiškiausių.

Vieni įspūdingiausių dokumentų buvo sukurti Viduramžių ir Renesanso laikotarpiais. Įvairių sričių tyrėjus domina skirtingų sudėtinių dalių kilmė, medžiagos, iš kurių jie gaminami, receptūros, įvairūs degradacijos procesai ir kt. Ypač svarbu atkreipti dėmesį į senųjų rankraščių pigmentus, kurie yra vieni iš nedaugelio komponentų, dažnai aptinkami jų originalia spalvine išvaizda. Pigmentai knygų tomuose dažnai buvo geriau apsaugoti nuo išorinio aplinkos poveikio: agresyvios atmosferos, drėgmės, temperatūros svyravimų, šviesos ar kitų galimų žalingų veiksnių. Todėl, analizuodami pigmentus ir jų dažų kompozicijas, galime pateikti išsamias išvagas apie Viduramžių ir Renesanso menininkų naudotas medžiagas ir receptūras, geografinę pigmentų kilmę, jų kaitą bėgant laikui ir įvertinti cheminius bei fizinius pokyčius.

Lietuvos paveldo institucijos, kaip ir visame pasaulyje, renka, saugo, tiria ir teikia visuomenei vertingus dokumentinio paveldo objektus. Tačiau rankraščių, ypač su įvairiais dekoru elementais (miniatiūromis, rubrikomis ir kt.), gamybos procesai nėra pakankamai tyrinėjami. Ilgą laiką lietuviškos knygos kultūros paveldas buvo tiriamas tik knygotyros ar meno istorijos požiūriu. Atsiradus daugiau tyrimų galimybių, svarbu pradėti tirti Lietuvos Didžiosios Kunigaikštystės (LDK) laikotarpio rankraščius. Šių rankraščių tyrimas ypač svarbus ne tik istoriniu ar tapatybės požiūriu, bet ir apibrėžiant jų gamybos procesus, rankraščių struktūrą, naudotas medžiagas ir jų kitimą LDK laikotarpiu.

Informacija apie pigmentų ar dažų sudėtį ypač naudinga restauratoriams, kai restauravimo darbams atlikti reikia pasirinkti tinkamas medžiagas ir restauravimo metodus. Rišiklius dažuose apibūdinti ypač sunku dėl mėginio dydžio, didelio neorganinio pigmento kiekio, laikui bėgant įvykusių skilimo procesų, ir tuo pačiu kitų priedų. Atsiradę spalvos pokyčiai ir degradacijos reiškiniai yra sudėtingas procesas, o juos mokslininkams, ypač restauratoriams, ne visada lengva atpažinti. Idealiausias būdas tirti šias medžiagas yra neinvaziniais analizės metodais, tačiau daugelis Lietuvos ir pasaulio paveldo institucijų turi galimybes taikyti mikrodestruktyvius, o

neinvaziniai – pilnai nepatenkina savo tyrimo galimybėmis ir turi tam tikrus trūkumus. Dėl šios priežasties daugeliu atvejų naudojami keli tyrimo metodai.

Lietuvos ir pasaulio restauratoriai turi restauruoti knygas, kuriose yra ypač dažni raudonos spalvos dažai: rubrikos, miniatiūros, įvairios išnašos, piešiniai ir kt. Laikui bėgant, juose dažnai stebimos įvairios destruktijos, dažai tampa takūs plovimo metu. Todėl labai svarbu žinoti jų sudėtį, kokie pigmentai ar mišiniai buvo naudojami.

Šios disertacijos naujumas – šešių istorinių raudonų pigmentų ir trijų skirtingų rišiklių duomenų bazės sukūrimas ir jos taikymas visiškai netyrinėtiems chemijos tyrėjų knygų rinkiniams, saugomiems Lietuvos mokslų akademijos Vrublevskių bibliotekos Rusiškų rankraštinųjų knygų (F19), Vilniaus viešosios bibliotekos (F22) bei Vilniaus baltarusių (F21) knygų fonduose. Šie, ypač gerai atspindi knygų raidos tendencijas Lietuvos Didžiosios Kunigaikštystės teritorijoje.

Pagrindinis šios daktaro disertacijos tikslas buvo šešių istorinių raudonų pigmentų (cinoberio, raudonojo švino, realgaro, raudonosios ochros, raudonojo molio ir hematito), bei trijų skirtingų rišiklių (gumiarabiko, pergamento ir žuvų klijų) duomenų bazės sukūrimas ir kapiliarinio plovimo taikymas vadeniui jautriems objektams. Šiam tikslui įgyvendinti buvo suformuluoti tokie disertacijos uždaviniai:

1. Ištirti šešis skirtingus raudonus pigmentus bei tris rišiklius kaip standartines medžiagas SEM/EDX, FTIR, XRD ir TG/DTG/DSC analizės metodais.

2. Remiantis senosiomis receptūromis, pagaminti analogiškas istoriniams, 18 skirtingų rūšių raudonų dažų kompozicijas. Jas dirbtinai pasendinti fotocheminio sendinimo kameroje, ir atlikti SEM/EDX, FTIR, XRD ir TG/DTG/DSC analizės tyrimus prieš ir po sendinimo.

3. Praktiškai pritaikyti surinktą raudonų dažų duomenų bazę senųjų knygų raudonų dažų ir rišiklių identifikavimui.

4. Išbandyti jautrių vadeniui objektų plovimą ant kapiliarinio neaustinio audinio Paraprint OL60.

## 1. EKSPERIMENTO METODIKA

Šeši istoriniai raudoni pigmentai ir trys rišikliai buvo išigyti iš *Kremer Pigmente*. Vieninės medžiagos ištirtos SEM/EDX, FTIR, XRD ir TG/DTG/DSC analizės metodais. Po to paruošta 18 skirtingų raudonų dažų kompozicijų analogiškų senosioms. Mėginiai dirbtinai pasendinti

fotocheminio sendinimo kameroje 1, 4, 7, 14, 21, 28 ir 35 dienas, veikiant šviesai, temperatūrai ir drėgmei. Pagaminti dažai prieš ir po dirbtinio fotocheminio sendinimo tirti ankčiau minėtais tyrimo metodais. Sukurta trumpa raudonų pigmentų, rišiklių ir jų kompozicijų duomenų bazė. Po to imti realūs mėginiai iš knygų fonduose F19, F21, F22 ir lyginti su turimais duomenis. Išbandytas paruoštų dažų pavyzdžių plovimas ant kapiliarinio neaustinio audinio Paraprint OL60. Atlikti OM, FTIR, SEM/EDX tyrimai.

## 2. REZULTATAI IR JŲ APTARIMAS

### 2.1. Pigmentų, analogiškų istoriniams raudoniems pigmentams, ir rišamųjų terpių apibūdinimas

Šioje disertacijos dalyje pateikiami komercinių, analogiškų istoriniams raudoniems pigmentams, ir rišiklių apibūdinimo rezultatai naudojant SEM/EDX, FTIR, XRD ir TGA/DTA/DSK analizės metodus.

#### 2.1.1. SEM/EDX analizės rezultatai

Pirmiausia buvo nustatyta komercinių raudonų pigmentų ir rišiklių elementinė sudėtis. EDX analizės duomenys pateikti 1 ir 2 lentelėje.

**Lentelė 1.** Komercinių raudonų pigmentų EDX analizės rezultatai

Pigmentas	Elementas, m. %						
	Hg	S	Si	Al			
Cinoberis	77,17	15,68	5,03	2,12			
Raudonasis švinas	Pb	O					
	84,52	15,48					
Realgaras	As	S	C				
	42,80	16,42	40,78				
Raudonoji ochra	Fe	O	Si	Al	C		
	48,16	16,80	7,43	2,23	25,38		
Raudonasis molis	Fe	O	Si	Al	C	K	Mg
	12,73	48,67	16,84	8,79	9,90	2,32	0,75
Hematitas	Fe	O	Si	Al	C	Ca	
	34,74	45,10	1,39	0,97	17,30	0,50	

**Lentelė 2.** Rišiklių EDX analizės rezultatai

Rišiklis	Elementas, m.%					
	C	O	Ca	Al	K	
Gumiarabikas	49,48	43,85	3,52	2,51	0,64	
Pergamento klėjai	C	O	Al	Ca	S	Na
	68,16	30,34	0,61	0,31	0,30	0,28
Žuvų klėjai	C	O	Mg	Al	S	Ca
	35,77	49,43	9,23	4,37	0,94	0,26

SEM analizės rezultatai parodė, kad cinoberis sudarytas iš į plokštelę panašių apie 2–5  $\mu\text{m}$  dydžio kristalų. Raudonojo švino dalelės sferinės, mažesnės nei 100  $\mu\text{m}$ . Realgaro dalelės labai skirtingų formų, jų dydis svyruoja nuo 5 iki 40  $\mu\text{m}$ . Raudonoji ochra ir raudonasis molis turi panašių plokštelių mikrostruktūrą, dalelių dydis svyruoja 2–10  $\mu\text{m}$  intervale. Pigmentas hematitas susideda iš nanodalelių, kurios sudaro sferinius aglomeratus. Gumiarabikas – gamtinis polisacharidas, susideda iš pailgų, maždaug 15  $\mu\text{m}$  pločio ir 50–60  $\mu\text{m}$  ilgio kristalų, pergamento ir žuvų klėjai – baltyminės kilmės medžiagos, todėl SEM nuotraukose stebima monolitinė mikrostruktūra.

### 2.1.2. FTIR analizės rezultatai

Infraraudonųjų spindulių spektroskopijos metodas buvo panaudotas analogiškų istoriniams raudonų pigmentų ir rišiklių apibūdinimui, bei identifikavimo galimybėms nustati. Visų komercinių mėginių FTIR spektrų sugerties juostos pateiktos 3 ir 4 lentelėse.

**Lentelė 3.** Komerciniams pigmentams būdingos IR sugerties juostos

Pigmentas	Būdingos IR sugerties juostos, $\text{cm}^{-1}$
Cinoberis	1017 $\text{cm}^{-1}$ (Si–O); 773, 692 $\text{cm}^{-1}$ (Si–O–Al).
Raudonasis švinas	1398, 682, 521 $\text{cm}^{-1}$ (Pb–O).
Realgaras	-
Raudonoji ochra	1030 $\text{cm}^{-1}$ (Si–O–Si); 795 $\text{cm}^{-1}$ (Si–O–Al); 531, 431 $\text{cm}^{-1}$ (Fe–O).
Raudonasis molis	3689, 3616 $\text{cm}^{-1}$ (O–H); 1001 $\text{cm}^{-1}$ (Si–O–Si); 913 $\text{cm}^{-1}$ (Si–O); 795,694 $\text{cm}^{-1}$ (Si–O–Al); 526, 464 $\text{cm}^{-1}$ (Fe–O).
Hematitas	1432, 876 $\text{cm}^{-1}$ ( $\text{CO}_3^{2-}$ ); 1028 $\text{cm}^{-1}$ (Si–O–Si); 519 ir 431 $\text{cm}^{-1}$ (Fe–O).



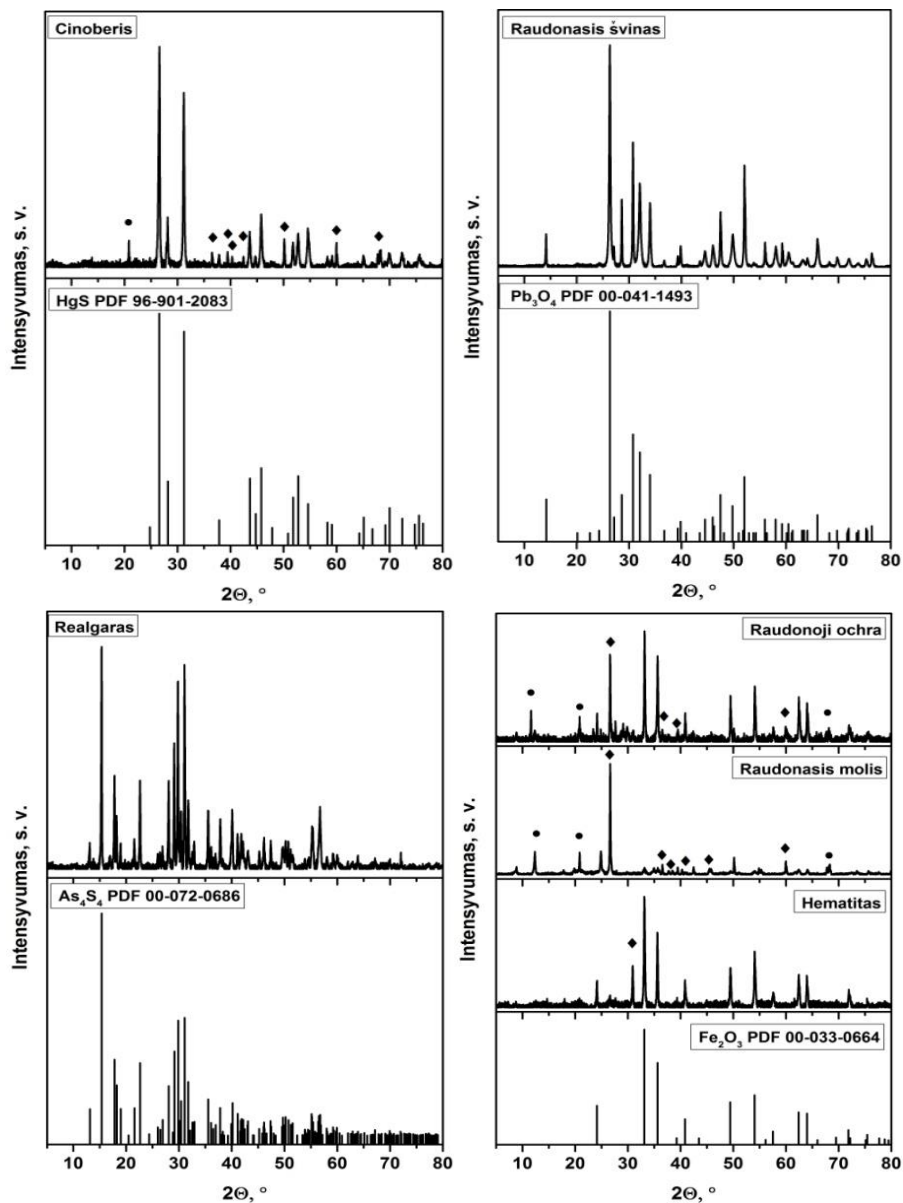
**Lentelė 4.** Rišikliams būdingos IR sugerties juostos

Rišiklis	Būdingos IR sugerties juostos, $\text{cm}^{-1}$
Gumiarabikas	$3300 \text{ cm}^{-1}$ (OH); $2923 \text{ cm}^{-1}$ (CH); $1600 \text{ cm}^{-1}$ (C=C, NH, $\text{NO}_2$ ); $1413, 1364 \text{ cm}^{-1}$ (C=O, OH); $1008 \text{ cm}^{-1}$ (C–H).
Pergamento ir žuvų klįjai	$3500\text{--}3400 \text{ cm}^{-1}$ (NH); $\sim 1630 \text{ cm}^{-1}$ (amidas I (C=O)); $\sim 1530 \text{ cm}^{-1}$ (amidas II (CN ir NH)); $1450 \text{ cm}^{-1}$ (CN); $\sim 1230 \text{ cm}^{-1}$ (amidas III); $1070\text{--}1020 \text{ cm}^{-1}$ (C–O).

Pigmentai – cinoberis ir realgaras nesugeria infraraudonųjų spindulių  $4000\text{--}350 \text{ cm}^{-1}$  srityje, o pergamento ir žuvų klijų FTIR spektrai beveik identiški, stebimi tik nežymūs sugerties juostų poslinkiai.

### 2.1.3. XRD analizės rezultatai

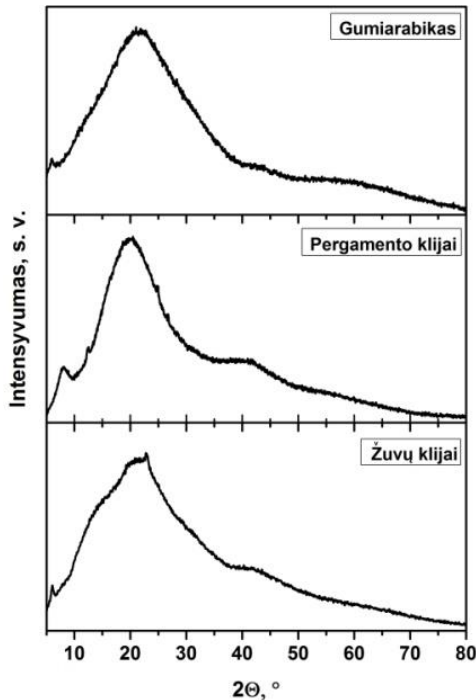
Skirtingų raudonų pigmentų ir rišiklių difraktogramos pateiktos 1 ir 2 paveiksluose. Cinoberio difraktograma rodo, kad įsigytame pigmente yra pagrindinė HgS fazė (PDF 96-901-2083), taip pat papildomos  $\text{SiO}_2$  (PDF 00-078-1253) ir  $\text{Al}_2\text{Si}_2\text{O}_5(\text{OH})_4$  (PDF 00-075-1593) fazės. Kitus du pigmentus raudonąjį šviną ir realgarą sudaro tik  $\text{Pb}_3\text{O}_4$  (PDF 00-041-1493) ir  $\text{As}_4\text{S}_4$  (PDF 00-072-0686) fazės. Raudonų geležies pigmentų difraktogramose visuose mėginiuose identifikuota pagrindinė  $\text{Fe}_2\text{O}_3$  fazė (PDF 00-033-0664). Raudonoji ochra ir raudonasis molis turi papildomas  $\text{SiO}_2$  (PDF 00-078-1253) ir  $\text{Al}_2\text{Si}_2\text{O}_5(\text{OH})_4$  (PDF 00-075-1593) fazes. Pigmento hematito XRD difraktograma labai gerai koreliuoja su standartine  $\text{Fe}_2\text{O}_3$  faze, tačiau taip pat turi  $\text{SiO}_2$  fazės priemaišų. Remiantis SEM/EDX, FTIR ir XRD analizės rezultatais, iš *Kremer Pigmente* įsigytų pigmentų realgaro ir raudonojo švino cheminė sudėtis atitinka aprašytą kataloge, o likusiuose keturiuose pigmentuose yra skirtingų priemaišų.



**1 pav.** Raudonų pigmentų difraktogramos (viršuje: kairė – cinoberis, dešinėje – raudonasis švinas, apačioje: kairėje – realgaras, dešinėje – geležies pigmentai). Pažymėtos fazės:  $\blacklozenge$  SiO<sub>2</sub>  $\bullet$  Al<sub>2</sub>Si<sub>2</sub>O<sub>5</sub>(OH)<sub>4</sub>

Remiantis literatūros šaltiniais, gryno gumiarabiko XRD pagrindinė difrakcijos linija yra prie  $2\theta = 18,9^\circ$ , o pergamento ir žuvų klijų, kurių pagrindinė sudedamoji dalis kolagenas, ties  $2\theta = 7^\circ$  ir  $20^\circ$ . Mūsų tirtuose mėginiuose (žr. 2 pav.), charakteringos difrakcijos smailės gerai koreliuoja pergamento klijų mėginyje ir šiek tiek pasislinkusios gumiarabiko ir žuvų

klijų pavyzdžiuose. Tam įtakos galėjo turėti nedidelis neorganinių priemaišų kiekis šių medžiagų sudėtyje.



2 pav. Skirtingų rišiklių difraktogramos, viršuje – gumiarabikas, viduryje – pergamento klijai, apačioje – žuvų klijai

#### 2.1.4. TG/DTG/DSC analizės rezultatai

Cinobrio TG/DTG/DSC analizės metu, pirmasis ir pagrindinis masės nuostolis (apie 55%) stebimas ties 400 °C temperatūra, kai heksagoninės struktūros raudonas gyvsidabrio sulfidas  $\alpha$ -HgS virsta į kubinės struktūros juodąjį metacinoberį  $\beta$ -HgS 300–410 °C temperatūrų intervale. Taip pat, šiame temperatūrų intervale vyksta HgS garavimas. Kameroje esant deguoniui susidaro  $\text{Hg}^0$  ir  $\text{S}_2$ , o reakcijoms vykstant toliau, gali susidaryti  $\text{SO}_2$  ar  $\text{HgSO}_3$ . Antrasis masės nuostolis ~ 2% (510–600 °C) yra susijęs su metacinoberio  $\beta$ -HgS virsmu į hipercinoberį  $\gamma$ -HgS ties 527 °C temperatūra. Šie virsmai taip pat gali būti siejami su susidariusių tarpinių produktų, tokių kaip HgO ar  $\text{HgSO}_4$ , skilimu ore. Raudonasis švinas susidaro oksidacijos metu, kai  $\alpha$ -PbO pašildomas iki maždaug 450–500 °C temperatūros, tačiau atmosferos slėgyje suyra iki geltonos spalvos  $\beta$ -PbO, kai temperatūra viršija 585 °C. Masės nuostoliai skylant  $\text{Pb}_3\text{O}_4$  iki PbO buvo apie 2%. Realgaro terminės analizės metu, pirmasis masės nuostolis (~ 18%) stebimas 307–370

°C temperatūroje. Raudonas pigmentas  $As_4S_4$ , esant maždaug 256 °C temperatūrai, virsta geltona  $As_4S_4$  faze, kuri lydosi esant maždaug 307 °C. Antrasis (~ 45%) masės nuostolis įvyksta 370–430 °C temperatūroje, o tai gali būti siejama su geltonos  $As_4S_4$  fazės virsmu į arsenolitą  $As_2O_3$ . Ir galiausiai trečiasis (~ 37%) masės nuostolis prasideda nuo 430–500 °C ir nuolat tęsiasi iki 100%, susijęs su medžiagos garavimu. Raudonų geležies pigmentų TG/DTG/DSC analizės duomenys šiek tiek skiriasi dėl skirtingo priemaišų kiekio. Tačiau pagrindinės nustatytos endoterminės smailės esant 450–650 °C temperatūrai stebimos visuose trijuose mėginiuose:  $\alpha$ - $Fe_2O_3$  virsta į  $\gamma$ - $Fe_2O_3$ .  $\gamma$ - $Fe_2O_3$  fazės susidarymo temperatūra yra apie 500 °C. Nustatyta, kad visais atvejais masės nuostoliai yra apie 6–7%.

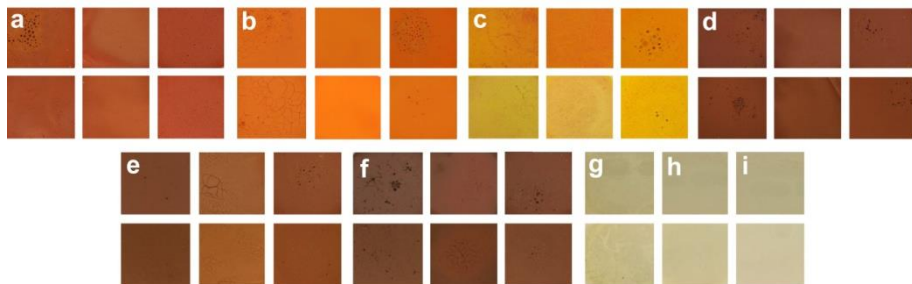
Gumiarabiko TG kreivė rodo tris pagrindinius masės nuostolius. Pirmasis masės praradimas (10–15%) nuo 30 iki 200 °C atsiranda dėl adsorbuoto ir struktūrinio vandens praradimo. Antrasis ~ 50% masės nuostolis 250–350 °C temperatūros intervale yra susijęs su polisacharidų skilimu, o paskutinis masės nuostolis (30%) 400–600 °C temperatūros intervale gali būti siejamas su tarpinių likučių, susidariusių karboksimetilintuose junginiuose skilimu. Pergamento ir žuvų klijų terminis skilimas kaitinimo metu yra labai panašus, nedideli skirtumai stebimi tik dėl skirtingų priemaišų kiekio. Plati endoterminė smailė susijusi su drėgmės praradimu ir visiškai sutampa su fibrilinio kolageno denatūracine endoterma 30–270°C. Masės nuostolis apie 10–12%. Pagrindinę DTG smailę galima priskirti terminiam kolageno skilimui tarp 270 ir 530 °C. Esant 300–315 °C temperatūrai, vyksta pirmasis kolageno skilimo procesas. Masės nuostolis yra apie 52%. Antroji smailė yra tarp 530–670 °C, kuri siejama su antruoju želatinos matricos skilimo etapu ir tarpinių neorganinių junginių skilimu. Paskutinis masės nuostolis yra apie 36–38%.

## 2.2. Rekonstruotų raudonų dažų apibūdinimas

Šioje disertacijos dalyje pateikiami rekonstruotų analogiškų istorinių raudonų pigmentų apibūdinimo prieš ir po dirbtinio fotocheminio sendinimo, naudojant kolorimetrinius, SEM, FTIR, XRD ir TG/DTG/DSC analizės metodus, rezultatai. Aptariami duomenys tik po 35 dienų fotocheminio sendinimo, nes tarpiniuose žymių pokyčių nepastebėta.

### 2.2.1. Kolorimetrinių matavimų rezultatai

Norint iširti pigmentų ir rišiklių stabilumą, rekonstruoti raudoni dažai su skirtingais rišikliais buvo dirbtinai fotochemiškai pasendinti. Spalvų pokyčiai prieš ir po dirbtinio fotocheminio sendinimo pateikti 3 pav.



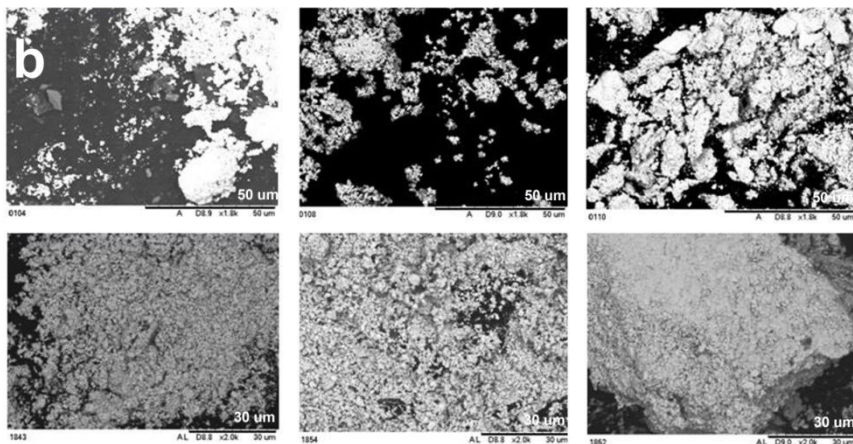
**3 pav.** Rekonstruotų raudonų dažų vaizdai: a – cinoberis, b – raudonasis švinas, c – realgaras, d – raudonoji ochra, e – raudonasis molis, f – hematitas su gumiarabiku, pergamento ir žuvų kljais (iš kairės į dešinę); ir rišikliai: g – gumiarabikas, h – pergamento kljiai ir i – žuvų kljiai. Prieš (viršuje) ir po 35 dienų dirbtinio sendinimo (apačioje)

Kaip matyti iš nuotraukų, cinoberio dažuose ryškiai raudonos spalvos pokytis nežymus, išskyrus kompoziciją su žuvų kljais, kur  $\Delta E$  vertė buvo 6,9 ir dažai atrodė šiek tiek ryškesni. Pagaminti raudonojo švino dažai buvo raudonai oranžinės spalvos. Intensyviausias spalvos pasikeitimas stebimas pavyzdyje su pergamento kljais, o  $\Delta E$  vertė buvo 7,7. Visos švino dažų kompozicijos po dirbtinio sendinimo buvo suskeldėjusios, silpnai laikėsi ant padėklo paviršiaus. Didžiausias spalvų pokytis stebėtas realgaro dažų kompozicijose. Prieš dirbtinį fotocheminį sendinimą, dažai buvo ryškiai raudonai oranžinės spalvos, nesuskilinėję. Po sendinimo – dažų paviršius sutrūkinėjo, spalvos išbluko ar perėjo į žalsvą, gelsvą, o  $\Delta E$  vertės buvo nuo 20 iki 41. Dažai, pagaminti naudojant raudonąją ochrą buvo tamsiai raudonos spalvos nepriklausomai nuo rišiklio. Tačiau kompozicijos su raudonuoju moliu ir pergamento ar žuvų kljais, turėjo šiek tiek gelsvą atspalvį. Hematito dažų spalva – raudonai rusva. Pergamento kljiai po dirbtinio sendinimo labiausiai pakeitė savo spalvą,  $\Delta E$  vertė buvo 13,2, gumiarabiko – 6,7, žuvų kljū – 4,2.

### 2.2.2. SEM analizės rezultatai

SEM analizė buvo atlikta siekiant įvertinti dažų morfologinius pokyčius prieš ir po dirbtinio sendinimo. Cinoberio dažų paviršiaus morfologija visais

atvejais buvo labai panaši, nepriklausomai nuo naudojamų rišiklių. Dirbtinis sendinimas beveik neturėjo įtakos dalelių dydžiui: 1–15  $\mu\text{m}$  prieš ir 1–10  $\mu\text{m}$  po sendinimo. Tik kompozicijoje su pergamento klėjais dalelių dydis svyravo nuo 1 iki 15  $\mu\text{m}$  prieš ir nuo 1 iki 3  $\mu\text{m}$  po sendinimo. Realgaro dažų morfologija buvo beveik identiška cinoberio dažų atveju. Didžiausi paviršiaus morfologijos pokyčiai prieš ir po dirbtinio sendinimo pastebėti dažų kompozicijoms su raudonojo švino pigmentu (žr. 4 pav.) ir raudonų geležies pigmentų.



**4 pav.** Skirtingos raudonos švino dažų kompozicijos SEM nuotraukos (iš kairės į dešinę) su gumiarabiku, pergamento ir žuvų klėjais prieš (viršuje) ir po 35 dienų dirbtinio sendinimo (apačioje)

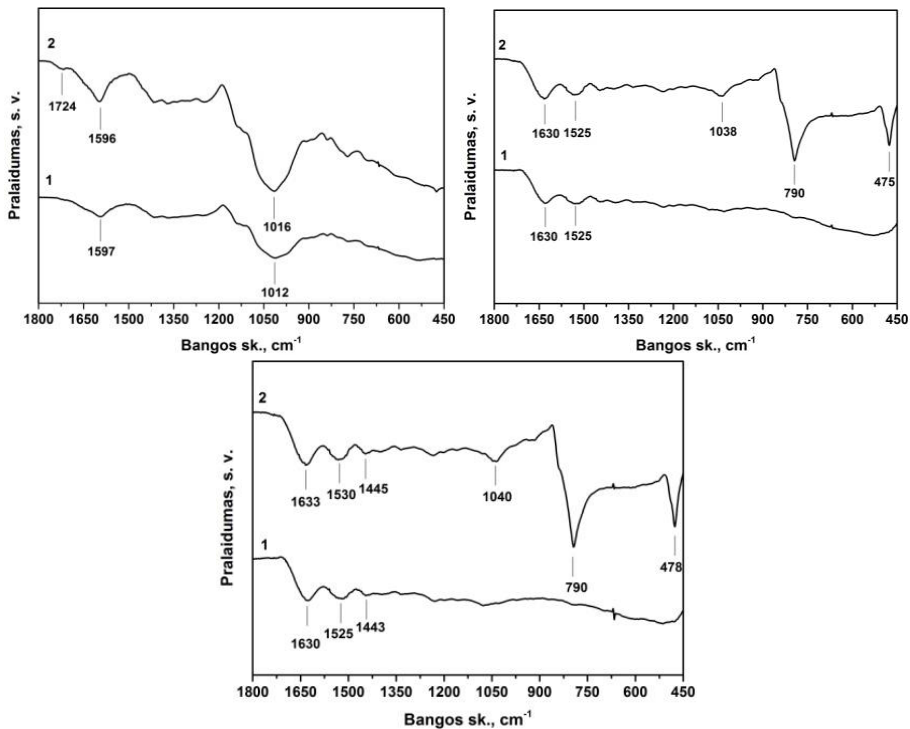
Prieš sendinimą, raudono švino dažų kompozicijas sudarė skirtingos formos dalelės, kurių dydis svyravo nuo 1–10  $\mu\text{m}$ . Tačiau po sendinimo, dalelės stipriai sumažėjo, buvo linkusios formuoti aglomeratus. Raudonų geležies dažų kompozicijos po sendinimo taip pat formavo aglomeratus, dalelių dydis stipriai sumažėjo nuo 50–60  $\mu\text{m}$  prieš iki 3–20  $\mu\text{m}$  po sendinimo.

### 2.2.3. FTIR analizės rezultatai

FTIR spektroskopija buvo naudojama siekiant geriau suprasti dažų spalvos pasikeitimą dirbtinio sendinimo metu ir nustatyti naujas funkcines grupes. Rišiklių FTIR spektrai prieš ir po sendinimo nepasikeitė arba jų pokyčiai buvo nereikšmingi. Nauja, nedidelio intensyvumo absorbcijos juosta gumiarabiko spektre po sendinimo buvo pastebėta prie 1727  $\text{cm}^{-1}$ ,

kurią galima priskirti C=O grupei, vykstant dalinei polisacharidų grandinių hidrolizei.

Raudonų dažų kompozicijose prieš ir po dirbtinio sendinimo pokyčiai stebėti tik realgaro dažų spektruose (5 pav.). Likę dažai pokyčių nerodė. Prieš sendinimą realgaro dažų FTIR spektruose nebuvo matoma kitų smailių, išskyrus rišiklio. Po dirbtinio sendinimo realgaro dažų su gumiarabiku FTIR spektre stebima nauja smailė prie  $1724\text{ cm}^{-1}$ , priskiriama susidariusiai rišiklio C=O grupei, ir labai nežymios prie  $790$  ir  $480\text{ cm}^{-1}$ . Apie  $1040$ ,  $790$  ir  $480\text{ cm}^{-1}$  realgaro dažų kompozicijų su pergamento ir žuvų klijais FTIR spektruose stebimos trys naujos smailės. Pirmoji smailė siejama su C–O ryšiu kolagene, antroji su As–O grupės ryšiu, o trečioji su As–S grupės ryšiu. Arseno trioksidas ir įvairūs sulfatų junginiai yra arseno sulfido pigmentų skilimo produktai, dėl šios priežaties dažų kompozicijos šviesėja ir blunka.

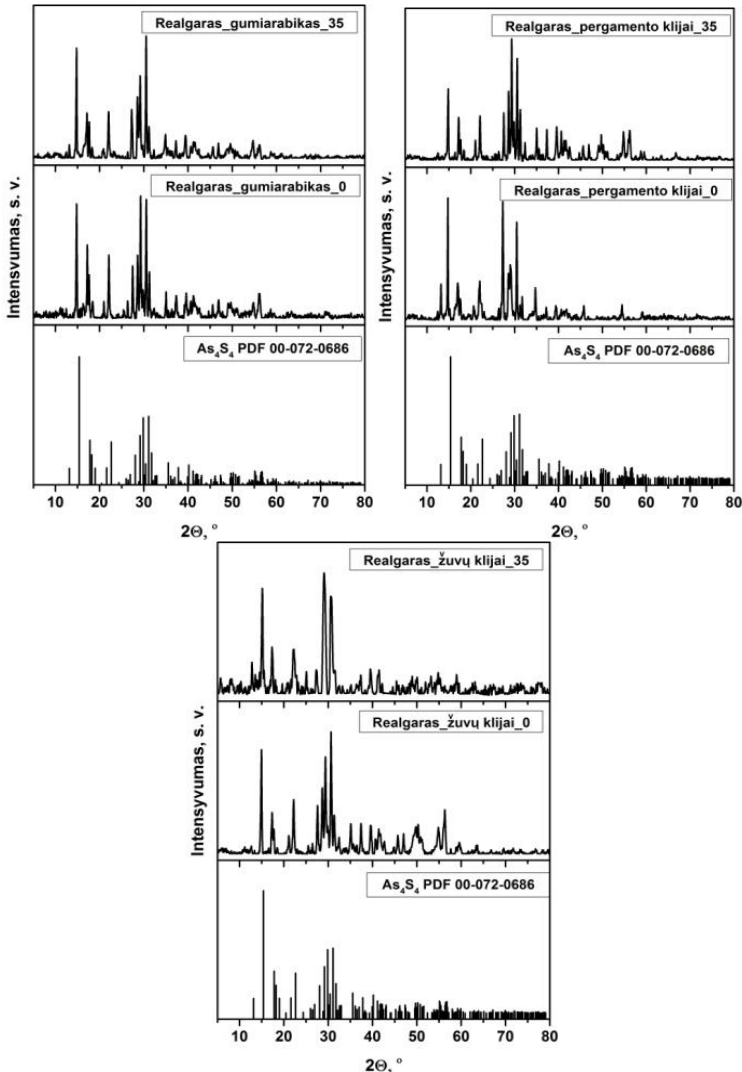


**5 pav.** Realgaro dažų FTIR spektrai su gumiarabiku (viršuje, kairėje), pergamento klijais (viršuje, dešinėje) ir žuvų klijais (apačioje), prieš (1) ir po (2) 35 dienų dirbtinio sendinimo

#### 2.2.4. XRD analizės rezultatai

Atlikus XRD analizę rišikliams po dirbtinio fotocheminio sendinimo, kaip ir buvo galima tikėtis, kristalinių fazių nenustatyta. Cinoberio dažų

XRD difraktogramose prieš ir po dirbtinio sendinimo reikšmingų pokyčių taip pat neįvyko. Buvo stebimos priemašinių fazių linijos, o dažuose su pergamento ir žuvų klijais buvo aptiktos mažo intensyvumo linijos prie  $2\theta = 7^\circ$  prieš sendinimą, ir tik žuvų klijuose po 35 dienų sendinimo. Raudonojo švino dažų kompozicijos su pergamento ir žuvų klijais po dirbtinio sendinimo turėjo naujas difrakcines linijas prie  $2\theta = 17,69^\circ$  ir tarp  $50\text{--}60^\circ$ , kurios rodo PbO formavimąsi. PbO susidarymas turėjo įtakos dažų spalvos pokyčiui.



**6 pav.** Realgaro su gumiarabiku (viršuje, kairėje), pergamento klijais (viršuje dešinėje) ir žuvų klijais (apačioje) XRD modeliai prieš ir po 35 dienų dirbtinio sendinimo



Didžiausi XRD pokyčiai difraktogramose stebimi dažų kompozicijose su realgaru (6 pav.). Po dirbtinio sendinimo, dažų kompozicijose buvo nustatytos arsenolitui ir pararealgarui būdingos difrakcinės linijos. Realgaro dažuose su gumiarabiku ir žuvų klijais difrakcinės linijos prie  $2\theta = 8,99^\circ$  ir  $12,85^\circ$  yra priskiriamos pararealgarui, o  $2\theta = 13,62^\circ$  ir  $25,13^\circ$  – arsenolitui. Dažuose su pergamento klijais nustatytos tiek pararealgarui, tiek arsenolitui priskiriamos difrakcinės linijos.

Raudonose geležies dažų kompozicijose didelių pokyčių nepastebėta. Stebimos priemaišinių ir rišiklių fazių smailės, hematito dažuose matoma  $\text{CaCO}_3$  būdinga linija prie  $2\theta = 29,64^\circ$ .








### 2.2.5. TG/DTG/DSC analizės rezultatai

Rišiklių terminė analizė neparodė didelių pokyčių po 35 dienų dirbtinio sendinimo. Buvo nežymūs TG/DTG/DSC kreivių poslinkiai  $\sim 10\text{--}20^\circ\text{C}$  temperatūros intervale. Cinoberio dažų kompozicijose pokyčių taip pat mažai. Raudonojo švino dažuose pastebėti tie patys pagrindiniai masės nuostoliai. Realgaro dažų su pergamento ir žuvų klijais DTG kreivės po sendinimo pasislinko į žemesnių temperatūrų intervalą apie  $20\text{--}50^\circ\text{C}$ , o tai gerai koreliuoja su kitais analizės rezultatais, kur buvo patvirtintas pastebimas degradacijos procesas. Raudonų geležies pigmentų terminės analizės pokyčiai nereikšmingi, daugiausia skirtumai susiję su neorganinių priemaišų buvimu.

### 2.3. Rekonstruotų raudonų dažų duomenų bazės taikymas originaliems rankraščiams

Šioje disertacijos dalyje anksčiau sukurta raudonų dažų duomenų bazė pritaikyta tirti ir apibūdinti LDK laikų rankraščius. Dauguma tirtų rankraščių priklausė F19 fondui, tačiau vyraujant vienos rūšies raudonam pigmentui (cinoberiui), buvo tirti F21 ir F22 fondai, siekiant surasti ir pritaikyti kitų raudonų pigmentų duomenų bazę. Pagrindinė informacija apie analizuojamus rankraščius (kurie saugomi LMAVB RS, Vilniuje), pateikta 5 lentelėje. Originalūs mėginiai buvo analizuojami SEM/EDX, FTIR, XRD ir TG/DTG/DSC analizės metodais.

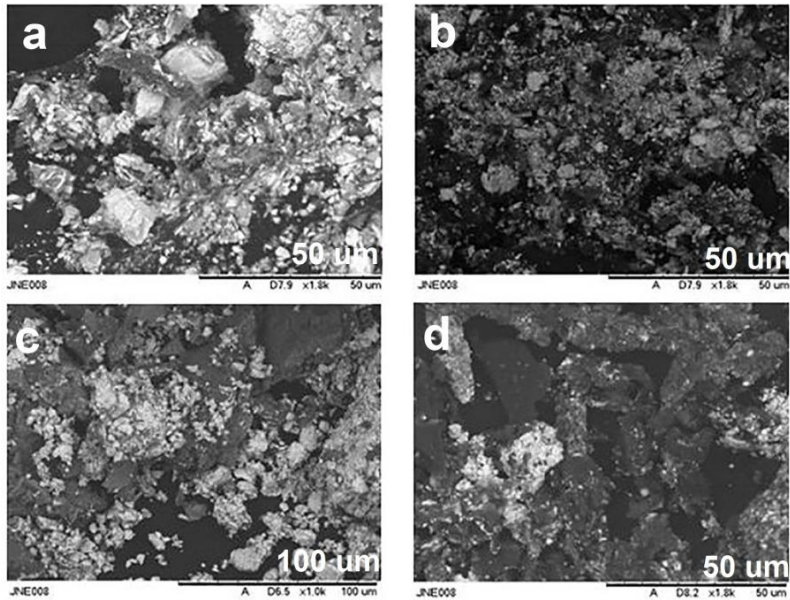
Lentelė 5. Pagrindinė informacija apie analizuojamus rankraščius

F19-115 (1662), psl. 170	F19-116 (1638-1639), psl. 5, 154, 260	F21-805 (XVI a.), psl. 250	F22-101 (1469-1494, 1607), psl. 6, 81, 138
	  		  

### 2.3.1. SEM/EDX analizės rezultatai

Raudona spalva yra dominuojanti visų tiriamų keturių knygų miniatiūrose ir rubrikose (žr. 5 lentelę). Pigmentų atspalviai labai įvairūs – nuo raudonai oranžinės, šviesiai raudonos iki ryškiai raudonos spalvos. Raudonų pigmentų mišiniai, ypač cinoberio su raudonuoju švinu, labai paplitę senuosiuose rankraščiuose, tačiau fondo F19, F21 ir F22 knygose jų nebuvo rasta. Cinoberis buvo nustatytas visuose tirtuose rankraščiuose, išskyrus vieną, kuriame buvo identifikuotas raudonasis švinas. Cinoberio dažų morfologija toje pačioje knygoje, bet skirtinguose puslapiuose buvo labai panaši. Reprezentacinės skirtingų mėginių SEM nuotraukos pateiktos 7 pav.

Raudoni dažai knygoje F19-115 buvo sudaryti iš skirtingos formos dalelių, kurių dydis svyravo nuo 1 iki 20  $\mu\text{m}$ . EDX elementinė analizė parodė, kad švino kiekis mėginyje buvo 63,5 m.%, taip pat nustatyta anglis (26,3 m.%) ir aliuminis (3,4 m.%). Likusiose knygose identifikuotas cinoberis. F19-116 knygoje pigmentas plokštelių pavidalo, tolygiai pasiskirstęs ant rišamosios medžiagos paviršiaus, nuo 1 iki 10  $\mu\text{m}$  dyžiu. EDX elementinė analizė parodė gyvsidabrį (62,3 m.%), sierą (11,4 m.%) ir popieriaus ar rišiklio priemaišas: anglį (19,5 m.%), deguonį (6,1 m.%) ir aliuminį (0,7 m.%).



**7 pav.** Raudonų dažų mėginių SEM nuotraukos iš analizuotų rankraščių: F19-115, psl. 170 (a); F19-116, psl. 154 (b); F22-805, psl. 250 (c) ir F21-101, psl. 6 (d)

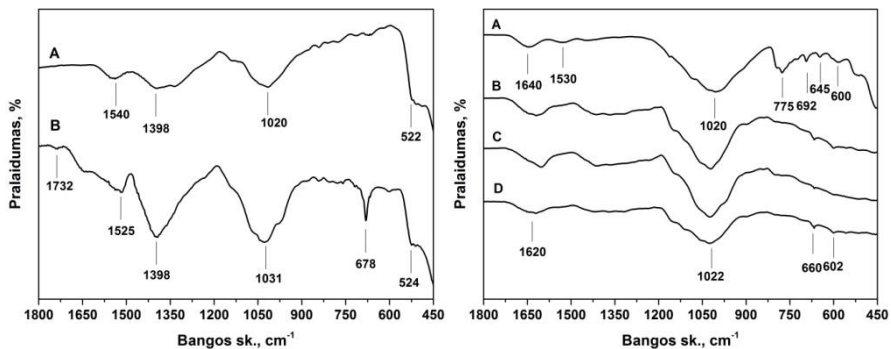
F21-805 knygos dažai sudaryti iš skirtingo dydžio aštrių aglomeratų, kurių dydis nuo 1 iki 20  $\mu\text{m}$ . EDX elementinė analizė parodė gyvsidabrij (72,1 m.%) ir sierą (14,5 m.%), be šių pagrindinių elementų nustatytas deguonis (10,8 m.%) ir aliuminis (2,6 m.%). Paskutinėje knygoje F22-101 pigmentas gerai sumaišytas su rišikliu. Dalelių dydis svyruoja nuo 1 iki 5  $\mu\text{m}$ . EDX elementinė analizė vėl parodė gyvsidabrio – 67,3 m.%, sieros – 13,7 m.% ir priemaišų (anglies – 15,7 m.%, deguonies 2,5 m.% ir aliuminio 0,6 m.%) buvimą.

Taigi, šiose knygoose tirti raudoni dažai buvo pakankamai gryni. Įdomu tai, kad dažuose neaptikta halogenų, kurie turi įtakos cinoberio tamsėjimui, arba sieros junginių, kurie sukelia  $\text{Pb}_3\text{O}_4$  patamsėjimą. Galima manyti, kad pigmentai buvo ypač kruopščiai paruošti ir naudoti tik aukščiausios kokybės.

### 2.3.1. FTIR analizės rezultatai

FTIR analizės metodas buvo puikus būdas identifikuoti rišikliams. Originalių raudonų dažų mėginių, paimtų iš rankraščių, FTIR spektrai buvo sėkmingai lyginami su užrašytais rekonstruotais ir dirbtinai pasendintais raudonų dažų, turinčių skirtingas rišamąsias medžiagas, spektrais. Tipiniai FTIR spektrai pateikti 8 pav. Knygos F19-115 dažai palyginti su

rekonstruotais raudonojo švino ir gumiarabiko dažais. Knygos dažuose aiškiai matomos Pb–O būdingos smailės prie 1398 ir 678  $\text{cm}^{-1}$ .



**8 pav.** Palyginamieji FTIR spektrai: kairėje F19-115, psl. 170 (B), (A) – raudonasis švinas su gumiarabiku po 35 dienų dirbtinio sendinimo, dešinėje F19-116, psl. 5 (B), 154 (C), 260 (D), (A) – cinoberis su žuvų klijais po 35 dienų dirbtinio sendinimo.

Intensyvesnės originalaus mėginio, nei dirbtinai sendinto rekonstruoto dažų mėginio smailės, gali būti siejamos su švino (II) oksido susidarymu, kuris turi įtakos pigmento spalvos pokyčiams. Naują absorbcijos smailę, esančią prie 1732  $\text{cm}^{-1}$ , galima priskirti polisacharidinių grandinių hidrolizei rišklyje. Likusios smailės taip pat priskiriamos gumiarabikui.

Knygos F19-116 mėginiai palyginti su cinoberio ir žuvų klijais. Rekonstruotų raudonų dažų (A) ir originalių mėginių (B, C, D) spektrai parodė nedidelius amidų grupės absorbcijos juostų skirtumus. Knygoje F19-116 matoma smailė prie 1620  $\text{cm}^{-1}$  (amidas I), o sendintų rekonstruotų dažų spektre prie 1640  $\text{cm}^{-1}$ . Tiriamuose spektruose nėra matoma amido II absorbcijos smailė ~ 1530  $\text{cm}^{-1}$ . Likusios smailės priskiriamos riškliui ir neorganiniams priedams. Knygoje F21-805 nustatytas cinoberis su pergamento klijais. FTIR spektrai beveik vienodi.

### 2.3.2. XRD analizės rezultatai

Atlikus XRD analizę, remiantis rekonstruota raudonų dažų duomenų baze, originaliuose mėginiuose iš knygų, buvo bandoma nustatyti ir palyginti komponentų kristalines formas. Raudonų dažų, surinktų iš tos pačios knygos, bet skirtingų puslapių, XRD duomenys buvo labai panašūs, o rezultatai gerai koreliavo su EDX ir FTIR analizės rezultatais. Pirmajame mėginyje F19-115 nustatyta raudonojo švino ( $\text{Pb}_3\text{O}_4$  PDF 00-041-1493) fazė. Reikšmingų skirtumų, palyginus su rekonstruotų dažų bazės duomenimis, nepastebėta, tik

nedideli PbO fazės intensyvumo svyravimai esant  $2\theta = 50\text{--}60^\circ$ . Kiti mėginiai F19-116, F21-805, F22-101 susideda iš HgS kristalinės fazės (PDF 96-901-2083). Vėlgi, XRD difraktogramose nestebimos rišiklio (gumiarabiko, pergamento ir žuvų klijų) difrakcijos linijos. Standartiniai XRD modeliai gerai sutampa su originalių pavyzdžių modeliais. Tačiau F21-805 ir F22-101 knygų mėginiuose matomos naujos difrakcijos linijos prie  $2\theta = 29,64^\circ$ , kurias galima priskirti  $\text{CaCO}_3$  fazei.

### 2.3.3. TG/DTG/DSC analizės rezultatai

Originaliems mėginiams iš knygų buvo atlikta terminė analizė, o gauti duomenys palyginti su rekonstruotų raudonų dažų terminės analizės rezultatais. Raudonojo švino su gumiarabiku pavyzdys iš knygos F19-115 pradėjo skilti tarp  $30\text{--}150^\circ\text{C}$  dėl adsorbuoto ir struktūrinio vandens išsiskyrimo, o masės nuostoliai buvo  $\sim 2,5\%$ . Antrasis, apie  $12\%$  masės nuostolis, esant maždaug  $200\text{--}370^\circ\text{C}$  temperatūrai, susijęs su polisacharidų skilimu, o trečiasis –  $\sim 8\%$  masės nuostolis, esant maždaug  $370\text{--}500^\circ\text{C}$  temperatūrai, yra susijęs su terminiu tarpinių liekanų, susidariusių karboksimetilintuose junginiuose, skaidymu. Maždaug  $2\%$  masės nuostolis nuo  $480\text{--}600^\circ\text{C}$  yra susijęs su raudonojo švino grįžtamuoju oksidacijos-redukcijos procesu, kai formuojasi PbO. Paskutinis,  $\sim 1,5\%$  masės nuostolis yra susijęs su kitais neorganiniais komponentais (aliuminiu ar kt.), kurie galėjo patekti į mėginį nuo popieriaus paviršiaus. Originalaus mėginio termogravimetrinės kreivės, palyginti su rekonstruotais raudonais dažais, yra apie  $50\text{--}70^\circ\text{C}$  žemesniame temperatūrų intervale. Tai gali būti susiejama su daline gumiarabiko hidrolize. Panašūs rišiklio terminiai procesai vyksta ir paskutiniame mėginyje F22-101, kur buvo nustatytas cinoberis su gumiarabiku. Cinoberis iš heksagoninės struktūros  $\alpha\text{-HgS}$  persitvarko į kubinės struktūros judąjį metacinoberį  $\beta\text{-HgS}$   $350\text{--}450^\circ\text{C}$  temperatūros intervale, taip pat gali vykti HgS garavimas ir esant deguoniui susidaryti  $\text{SO}_2$  ar  $\text{HgSO}_3$ .

Likusių mėginiuose (F19-116 ir F21-805) yra baltyminis rišiklis ir tas pats neorganinis pigmentas HgS. Baltyminių medžiagų skilimas visada vyksta dviem etapais. Pirmasis skilimas vyksta apie  $300^\circ\text{C}$  temperatūroje, antrasis – maždaug  $500^\circ\text{C}$  temperatūroje, kurie būdingi polipeptido grandinės terminiam oksidaciniam skilimui. Mūsų tiriamu atveju rišikliai yra beveik identiški (žuvų ir pergamento klijai), tačiau tik vienu atveju (F19-116) terminis skilimas yra aiškiai matomas. Antruoju atveju (F21-805) terminis kitimas yra labai nereikšmingas. HgS struktūriniai pokyčiai vyksta beveik vienodoje temperatūroje.

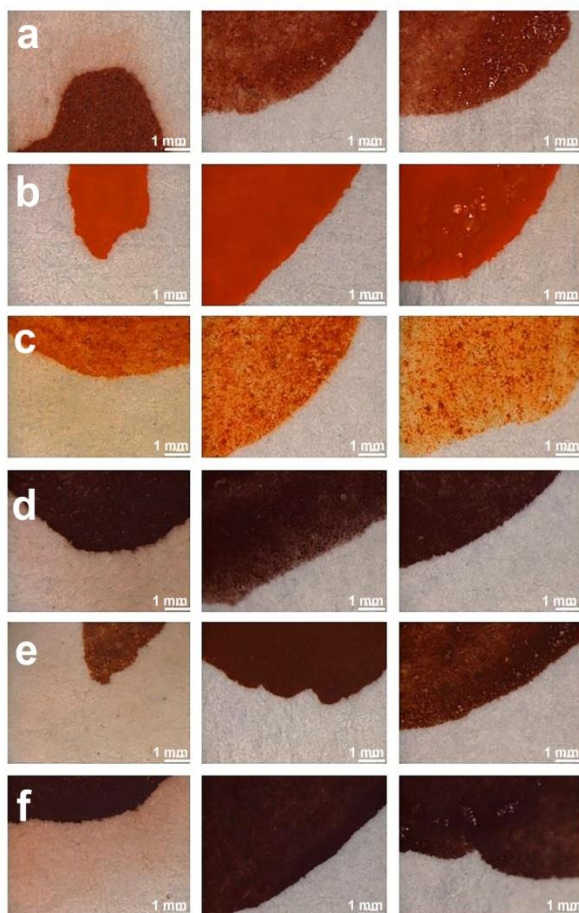
### 3. Jautrių vandeniui objektų plovimas ant kapiliarinio audinio

Restauravime nuo 2001 metų yra žinomas ir naudojamas kapiliarinis neaustinis audinys Paraprint OL60 spalvotų, vandeniui jautrių objektų, plovimui. Tačiau iki šiol nebuvo žinių apie jo panaudojimą Lietuvos restauravimo dirbtuvėse. Paraprint OL60 audinys yra 100% atsparus šarmams, plovimo metu ypač patogus, nes galima į plaunamą objektą iš karto įvesti norimas medžiagas (rišiklius, šarminį agentą, rankraščius, parašytus geležies-galo rašalais, apdoroti fitatais ir t.t.). Šis neaustinis audinys taip pat įdomus restauratoriams dėl savo stipraus kapiliarinio veikimo mechanizmo, didelio difuzijos greičio ir savo fizinio stabilumo. Tai neleidžia plovimo metu ištirpusiems junginiams migruoti atgal į plaunamą objektą.

Plaunant vandeniui jautrius objektus, restauratoriui yra didelis iššūkis pašalinti tirpius degradacijos produktus ir išaugoti takius įrašus.

Šiame darbe buvo išbandytas plovimas ant Paraprint OL60 audinio. Iš pradžių ant filtrinio popieriaus (5 cm x 10 cm) lakštų buvo paruošti skirtingi rekonstruotų raudonų dažų kompozicijų pavyzdžiai. Paraprint OL60 audinys buvo uždėtas ant organinio stiklo ir kruopščiai sudrėkintas. Paruošti mėginiai buvo švelniai drėkinami „GoreTex<sup>®</sup>“ sistemoje. Viršutinis Paraprint OL60 kraštas dedamas į rezervuarą su švariu vandeniu, apatinis kraštas kabo žemiau, ir į indą renkamas pratekėjęs vanduo. Apatinis Paraprint OL60 kraštas nukirptas 145 ° kampu, kad būtų lengiau surinkti vandenį. Sudrėkinti mėginiai buvo dedami ant Paraprint OL60 ir uždengiami antru organinio stiklo lakštu, siekiant sumažinti vandens garavimą iš popieriaus paviršiaus. Mūsų atveju plovimo procesas užtruko apie 1 val, o pratekėjęs vanduo surinktas tolimesniems tyrimams.

Originalaus objekto plovimas sustabdomas, kai ištekantis vanduo yra visiškai skaidrus. Procesas taip pat turėtų būti visą laiką stebimas, jei rašalai ar dažai pradėtų migruoti ar „judėti“ per popierių. Po plovimo, tiriami mėginiai buvo fotografuoti optiniu mikroskopu. Surinkti plovimo vandenys išgarinti iki sausos liekanos ir tirti FTIR ir SEM/EDX analizės metodais. Dažai su pergamento ir žuvų klijais po plovimo ant Paraprint OL60 kapiliarinio audinio nerodė jokių pokyčių, tačiau kompozicijose su gumiarabiku stebėta dažų migracija plovimo kryptimi (9 pav.).



**9 pav.** Dažų išplautų ant Paraprint OL60 audinio optinės nuotraukos: kairėje – gumiarabikas, viduryje – pergamento klėjai, dešinėje – žuvų klėjai. a – cinobris, b – raudonasis švinas, c – realgaras, d – raudonoji ochra, e – raudonasis molis, f – hematitas

Ištirus visas nuosėdas FTIR analizės metodu, nustatytos acto rūgštis, kuri buvo naudota dažų kompozicijų gamybos procese, būdingos absorbcijos smailės prie  $1780\text{--}1720\text{ cm}^{-1}$  C=O, ir  $700\text{--}500\text{ cm}^{-1}$  C=O ir C–O, taip pat nežymūs baltyminių rišiklių amidų poslinkiai. Nė viename FTIR spektre nebuvo identifikuotos smailės, priskiriamos konkrečiam pigmentui.

Nuosėdų SEM/EDX analizė parodė, kad visuose mėginiuose pagrindiniai elementai buvo C (~ 50–60 m.%) ir O (~ 20–30 m.%), likę elementai buvo Na, Mg, Al, Si, P, S, Cl, K, Ca ir Cu. Tik gumiarabiko su cinobriu, realgaru ir hematitu mėginiuose buvo nedidelis pigmento priemaišų kiekis (~ 0,4–0,7 m.%). Filtro popieriaus SEM/EDX analizės rezultatai: C (61,17 m.%), O (36,51 m.%), Al (1,77 m.%), Si (0,20 m.%), Ca (0,20 m.%), Cu (0,15 m.%),

o po plovimo – C (59,13 m.%), O (38,81 m.%), Al (1,85 m.%), Si (0,07 m.%), Cu (0,14 m.%).

Kapiliarinis plovimo būdas buvo tinkamas ir saugus mėginiams su pergamento ir žuvų kljais, tačiau netiko mėginiams su gumiarabiku. Kaip ir visi plovimo būdai, šis turi savo privalumų: patogus, lengvai kontroliuojamas procesas, plovimo metu viršutinis dažų sluoksnis mažiau veikiamas vandens, ekonomišką.

## IŠVADOS

1. Šiame darbe SEM/EDX, FTIR, XRD ir TG/DTG/DSC analizės metodais ištyrus šešis skirtingus istorinius raudonus pigmentus (natūralų cinoberį, Monte Amiata (HgS), raudonąjį šviną (Pb<sub>3</sub>O<sub>4</sub>), realgarą (As<sub>4</sub>S<sub>4</sub>), Andalūzijos raudonąją ochrą (Fe<sub>2</sub>O<sub>3</sub>), raudonąjį molį (Fe<sub>2</sub>O<sub>3</sub>·xSiO<sub>2</sub>·yAl<sub>2</sub>O<sub>3</sub>), hematitą (Fe<sub>2</sub>O<sub>3</sub>)) ir tris rišiklius (gumiarabiką, pergamento ir žuvų kljus) kaip standartines medžiagas, pagaminta aštuoniolika skirtingų, analogiškų istoriniams, raudonų dažų kompozicijų. Paruoštas kompozicijas pasendinus 35 dienas dirbtinio fotocheminio sendinimo kameroje ir atlikus spalvos pokyčio, SEM/EDX, FTIR, XRD ir TG/DTG/DSC tyrimus prieš ir po sendinimo sukurta raudonų pigmentų, dažų ir rišiklių duomenų bazė.

2. Vieninių medžiagų SEM analizė parodė, kad medžiagų morfologija labai priklauso nuo jų prigimties, o EDX parodė, kad tirtuose mėginiuose yra priemaišinių cheminių elementų. FTIR spektruose buvo stebimos papildomos priemaišinių junginių absorbcijos juostos, o XRD rezultatai gerai sutapo su SEM/EDX ir FTIR analizės rezultatais. Iš *Kremer Pigmente* įsigytų realgaro ir raudonojo švino pigmentų cheminė sudėtis atitiko aprašytą kataloge, tačiau likusiuose keturiuose pigmentuose buvo skirtingų priemaišų.

3. Pagamintos raudonų dažų kompozicijos, nepriklausomai nuo naudotų rišiklių, su cinoberiu buvo ryškiai raudonos spalvos, raudonojo švino ir realgaro – raudonai oranžinės, raudonosios ochros – tamsiai raudonos spalvos. Kompozicijos su raudonojo molio ir pergamento ar žuvų kljais turėjo šiek tiek gelsvą atspalvį. Raudonai rusvos spalvos dažai buvo gauti naudojant hematitą. Po dirbtinio sendinimo didžiausias spalvų pokytis buvo realgaro dažų kompozicijoms. Šie dažai pašviesėjo ir įgijo žalsvą, gelsvą atspalvį. Nežymiai pakeitė spalvą raudoni švino dažai, o cinoberio ir raudoni geležies dažai beveik nepasikeitė.

4. Remiantis SEM rezultatais, po 35 dienų dirbtinio sendinimo raudonų dažų paviršiaus morfologija reikšmingai nepasikeitė. Tačiau daugeliu atvejų dalelių dydis sumažėjo. FTIR spektroskopijos rezultatai leido daryti išvadą,



kad dirbtinis sendinimas turėjo žalingą poveikį. Naujos absorbcijos juostos prie 790 ir 480  $\text{cm}^{-1}$  buvo matomos realgaro dažuose su visais riškiais. XRD analizės rezultatai taip pat patvirtino FTIR spektroskopijos rezultatus. Raudonojo švino su pergamento ir žuvų klijais XRD difraktogramose po senėjimo buvo nustatytos difrakcinės linijos, priskirtos PbO. Realgaro XRD difraktogramos po dirbtinio sendinimo parodė balto arsenolito  $\text{As}_2\text{O}_3$  ir geltono pararealgaro  $\text{As}_4\text{S}_4$  susidarymą. TG/DTG/DSC kreivės po dirbtinio sendinimo buvo nežymiai pasislinkusios į žemesnių temperatūrų intervalą.

5. Pirmą kartą LDK laikų rankraščiams tirti ir apibūdinti buvo pritaikyta sukurta raudonų dažų duomenų bazė. SEM/EDX ir XRD analizės duomenys parodė, kad tiriamuoju laikotarpiu F19 fonde vyravo cinoberio pigmentas, tačiau buvo aptiktas ir raudonasis švinas. Raudoni dažai buvo pakankamai grynai ir neturėjo daug priemaišų, tik knygoje F19-115 identifikuotas PbO, kuris turi įtakos dažų šviesėjimui.

6. Knygų F19-115 ir F19-116 dažų mėginių FTIR spektruose matomos rišklio destrukcijai būdingos absorbcijos juostos. Gumiarabike identifikuotas C=O grupių formavimasis, susijęs su polisacharidų grandinės hidrolize ir turintis įtakos blogam dažų sukibimui su paviršiumi. Žuvų klijų FTIR spektras nerodė amido II grupės, o tai gali būti siejama su kolageno daline hidrolize dažuose.

7. Išbandytas naujas, iki šiol Lietuvos restauratorių netaikytas, vandeniui jautrių objektų kapiliarinis plovimas ant neaustinio Paraprint OL60 audinio. Plovimas atliktas visoms rekonstruotų raudonų dažų kompozicijoms. Šis būdas buvo tinkamas ir saugus mėginiam su pergamento ir žuvų klijais, tačiau mėginiai su gumiarabiku buvo takūs. Norint pritaikyti šį plovimo būdą originaliems kultūros paveldo objektams, reikėtų žinoti tikslią dažų sudėtį.

8. Šis darbas dar kartą parodė, kaip svarbu tiriant kultūros paveldo objektus taikyti kelis tyrimo metodus. Neinvaziniai kultūros paveldo objektų tyrimo metodai visada galėtų būti naudingesni, tačiau, turint pakankamą mėginio kiekį, galima sėkmingai naudoti FTIR, SEM/EDX, XRD ir TG/DTG/DSC analizės metodus, taip išvengiant galimos sudedamųjų dalių įtakos rezultatų patikimumui.

## MOKSLINIŲ PUBLIKACIJŲ DISERTACIJOS TEMA SĄRAŠAS

### **Straipsniai recenzuojamuose žurnaluose:**

1. Čiuladienė, Aušra, Kareiva, Aivaras. (2021). Application of red paint data library for the characterization of the manuscript from Grand Duchy of Lithuania. *Microchemical Journal*, 164, 105961. <https://doi.org/10.1016/j.microc.2021.105961>
2. Čiuladienė, Aušra, Beganskienė, Aldona, Senvaitienė, Jūratė, Kareiva, Aivaras. (2021). Study of the red iron paints for rubrics and miniatures: accelerated aging and analytical data. *Materials Science (Medžiagotyra)*, 27(1), 77–83. <https://doi.org/10.5755/j02.ms.25190>
3. Čiuladienė, Aušra, Kareiva, Aivaras, Raudonis, Rimantas. (2020). From model to artefact: Versatile characterization of cinnabar, red lead and realgar red paints for rubrics and miniatures. *Chemija*, 31(4), 238–246. <https://doi.org/10.6001/chemija.v31i4.4320>
4. Čiuladienė, Aušra, Luckutė, Austėja, Kiuberis, Jonas, Kareiva, Aivaras. (2018). Investigation of the chemical composition of red pigments and binding media. *Chemija*, 29(4), 243–256. <https://doi.org/10.6001/chemija.v29i4.3840>

### **Pranešimų mokslinėse konferencijose tezės:**

1. Čiuladienė, Aušra, Kareiva, Aivaras. (2021). Identifying an illuminated and rubricated manuscript using red paint database. *Meetings of conservators and restorers of archival and library materials and art on paper, May 26-28, 2021, Dubrovnik, Croatia*.
2. Čiuladienė, Aušra, Kareiva, Aivaras. (2020). Determination of red paint using the database of analysis of red pigments. *Research. Dilemmas. Solutions: The 12-Th Baltic States Triennial Conservators' Meeting, Vilnius, Lithuania, 2020: Preprints, 399–400*.
3. Čiuladienė, Aušra, Kareiva, Aivaras. (2019). Painting the page – the red paint analysis an illuminated and rubricated manuscript. *4th*

*International Student Conference of Conservation and Restoration of Works of Art, November 6-8, 2019, Cracow, Poland.*

4. Čiuladienė, Aušra, Luckutė, Austėja, Kareiva, Aivaras. (2018). Investigation of red ballpoint pen inks. *EcoBalt 2018: The International Conference Proceedings Book, October 25-27, 2018, Vilnius, Lithuania.* p. 45.

5. Čiuladienė, Aušra, Luckutė, Austėja, Kareiva, Aivaras. (2018). On the chemical composition of red pigments and binding medium. *Advanced Materials and Technologies 2018: Book of Abstracts of 20th International Conference-School, August 27-31, 2018, Palanga, Lithuania, Kaunas: Technologija.* p. 100.

## CURRICULUM VITAE

---

### ASMENINĖ INFORMACIJA

---

Vardas, pavardė	Aušra Čiuladienė
Gimimo data	1987 09 04
El. pašto adresas	ciuladiene.ausra@gmail.com
Telefono numeris	+370 626 46311

---

### IŠSILAVINIMAS IR KVALIFIKACIJA

---

2010 – 2012 m.	Chemijos magistro kvalifikacinis laipsnis Vilniau universitetas
2006 – 2010 m.	Konservavimo ir restauravimo chemijos bakalauro kvalifikacinis laipsnis Vilniaus universitetas

---

### DARBO PATIRTIS

---

2011 – iki dabar	LMA Vrublevskių bibliotekos Dokumentų konservavimo ir restaruravimo skyriaus restauratorė, chemikė-technologė
------------------	---

---

### DALYVAVIMAS MOKYMUOSE IR TARPTAUTINĖSE MOKYKLOSE

---

2019 06 10 – 2019 06 13	Tarptautiniai pigmentų identifikavimo kursai, „Identification of Pigments“, Londonas, Jungtinė Karalystė
-------------------------	--

---

## REFERENCES

- [1] Faubel, W.; Staub, S.; Simon, R.; Heissler, S.; Pataki, A.; Banik, G. Non-Destructive Analysis for the Investigation of Decomposition Phenomena of Historical Manuscripts and Prints. *Spectrochimica Acta - Part B Atomic Spectroscopy*, **2007**, *62* (6-7 SPEC. ISS.), 669–676. <https://doi.org/10.1016/j.sab.2007.03.029>.
- [2] Fierascu, I.; Fierascu, R. C.; Stirban, A.; Panaitescu, D. M.; Nicolae, C. A.; Raditoiu, V.; Zgarciu, M. S.; Leahu, A. C. Chemical and Mineral Characterization of Romanian Book Paper Materials (XVII–XIXth Century). *Microchemical Journal*, **2020**, *152*, 104307. <https://doi.org/10.1016/j.microc.2019.104307>.
- [3] Legrand, S.; Ricciardi, P.; Nodari, L.; Janssens, K. Non-Invasive Analysis of a 15th Century Illuminated Manuscript Fragment: Point-Based vs Imaging Spectroscopy. *Microchemical Journal*, **2018**, *138*, 162–172. <https://doi.org/10.1016/j.microc.2018.01.001>.
- [4] Cucci, C.; Bracci, S.; Casini, A.; Innocenti, S.; Picollo, M.; Stefani, L.; Rao, I. G.; Scudieri, M. The Illuminated Manuscript Corale 43 and Its Attribution to Beato Angelico: Non-Invasive Analysis by FORS, XRF and Hyperspectral Imaging Techniques. *Microchemical Journal*, **2018**, *138*, 45–57. <https://doi.org/10.1016/j.microc.2017.12.021>.
- [5] Aceto, M.; Agostino, A.; Fenoglio, G.; Gulmini, M.; Bianco, V.; Pellizzi, E. Non Invasive Analysis of Miniature Paintings: Proposal for an Analytical Protocol. *Spectrochimica Acta - Part A: Molecular and Biomolecular Spectroscopy*, **2012**, *91*, 352–359. <https://doi.org/10.1016/j.saa.2012.02.021>.
- [6] Janssens, K.; Van der Snickt, G.; Vanmeert, F.; Legrand, S.; Nuyts, G.; Alfeld, M.; Monico, L.; Anaf, W.; De Nolf, W.; Vermeulen, M.; et al. Non-Invasive and Non-Destructive Examination of Artistic Pigments, Paints, and Paintings by Means of X-Ray Methods. *Topics in Current Chemistry*, **2016**, *374* (6), 1–52. <https://doi.org/10.1007/s41061-016-0079-2>.
- [7] Cicėnienė, R. Rankraštinė knyga Lietuvos Didžiojoje Kunigaikštystėje XIV a. pradžioje - XVI a. viduryje: sklaidos ir funkcionavimo sąlygos. *Knygotyra*, **2015**, *53*, 7–37. <https://doi.org/10.15388/kn.v53i0.7803>.
- [8] Van Der Snickt, G.; De Nolf, W.; Vekemans, B.; Janssens, K.  $\mu$ -XRF/ $\mu$ -RS vs. SR  $\mu$ -XRD for Pigment Identification in Illuminated Manuscripts. *Applied Physics A: Materials Science and Processing*, **2008**, *92* (1), 59–68. <https://doi.org/10.1007/s00339-008-4447-9>.
- [9] Ghezzi, L.; Duce, C.; Bernazzani, L.; Bramanti, E.; Colombini, M. P.; Tiné, M. R.; Bonaduce, I. Interactions between Inorganic Pigments and Rabbit Skin Glue in Reference Paint Reconstructions. *Journal of Thermal Analysis and Calorimetry*, **2015**, *122* (1), 315–322.

- <https://doi.org/10.1007/s10973-015-4759-x>.
- [10] Vieira, M.; Nabais, P.; Angelin, E. M.; Araújo, R.; Lopes, J. A.; Martín, L.; Sameño, M.; Melo, M. J. Organic Red Colorants in Islamic Manuscripts (12th - 15th c.) Produced in Al-Andalus, Part 1. *Dyes and Pigments*, **2019**, *166*, 451–459. <https://doi.org/10.1016/j.dyepig.2019.03.061>.
- [11] Hogan, C.; Da Pieve, F. Colour Degradation of Artworks: An Ab Initio Approach to X-Ray, Electronic and Optical Spectroscopy Analyses of Vermilion Photodarkening. *Journal of Analytical Atomic Spectrometry*, **2015**, *30* (3), 588–598. <https://doi.org/10.1039/c4ja00327f>.
- [12] Bruni, S.; Cariati, F.; Casadio, F.; Toniolo, L. Identification of Pigments on a XV Century Illuminated Parchment by Raman and FTIR Microspectroscopies. *Spectrochimica Acta - Part A: Molecular and Biomolecular Spectroscopy*, **1999**, *55* (7–8), 1371–1377. [https://doi.org/10.1016/S1386-1425\(98\)00300-X](https://doi.org/10.1016/S1386-1425(98)00300-X).
- [13] Whitney, A. V.; Casadio, F.; Van Duyne, R. P. Identification and Characterization of Artists' Red Dyes and Their Mixtures by Surface-Enhanced Raman Spectroscopy. *Applied Spectroscopy*, **2007**, *61* (9), 994–1000. <https://doi.org/10.1366/000370207781745838>.
- [14] Vila, A.; García, J. F. Analysis of the Chemical Composition of Red Pigments and Inks for the Characterization and Differentiation of Contemporary Prints. *Analytical Letters*, **2012**, *45* (10), 1274–1285. <https://doi.org/10.1080/00032719.2012.673100>.
- [15] Wallert, A.; Hermens, E.; Peek, M. 1995. *Historical Painting Techniques, Materials, and Studio Practice: Preprints of a Symposium, University of Leiden, the Netherlands, 26-29 June, 1995*. Marina Del Rey, CA: Getty Conservation Institute.
- [16] Barnett, J. R.; Miller, S.; Pearce, E. Colour and Art: A Brief History of Pigments. *Optics and Laser Technology*, **2006**, *38* (4–6), 445–453. <https://doi.org/10.1016/j.optlastec.2005.06.005>.
- [17] Abel, A. *The History of Dyes and Pigments* (Second Edi.). Elsevier Ltd. 2012. <https://doi.org/10.1016/b978-0-08-101270-3.00024-2>.
- [18] Goltz, D. M. A Review of Instrumental Approaches for Studying Historical Inks. *Analytical Letters*, **2012**, *45* (4), 314–329. <https://doi.org/10.1080/00032719.2011.644712>.
- [19] Bagdzevičienė, J.; Kruopaitė, L. *Pigmentai Ir Dažikliai Restauruojant Kultūros Vertybes*; Vilnius : Savastis, 2005.
- [20] Doménech-Carbó, M. T. Novel Analytical Methods for Characterising Binding Media and Protective Coatings in Artworks. *Analytica Chimica Acta*, **2008**, *621* (2), 109–139. <https://doi.org/10.1016/j.aca.2008.05.056>.
- [21] Kroustallis, S. Binding Media in Medieval Manuscript Illumination: A Source Research. *Revista de História da Arte*, **2011**, *W* (1), 112–125.

- [22] Melo, M. J.; Castro, R.; Nabais, P.; Vitorino, T. The Book on How to Make All the Colour Paints for Illuminating Books: Unravelling a Portuguese Hebrew Illuminators' Manual. *Heritage Science*, **2018**, *6* (1), 1–8. <https://doi.org/10.1186/s40494-018-0208-z>.
- [23] Zhao, C.; Zhang, Y.; Wang, C. C.; Hou, M.; Li, A. Recent Progress in Instrumental Techniques for Architectural Heritage Materials. *Heritage Science*, **2019**, *7* (1), 1–50. <https://doi.org/10.1186/s40494-019-0280-z>.
- [24] Thompson, D. *The Materials and Techniques of Medieval Painting*; New York : Dover Publications, 1956.
- [25] Johnston, M.; Van Dussen, M. *The Medieval Manuscript Book*; Cambridge : Cambridge University Press, 2015. <https://doi.org/10.1017/CBO9781107588851>.
- [26] Whetter, K. S., Kevin S. *The Manuscript and Meaning of Malory's 'Morte d'Arthur' : Rubrication, Commemoration, Memorialization*; Boydell & Brewer, D. S. Brewer, 2017.
- [27] Hamel, C. De. *The British Library Guide to Manuscript Illumination : History and Techniques*; Toronto : University of Toronto Press, 2001.
- [28] Miguel, C.; Pinto, J. V.; Clarke, M.; Melo, M. J. The Alchemy of Red Mercury Sulphide: The Production of Vermilion for Medieval Art. *Dyes and Pigments*, **2014**, *102*, 210–217. <https://doi.org/10.1016/j.dyepig.2013.10.041>.
- [29] Tumer, N. The Recipe Collection of Johannes Alcherius and the Painting Materials Used in Manuscript Illumination in France and Northern Italy, c. 1380-1420 . *Studies in Conservation*, **2014**, *43* (sup1), 45–50. <https://doi.org/10.1179/sic.1998.43.supplement-1.45>.
- [30] Melo, M. J.; Araújo, R.; Castro, R.; Casanova, C. Colour Degradation in Medieval Manuscripts. *Microchemical Journal*, **2016**, *124*, 837–844. <https://doi.org/10.1016/j.microc.2015.10.014>.
- [31] Moura, L.; Melo, M. J.; Casanova, C.; Claro, A. A Study on Portuguese Manuscript Illumination: The Charter of Vila Flor (Flower Town), 1512. *Journal of Cultural Heritage*, **2007**, *8* (3), 299–306. <https://doi.org/10.1016/j.culher.2007.02.003>.
- [32] Siddall, R. Mineral Pigments in Archaeology: Their Analysis and the Range of Available Materials. *Minerals*, **2018**, *8* (5), 1–35. <https://doi.org/10.3390/min8050201>.
- [33] Iriarte, E.; Foyo, A.; Sánchez, M. A.; Tomillo, C.; Setién, J. The Origin and Geochemical Characterization of Red Ochres from the Tito Bustillo and Monte Castillo Caves (Northern Spain). *Archaeometry*, **2009**, *51* (2), 231–251. <https://doi.org/10.1111/j.1475-4754.2008.00397.x>.
- [34] Shrimali, K.; Jin, J.; Hassas, B. V.; Wang, X.; Miller, J. D. The Surface State of Hematite and Its Wetting Characteristics. *Journal of Colloid and Interface Science*, **2016**, *477*, 16–24.

- <https://doi.org/10.1016/j.jcis.2016.05.030>.
- [35] Cornell, R. M.; Schwertmann, U. *The Iron Oxides: Structure, Properties, Reactions, Occurrences and Uses*. Weinheim : WILEY-VCH Verlag GmbH & Co. KGaA, 2003. <https://doi.org/10.1002/3527602097>.
- [36] Teja, A. S.; Koh, P. Y. Synthesis, Properties, and Applications of Magnetic Iron Oxide Nanoparticles. *Progress in Crystal Growth and Characterization of Materials*, **2009**, 55 (1–2), 22–45. <https://doi.org/10.1016/j.pcrysgrow.2008.08.003>.
- [37] Capel, J.; Huertas, F.; Pozzuoli, A.; Linares, J. Red Ochre Decorations in Spanish Neolithic Ceramics: A Mineralogical and Technological Study. *Journal of Archaeological Science*, **2006**, 33 (8), 1157–1166. <https://doi.org/10.1016/j.jas.2005.12.004>.
- [38] Eiselt, B. S.; Popelka-Filcoff, R. S.; Darling, J. A.; Glascock, M. D. Hematite Sources and Archaeological Ochres from Hohokam and O’odham Sites in Central Arizona: An Experiment in Type Identification and Characterization. *Journal of Archaeological Science*, **2011**, 38 (11), 3019–3028. <https://doi.org/10.1016/j.jas.2011.06.030>.
- [39] Opuchovic, O.; Kareiva, A. Historical Hematite Pigment: Synthesis by an Aqueous Sol-Gel Method, Characterization and Application for the Colouration of Ceramic Glazes. *Ceramics International*, **2015**, 41 (3), 4504–4513. <https://doi.org/10.1016/j.ceramint.2014.11.145>.
- [40] Sanson, A.; Mathon, O.; Pascarelli, S. Local Vibrational Dynamics of Hematite ( $\alpha$ -Fe<sub>2</sub>O<sub>3</sub>) Studied by Extended x-Ray Absorption Fine Structure and Molecular Dynamics. *Journal of Chemical Physics*, **2014**, 140 (22), 1–8. <https://doi.org/10.1063/1.4882282>.
- [41] Hradil, D.; Grygar, T.; Hradilová, J.; Bezdička, P. Clay and Iron Oxide Pigments in the History of Painting. *Applied Clay Science*, **2003**, 22 (5), 223–236. [https://doi.org/10.1016/S0169-1317\(03\)00076-0](https://doi.org/10.1016/S0169-1317(03)00076-0).
- [42] Barata, C.; Rocha, F.; Cruz, A. J.; Andrejkovičová, S.; Reguer, S. Synchrotron X-Ray Diffraction of Bole Layers from Portuguese Gilded Baroque Retables. *Applied Clay Science*, **2015**, 116–117, 39–45. <https://doi.org/10.1016/j.clay.2015.08.012>.
- [43] Hradil, D.; Hradilová, J.; Bezdička, P.; Serendan, C. Late Gothic/Early Renaissance Gilding Technology and the Traditional Poliment Material “Armenian Bole”: Truly Red Clay, or Rather Bauxite? *Applied Clay Science*, **2017**, 135, 271–281. <https://doi.org/10.1016/j.clay.2016.10.004>.
- [44] Elert, K.; Cardell, C. Weathering Behavior of Cinnabar-Based Tempera Paints upon Natural and Accelerated Aging. *Spectrochimica Acta - Part A: Molecular and Biomolecular Spectroscopy*, **2019**, 216, 236–248. <https://doi.org/10.1016/j.saa.2019.03.027>.
- [45] King, R. J. Minerals Explained 37: Cinnabar. *Geology Today*, **2002**,



- 18 (5), 195–199.
- [46] Roy, A. *Artists' Pigments: A Handbook of Their History and Characteristics, Volume 2*; Washington : National Gallery of Art, 1986.
- [47] Nöller, R. Cinnabar Reviewed: Characterization of the Red Pigment and Its Reactions. *Studies in Conservation*, **2015**, 60 (2), 79–87. <https://doi.org/10.1179/2047058413y.0000000089>.
- [48] Chiriu, D.; Pala, M.; Pisu, F. A.; Cappellini, G.; Ricci, P. C.; Carbonaro, C. M. Time through Colors: A Kinetic Model of Red Vermilion Darkening from Raman Spectra. *Dyes and Pigments*, **2021**, 184, 108866. <https://doi.org/10.1016/j.dyepig.2020.108866>.
- [49] Miguel, C.; Claro, A.; Gonçalves, A. P.; Muralha, V. S. F.; Melo, M. J. A Study on Red Lead Degradation in a Medieval Manuscript Lorvão Apocalypse (1189). *Journal of Raman Spectroscopy*, **2009**, 40 (12), 1966–1973. <https://doi.org/10.1002/jrs.2350>.
- [50] Holley, E. A.; James McQuillan, A.; Craw, D.; Kim, J. P.; Sander, S. G. Mercury Mobilization by Oxidative Dissolution of Cinnabar ( $\alpha$ -HgS) and Metacinnabar ( $\beta$ -HgS). *Chemical Geology*, **2007**, 240 (3–4), 313–325. <https://doi.org/10.1016/j.chemgeo.2007.03.001>.
- [51] Spring, M.; Grout, R. The Blackening of Vermilion: An Analytical Study of the Process in Paintings. *National Gallery Technical Bulletin*, **2002**, 23, 50–61.
- [52] McCormack, J. K. The Darkening of Cinnabar in Sunlight. *Mineralium Deposita*, **2000**, 35 (8), 796–798. <https://doi.org/10.1007/s001260050281>.
- [53] Radepont, M.; Coquinot, Y.; Janssens, K.; Ezrati, J. J.; De Nolf, W.; Cotte, M. Thermodynamic and Experimental Study of the Degradation of the Red Pigment Mercury Sulfide. *Journal of Analytical Atomic Spectrometry*, **2015**, 30 (3), 599–612. <https://doi.org/10.1039/c4ja00372a>.
- [54] Vahur, S. *Expanding the Possibilities of ATR-FT-IR Spectroscopy in Determination of Inorganic Pigments*; Tartu : Tartu University Press, 2010.
- [55] Pessanha, S.; Carvalho, M. L.; Manso, M.; Guilherme, A.; Marques, A. F.; Perez, C. A. Hg Diffusion in Books of XVIII and XIX Centuries by Synchrotron Microprobe. *Spectrochimica Acta - Part B Atomic Spectroscopy*, **2009**, 64 (8), 805–807. <https://doi.org/10.1016/j.sab.2009.05.018>.
- [56] Terrapon, V.; Béarat, H. A Study of Cinnabar Blackening: New Approach and Treatment Perspective. *Conference paper: The 7th International Conference on Science and Technology in Archaeology and Conservation at Petra*, **2010**, No. December, 1–11.
- [57] Keune, K.; Mass, J.; Meirer, F.; Pottasch, C.; Van Loon, A.; Hull, A.; Church, J.; Pouyet, E.; Cotte, M.; Mehta, A. Tracking the Transformation and Transport of Arsenic Sulfide Pigments in Paints:

- Synchrotron-Based X-Ray Micro-Analyses. *Journal of Analytical Atomic Spectrometry*, **2015**, *30* (3), 813–827.  
<https://doi.org/10.1039/c4ja00424h>.
- [58] FitzHugh, E. W. *Artists' Pigments: A Handbook of Their History and Characteristics, Volume 3*; Washington : National Gallery of Art, 1997.
- [59] Wu, Y.; Zhou, X. yong; Lei, M.; Yang, J.; Ma, J.; Qiao, P. wei; Chen, T. bin. Migration and Transformation of Arsenic: Contamination Control and Remediation in Realgar Mining Areas. *Applied Geochemistry*, **2017**, *77*, 44–51.  
<https://doi.org/10.1016/j.apgeochem.2016.05.012>.
- [60] Kyono, A.; Kimata, M.; Hatta, T. Light-Induced Degradation Dynamics in Realgar: In Situ Structural Investigation Using Single-Crystal X-Ray Diffraction Study and X-Ray Photoelectron Spectroscopy. *American Mineralogist*, **2005**, *90* (10), 1563–1570.  
<https://doi.org/10.2138/am.2005.1785>.
- [61] Bonazzi, P.; Bindi, L.; Muniz-Miranda, M.; Chelazzi, L.; Rödl, T.; Pfitzner, A. Light-Induced Molecular Change in HgI<sub>2</sub> As<sub>4</sub>S<sub>4</sub>: Evidence by Single-Crystal X-Ray Diffraction and Raman Spectroscopy. *American Mineralogist*, **2011**, *96* (4), 646–653.  
<https://doi.org/10.2138/am.2011.3654>.
- [62] Bindi, L.; Popova, V.; Bonazzi, P. Uzonite, As<sub>4</sub>S<sub>5</sub>, from the Type Locality: Single-Crystal X-Ray Study and Effects of Exposure to Light. *Canadian Mineralogist*, **2003**, *41* (6), 1463–1468.  
<https://doi.org/10.2113/gscanmin.41.6.1463>.
- [63] Keune, K.; Mass, J.; Mehta, A.; Church, J.; Meirer, F. Analytical Imaging Studies of the Migration of Degraded Orpiment, Realgar, and Emerald Green Pigments in Historic Paintings and Related Conservation Issues. *Heritage Science*, **2016**, *4* (1), 1–14.  
<https://doi.org/10.1186/s40494-016-0078-1>.
- [64] Ballirano, P. Thermal Behavior of Realgar As<sub>4</sub>S<sub>4</sub>, and of Arsenolite As<sub>2</sub>O<sub>3</sub> and Non-Stoichiometric As<sub>8</sub>S<sub>8+x</sub> Crystals Produced from As<sub>4</sub>S<sub>4</sub> Melt Recrystallization. *American Mineralogist*, **2012**, *97* (8–9), 1320–1329. <https://doi.org/10.2138/am.2012.4114>.
- [65] Daniels, V.; Leach, B. The Occurrence and Alteration of Realgar on Ancient Egyptian Papyri. *Studies in Conservation*, **2004**, *49* (2), 73–84. <https://doi.org/10.1179/sic.2004.49.2.73>.
- [66] Macchia, A.; Campanella, L.; Gazzoli, D.; Gravagna, E.; Maras, A.; Nunziante, S.; Rocchia, M.; Roscioli, G. Realgar and Light. *Procedia Chemistry*, **2013**, *8*, 185–193.  
<https://doi.org/10.1016/j.proche.2013.03.024>.
- [67] Douglass, D. L.; Chichang Shing; Ge Wang. The Light-Induced Alteration of Realgar to Pararealgar. *American Mineralogist*, **1992**, *77* (11–12), 1266–1274.
- [68] Jovanovski, G.; Makreski, P. Intriguing Minerals: Photoinduced

- Solid-State Transition of Realgar to Pararealgar—Direct Atomic Scale Observation and Visualization. *ChemTexts*, **2020**, *6* (1), 1–14. <https://doi.org/10.1007/s40828-019-0100-9>.
- [69] Robert L. Feller. *Artists' Pigments: A Handbook of Their History and Characteristics, Volume 1*; Washington : National Gallery of Art, 1986.
- [70] McKinley, J. P.; Dlaska, M. K.; Batson, R. Red Lead: Understanding Red Lead in Lead-Acid Batteries. *Journal of Power Sources*, **2002**, *107* (2), 180–186. [https://doi.org/10.1016/S0378-7753\(01\)01003-5](https://doi.org/10.1016/S0378-7753(01)01003-5).
- [71] Aze, S.; Vallet, J. M.; Detalle, V.; Grauby, O.; Baronnet, A. Chromatic Alterations of Red Lead Pigments in Artworks: A Review. *Phase Transitions*, **2008**, *81* (2–3), 145–154. <https://doi.org/10.1080/01411590701514326>.
- [72] Coccato, A.; Moens, L.; Vandenaabeele, P. On the Stability of Mediaeval Inorganic Pigments: A Literature Review of the Effect of Climate, Material Selection, Biological Activity, Analysis and Conservation Treatments. *Heritage Science*, **2017**, *5* (1). <https://doi.org/10.1186/s40494-017-0125-6>.
- [73] Aze, S. V.; Baronnet, A.; Grauby, O. Red Lead Darkening in Wall Paintings: Natural Ageing of Experimental Wall Paintings versus Artificial Ageing Tests. *European Journal of Mineralogy*, **2007**, *19* (6), 883–890. <https://doi.org/10.1127/0935-1221/2007/0019-1771>.
- [74] Costantini, I.; Lottici, P. P.; Bersani, D.; Pontiroli, D.; Casoli, A.; Castro, K.; Madariaga, J. M. Darkening of Lead- and Iron-Based Pigments on Late Gothic Italian Wall Paintings: Energy Dispersive X-Ray Fluorescence,  $\mu$ -Raman, and Powder X-Ray Diffraction Analyses for Diagnosis: Presence of  $\beta$ -PbO<sub>2</sub> (Plattnerite) and  $\alpha$ -PbO<sub>2</sub> (Scrutinyite). *Journal of Raman Spectroscopy*, **2020**, *51* (4), 680–692. <https://doi.org/10.1002/jrs.5817>.
- [75] Ayalew, E.; Janssens, K.; De Wael, K. Unraveling the Reactivity of Minium toward Bicarbonate and the Role of Lead Oxides Therein. *Analytical Chemistry*, **2016**, *88* (3), 1564–1569. <https://doi.org/10.1021/acs.analchem.5b02503>.
- [76] Zhao, Y.; Tang, Y.; Tong, T.; Sun, Z.; Yu, Z.; Zhu, Y.; Tong, H. Red Lead Degradation: Monitoring of Color Change over Time. *New Journal of Chemistry*, **2016**, *40* (4), 3686–3692. <https://doi.org/10.1039/c5nj02426a>.
- [77] Bansa, H.; Ishii, R. The Effect of Different Strengthening Methods on Different Kinds of Paper. Die Wirkung Verschiedener Festigkeitsmethoden Auf Verschiedene Papierarten. *Restaurator*, **1997**, *18*, 51–72.
- [78] Moon, R. J.; Martini, A.; Nairn, J.; Simonsen, J.; Youngblood, J. Cellulose Nanomaterials Review: Structure, Properties and Nanocomposites. *Chemical Society Review*, **2011**, *40*, 3941–3994. <https://doi.org/10.1039/c0cs00108b>.

- [79] Baty, J. W.; Maitland, C. L.; Minter, W.; Hubbe, M. A.; Jordan-Mowery, S. K. Deacidification for the Conservation and Preservation of Paper-Based Works: A Review. *BioResources*, **2010**, *5* (3), 1955–2023. <https://doi.org/10.15376/biores.5.3.1955-2023>.
- [80] Cappitelli, F.; Sorlini, C.; Pedemonte, E.; Princi, E.; Vicini, S. Effectiveness of Graft Synthetic Polymers in Preventing Biodeterioration of Cellulose-Based Materials. *Macromolecular Symposia*, **2006**, *238*, 84–91. <https://doi.org/10.1002/masy.200650612>.
- [81] Kiuberis, J.; Tautkus, S.; Kazlauskas, R.; Pakutinskiene, I.; Kareiva, A. Protective Coating for Paper: New Development and Analytical Characterization. *Journal of Cultural Heritage*, **2005**, *6* (3), 245–251. <https://doi.org/10.1016/j.culher.2005.06.002>.
- [82] Senvaitiene, J.; Pakutinskiene, I.; Beganskienė, A.; Tautkus, S.; Kazlauskas, R.; Kareiva, A. Destructive Effects of Paper Conservation Procedure on the Writing Iron Gall Ink - Evidence from Transmetalation Reaction. *Polish Journal of Chemistry*, **2005**, *79*, 1575–1583.
- [83] Sivakova, B.; Beganskiene, A.; Kareiva, A. Investigation of Damaged Paper by Ink Corrosion. *Medziagotyra*, **2008**, *14* (1), 51–54.
- [84] Sivakova, B.; Darčanova, O.; Beganskiene, A.; Kareiva, A. Investigation of Impact of Stabilization System APTES/KI on Ageing Resistance of Inked Paper. *Medziagotyra*, **2009**, *15* (4), 311–315.
- [85] Darčanova, O.; Beganskiene, A.; Kareiva, A. Sol-Gel Synthesis of Calcium Nanomaterial for Paper Conservation. *Chemija*, **2015**, *26* (1), 25–31.
- [86] Darcanova, O.; Tamute, M.; Beganskienė, A.; Kareiva, A. Synthesis of Magnesium Oxide Nanoparticles via Sol-Gel Method and Hydrolysis and Application for Paper Deacidification Treatment. *Chemija*, **2016**, *27*, 170–178.
- [87] Liubiniene, M.; Kupčiūnaitė, J.; Beganskienė, A. Study of the Influence of Surfactants on the Paper Properties and Degradation. *Chemija*, **2018**, *29*, 157–165. <https://doi.org/10.6001/chemija.v29i3.3818>.
- [88] Capillary Washing and Light Bleaching – South Florida Art Conservation. <https://sflac.net/paper-conservation/capillary-washing-and-light-bleaching/> (accessed Dec 14, 2020).
- [89] Schalkx, H.; Iedema, P.; Reissland, B.; Van Velzen, B. Aqueous Treatment of Water-Sensitive. *Journal of Paper Conservation*, **2011**, *12*, 11–20.
- [90] Byron Bird, R.; Stewart, W. E.; Lightfoot, E. N. *Transport Phenomena*. (Second Edi.). New York : Wiley, 2001.
- [91] Huhsmann, E.; Hähner, U. Application of the Non-Woven Viscose Fabric Paraprint OL 60 for Float Screen Washing of Documents Damaged by Iron Gall Ink Corrosion. *Restaurator*, **2007**, *28*, 140–

151. <https://doi.org/10.1515/REST.2007.140>.
- [92] Mesmer, R. Book and Paper Group Tips Session 2013: Contemporary Treatment — Tips and Techniques. *Materials and Techniques for Mounts, Encapsulations, and Book Supports*; **2013**, 32, 84–87.
- [93] Dellapiana, L. Water and Paper Conservation Principles. *News in Conservation*, **2016**, 56, 16–18.
- [94] Miguel, C.; Lopes, J. A.; Clarke, M.; Melo, M. J. Combining Infrared Spectroscopy with Chemometric Analysis for the Characterization of Proteinaceous Binders in Medieval Paints. *Chemometrics and Intelligent Laboratory Systems*, **2012**, 119, 32–38. <https://doi.org/10.1016/j.chemolab.2012.09.003>.
- [95] Baer, N. S.; Feller, R. L. Accelerated Aging: Photochemical and Thermal Aspects. *Journal of the American Institute for Conservation*, **2006**, 35 (2), 163. <https://doi.org/10.2307/3179994>.
- [96] Sanchez, C.; Nigen, M.; Mejia Tamayo, V.; Doco, T.; Williams, P.; Amine, C.; Renard, D. Acacia Gum: History of the Future. *Food Hydrocolloids*, **2018**, 78, 140–160. <https://doi.org/10.1016/j.foodhyd.2017.04.008>.
- [97] Daoub, R. M. A.; Elmubarak, A. H.; Misran, M.; Hassan, E. A.; Osman, M. E. Characterization and Functional Properties of Some Natural Acacia Gums. *Journal of the Saudi Society of Agricultural Sciences*, **2018**, 17 (3), 241–249. <https://doi.org/10.1016/j.jssas.2016.05.002>.
- [98] De Campos Vidal, B.; Mello, M. L. S. Collagen Type I Amide I Band Infrared Spectroscopy. *Micron*, **2011**, 42 (3), 283–289. <https://doi.org/10.1016/j.micron.2010.09.010>.
- [99] Niu, F.; Kou, M.; Fan, J.; Pan, W.; Feng, Z. J.; Su, Y.; Yang, Y.; Zhou, W. Structural Characteristics and Rheological Properties of Ovalbumin-Gum Arabic Complex Coacervates. *Food Chemistry*, **2018**, 260, 1–6. <https://doi.org/10.1016/j.foodchem.2018.03.141>.
- [100] Davidenko, N.; Campbell, J. J.; Thian, E. S.; Watson, C. J.; Cameron, R. E. Collagen-Hyaluronic Acid Scaffolds for Adipose Tissue Engineering. *Acta Biomaterialia*, **2010**, 6 (10), 3957–3968. <https://doi.org/10.1016/j.actbio.2010.05.005>.
- [101] Wang, K.; Wang, W.; Ye, R.; Liu, A.; Xiao, J.; Liu, Y.; Zhao, Y. Mechanical Properties and Solubility in Water of Corn Starch-Collagen Composite Films: Effect of Starch Type and Concentrations. *Food Chemistry*, **2017**, 216, 209–216. <https://doi.org/10.1016/j.foodchem.2016.08.048>.
- [102] Back, S. K.; Bhatta, D.; Kim, S. H.; Jang, H. N.; Kim, J. H.; Kim, K. H.; Kim, Y. R.; Seo, Y. C. Thermal Decomposition Characteristics of Mercury Compounds in Industrial Sludge with High Sulfur Content. *Journal of Material Cycles and Waste Management*, **2018**, 20 (1), 622–631. <https://doi.org/10.1007/s10163-017-0630-4>.

- [103] Sedlar, M.; Pavlin, M.; Popovieč, A.; Horvat, M. Temperature Stability of Mercury Compounds in Solid Substrates. *Open Chemistry*, **2015**, *13* (1), 404–419. <https://doi.org/10.1515/chem-2015-0051>.
- [104] Zoppi, M.; Pratesi, G. The Dual Behavior of the  $\beta$ -As<sub>4</sub>S<sub>4</sub> Altered by Light. *American Mineralogist*, **2012**, *97* (5–6), 890–896. <https://doi.org/10.2138/am.2012.3968>.
- [105] Karunadasa, K. S. P.; Manoratne, C. H.; Pitawala, H. M. T. G. A.; Rajapakse, R. M. G. Thermal Decomposition of Calcium Carbonate (Calcite Polymorph) as Examined by in-Situ High-Temperature X-Ray Powder Diffraction. *Journal of Physics and Chemistry of Solids*, **2019**, *134* (May), 21–28. <https://doi.org/10.1016/j.jpics.2019.05.023>.
- [106] Darezereshki, E. One-Step Synthesis of Hematite ( $\alpha$ -Fe<sub>2</sub>O<sub>3</sub>) Nano-Particles by Direct Thermal-Decomposition of Maghemite. *Materials Letters*, **2011**, *65* (4), 642–645. <https://doi.org/10.1016/j.matlet.2010.11.030>.
- [107] Cao, S. W.; Zhu, Y. J.; Zeng, Y. P. Formation of  $\gamma$ -Fe<sub>2</sub>O<sub>3</sub> Hierarchical Nanostructures at 500 °C in a High Magnetic Field. *Journal of Magnetism and Magnetic Materials*, **2009**, *321* (19), 3057–3060. <https://doi.org/10.1016/j.jmmm.2009.05.005>.
- [108] Jamaludin, J.; Adam, F.; Rasid, R. A.; Hassan, Z. Thermal Studies on Arabic Gum - Carrageenan Polysaccharides Film. *Chemical Engineering Research Bulletin*, **2017**, *19*, 80–86. <https://doi.org/10.3329/ceerb.v19i0.33800>.
- [109] Silva, D. A.; Feitosa, J. P. A.; Maciel, J. S.; Paula, H. C. B.; de Paula, R. C. M. Characterization of Crosslinked Cashew Gum Derivatives. *Carbohydrate Polymers*. **2006**, *66* (1), 16–26. <https://doi.org/10.1016/j.carbpol.2006.02.021>.
- [110] Badea, E.; Usacheva, T. R.; Della Gatta, G.; Badea, E. The Use of Differential Scanning Calorimetry to Characterise Collagen Deterioration in Parchment. *Rossijskij Khimicheskij Zhurnal*, **2015**, *59* (1), 28–41.
- [111] Budrugaec, P.; Badea, E.; Gatta, G. Della; Miu, L.; Comănescu, A. A DSC Study of Deterioration Caused by Environmental Chemical Pollutants to Parchment, a Collagen-Based Material. *Thermochimica Acta*, **2010**, *500* (1–2), 51–62. <https://doi.org/10.1016/j.tca.2009.12.010>.
- [112] Sebestyén, Z.; Czégény, Z.; Badea, E.; Carsote, C.; Şendrea, C.; Barta-Rajnai, E.; Bozi, J.; Miu, L.; Jakab, E. Thermal Characterization of New, Artificially Aged and Historical Leather and Parchment. *Journal of Analytical and Applied Pyrolysis*, **2015**, *115*, 419–427. <https://doi.org/10.1016/j.jaap.2015.08.022>.
- [113] Tomassetti, M.; Marini, F.; Campanella, L.; Coppa, A. Study of Modern or Ancient Collagen and Human Fossil Bones from an Archaeological Site of Middle Nile by Thermal Analysis and

- Chemometrics. *Microchemical Journal*, **2013**, *108*, 7–13. <https://doi.org/10.1016/j.microc.2012.11.006>.
- [114] Bozec, L.; Odlyha, M. Thermal Denaturation Studies of Collagen by Microthermal Analysis and Atomic Force Microscopy. *Biophysical Journal*, **2011**, *101* (1), 228–236. <https://doi.org/10.1016/j.bpj.2011.04.033>.
- [115] Elert, K.; Herrera, A.; Cardell, C. Pigment-Binder Interactions in Calcium-Based Tempera Paints. *Dyes and Pigments*, **2018**, *148*, 236–248. <https://doi.org/10.1016/j.dyepig.2017.09.013>.
- [116] Dong, Y.; Sørensen, K. M.; He, S.; Engelsen, S. B. Gum Arabic Authentication and Mixture Quantification by near Infrared Spectroscopy. *Food Control*, **2017**, *78*, 144–149. <https://doi.org/10.1016/j.foodcont.2017.02.002>.
- [117] De Campos Vidal, B.; Mello, M. L. S. Collagen Type I Amide I Band Infrared Spectroscopy. *Micron*, **2011**, *42* (3), 283–289. <https://doi.org/10.1016/j.micron.2010.09.010>.
- [118] Bagdzevičiene, J.; Tautkus, S.; Senvaitiene, J.; Lukšeniene, J. Investigation of the Technique of Painting on a Tin Alloy Plate. *Chemija*, **2009**, *20* (2), 93–100.
- [119] Nodari, L.; Ricciardi, P. Non-Invasive Identification of Paint Binders in Illuminated Manuscripts by ER-FTIR Spectroscopy: A Systematic Study of the Influence of Different Pigments on the Binders' Characteristic Spectral Features. *Heritage Science*, **2019**, *7* (1), 1–13. <https://doi.org/10.1186/s40494-019-0249-y>.
- [120] Vermeulen, M.; Janssens, K.; Sanyova, J.; Rahemi, V.; McGlinchey, C.; De Wael, K. Assessing the Stability of Arsenic Sulfide Pigments and Influence of the Binding Media on Their Degradation by Means of Spectroscopic and Electrochemical Techniques. *Microchemical Journal*, **2018**, *138*, 82–91. <https://doi.org/10.1016/j.microc.2018.01.004>.
- [121] Manfredi, M.; Bearman, G.; France, F.; Shor, P.; Marengo, E. Quantitative Multispectral Imaging for the Detection of Parchment Ageing Caused by Light: A Comparison with ATR-FTIR, GC-MS and TGA Analyses. *International Journal of Conservation Science*, **2015**, *6* (1), 3–14.
- [122] Lashgari, A.; Ghamami, S.; Bahrami, Z.; Shomossi, F.; Salgado-Morán, G.; Glossman-Mitnik, D. Morphological Investigation and Fractal Properties of Realgar Nanoparticles. *Journal of Nanomaterials*, **2015**, No. Article ID 130698, 1–8. <https://doi.org/10.1155/2015/130698>.
- [123] Fessas, D.; Signorelli, M.; Schiraldi, A.; Kennedy, C. J.; Wess, T. J.; Hassel, B.; Nielsen, K. Thermal Analysis on Parchments I: DSC and TGA Combined Approach for Heat Damage Assessment. *Thermochimica Acta*, **2006**, *447* (1), 30–35. <https://doi.org/10.1016/j.tca.2006.04.007>.

- [124] Nastova, I.; Grupče, O.; Minčeva-Šukarova, B.; Ozcatal, M.; Mojsoska, L. Spectroscopic Analysis of Pigments and Inks in Manuscripts: I. Byzantine and Post-Byzantine Manuscripts (10-18th Century). *Vibrational Spectroscopy*, **2013**, *68*, 11–19. <https://doi.org/10.1016/j.vibspec.2013.05.006>.
- [125] Nastova, I.; Grupče, O.; Minčeva-Šukarova, B.; Kostadinovska, M.; Ozcatal, M. Spectroscopic Analysis of Pigments and Inks in Manuscripts. III. Old-Slavonic Manuscripts with Multicolored Rubication. *Vibrational Spectroscopy*, **2015**, *78*, 39–48. <https://doi.org/10.1016/j.vibspec.2015.03.005>.
- [126] Hospodarova, V.; Singovszka, E.; Stevulova, N. Characterization of Cellulosic Fibers by FTIR Spectroscopy for Their Further Implementation to Building Materials. *American Journal of Analytical Chemistry*, **2018**, *09* (06), 303–310. <https://doi.org/10.4236/ajac.2018.96023>.
- [127] Pellegrini, D.; Duce, C.; Bonaduce, I.; Biagi, S.; Ghezzi, L.; Colombini, M. P.; Tinè, M. R.; Bramanti, E. Fourier Transform Infrared Spectroscopic Study of Rabbit Glue/Inorganic Pigments Mixtures in Fresh and Aged Reference Paint Reconstructions. *Microchemical Journal*, **2016**, *124*, 31–35. <https://doi.org/10.1016/j.microc.2015.07.018>.
- [128] Jenkins, D. M. Empirical Study of the Infrared Lattice Vibrations (1100-350  $\text{cm}^{-1}$ ) of Phlogopite. *Physics and Chemistry of Minerals*, **1989**, *16* (4), 408–414. <https://doi.org/10.1007/BF00199563>.
- [129] Melo, M. J.; Nabais, P.; Araújo, R.; Vitorino, T. The Conservation of Medieval Manuscript Illuminations: A Chemical Perspective. *Physical Sciences Reviews*, **2019**, *4* (8), 1–13. <https://doi.org/10.1515/psr-2018-0017>.
- [130] Barth, A. Infrared Spectroscopy of Proteins. *Biochimica et Biophysica Acta – Bioenergetics*, **2007**, *1767* (9), 1073–1101. <https://doi.org/10.1016/j.bbabi.2007.06.004>.
- [131] Muyonga, J. H.; Cole, C. G. B.; Duodu, K. G. Fourier Transform Infrared (FTIR) Spectroscopic Study of Acid Soluble Collagen and Gelatin from Skins and Bones of Young and Adult Nile Perch (Lates Niloticus). *Food Chemistry*, **2004**, *86* (3), 325–332. <https://doi.org/10.1016/j.foodchem.2003.09.038>.
- [132] Parras-Guijarro, D.; Montejo-Gámez, M.; Ramos-Martos, N.; Sánchez, A. Analysis of Pigments and Coverings by X-Ray Diffraction (XRD) and Micro Raman Spectroscopy (MRS) in the Cemetery of Tutugi (Galera, Granada, Spain) and the Settlement Convento 2 (Montemayor, Córdoba, Spain). *Spectrochimica Acta - Part A: Molecular and Biomolecular Spectroscopy*, **2006**, *64* (5), 1133–1141. <https://doi.org/10.1016/j.saa.2005.11.035>.
- [133] Zohuriaan, M. J.; Shokrolahi, F. Thermal Studies on Natural and Modified Gums. *Polymer Testing*, **2004**, *23* (5), 575–579.



<https://doi.org/10.1016/j.polymertesting.2003.11.001>.

- [134] Nair, R. M.; Bindhu, B. An In-Depth Study on the Application of Gum Arabic: A Biopolymer. *International Journal of Recent Technology and Engineering*, **2019**, 8 (1C2), 1120–1121.
- [135] Duce, C.; Bramanti, E.; Ghezzi, L.; Bernazzani, L.; Bonaduce, I.; Colombini, M. P.; Spepi, A.; Biagi, S.; Tine, M. R. Interactions between Inorganic Pigments and Proteinaceous Binders in Reference Paint Reconstructions. *Dalton Transactions*, **2013**, 42 (17), 5975–5984. <https://doi.org/10.1039/c2dt32203j>.
- [136] Colomer, M. T. Straightforward Synthesis of Ti-Doped YSZ Gels by Chemical Modification of the Precursors Alkoxides. *Journal of Sol-Gel Science and Technology*, **2013**, 67 (1), 135–144. <https://doi.org/10.1007/s10971-013-3059-9>.

COPIES OF PUBLICATION

1

Application of red paint data library for the  
characterization of the  
manuscript from Grand Duchy of Lithuania

Aušra Čiuladienė, Aivaras Kareiva

2

Study of the Red Iron Paints for Rubrics and  
Miniatures: Accelerated Aging and Analytical  
Data

Aušra Čiuladienė, Aldona Beganskienė, Jūratė Senvaitienė, Aivaras Kareiva

## Study of the Red Iron Paints for Rubrics and Miniatures: Accelerated Aging and Analytical Data

Aušra ČIULADIENĖ<sup>1\*</sup>, Aldona BEGANSKIENĖ<sup>1</sup>, Jūratė SENVAITIENĖ<sup>1,2</sup>,  
Aivaras KAREIVA<sup>1</sup>

<sup>1</sup>*Institute of Chemistry, Faculty of Chemistry and Geosciences, Vilnius University, Naugarduko st. 24, LT-03225 Vilnius, Lithuania*

<sup>2</sup>*Pranas Gudynas Centre for Restoration, Lithuanian Art Museum, Didžioji st. 4, LT 01128, Vilnius, Lithuania*

**crossref** <http://dx.doi.org/10.5755/j02.ms.25190>

Received 30 January 2020; accepted 29 May 2020

In this study, the red iron paints used in ancient manuscripts for rubrics and miniatures were fabricated and investigated. The commercial three different iron pigments (red ochre (Fe<sub>2</sub>O<sub>3</sub>), red bolus (Fe<sub>2</sub>O<sub>3</sub>·xSiO<sub>2</sub>·yAl<sub>2</sub>O<sub>3</sub>), and hematite (Fe<sub>2</sub>O<sub>3</sub>)) and three binding media (gum Arabic, fish glue and parchment glue) were used for the preparation of analogous to historical red iron paints. The obtained model red iron paints were analyzed with the aim to create a short data library which could be used for the characterization of different model compositions of red paints as well as real historical and archaeological red paints. The obtained red paints and binding media were characterized using Fourier-transform infrared spectroscopy (FTIR), scanning electron microscopy coupled with energy-dispersive X-ray spectroscopy (SEM/EDX), X-ray diffraction (XRD) analysis and thermal (TG/DSC) analysis techniques. The accelerated aging test was also applied for the analogous to historical red iron paints. These results are useful to develop red paint guidelines for the storage and display for improved conservation and accessibility of manuscripts.

*Keywords:* iron pigments, binders, red iron paints, model compositions, accelerated aging.

### 1. INTRODUCTION

The accurate identification of pigments should be done by conservation and restoration scientists and specialists prior the restoration of the object of cultural heritage. Such necessity is related with several reasons. It is very important that the entire recovery will be done with the pigment having the same chemical composition as original rather than a similar shade. The alternative pigments can react with nearby original pigments and irreversible changes occur damaging the painting or other object of restoration. The second reason is necessity to identify any degradation products of pigments and to suspend or cancel proposals for possible treatments that can cause decomposition processes [1, 2]. In addition, the authenticity of the cultural heritage objects is very important as well. One of the possible ways to check the fake object is to check if the used pigments are in the first production or later period. Moreover, important information on the chemical composition of historical writing inks and paints could be useful for the investigation of various degradation mechanisms of cultural heritage artefacts [3, 4].

Clay and iron oxides were used as artistic pigments in pre-historic times and quickly become very common in all over the world. Clay minerals and iron oxides are closely related to their natural formation [5–7]. Their structural and mineralogical properties are directly related to their natural genesis and origin and help us to explore historical painting techniques and materials of each painting layer which the main building element [8–10]. Paint is the mixture of pigments and binding media, and their composition gives

colour quality. The main aspects of this quality are colour stability and coating capacity [11–13]. The colour quality can be highly dependent on the chemical interactions within the mixtures and the surrounding environment. Clay and iron oxides as artistic pigments are found in paintings of each region and at most of the historical periods [14].

If we want to identify an unknown person, we have to compare an unknown fingerprint with one of a specific individual and so know if it was left by that individual. This test method can be described as a “fingerprinting”. The study of the materials used for making manuscripts is not so much, probably because the research started in the late eighteenth century [15]. Knowledge of the composition of the original materials and pigments is very helpful for restorers when they have to choose suitable materials and relevant colour tones. The characterization of paint binders in general are in particular is complex due to the sample size, the high inorganic content, the degradation phenomena undergone with time, and the simultaneous presence of other additives [16, 17]. Therefore, non-invasive analytical techniques have not fully satisfied features and can not be used as a self-consistent analytical tool. The optimal strategy to recognize colourants and other additives used in miniatures or rubrics should, therefore, provide for a multi-technique approach.

This study is a continuous work carried out reconstructing red paints using proteinaceous and natural gums binders aimed to clarify how these materials are aging together and create a short data library which could be used for the characterization of red paints in ancient manuscripts. Nine different analogous to ancient red paints using three

\* Corresponding author. Tel.: +370-5-2193108;  
E-mail address: [ausra.ciuladiene@chgf.vu.lt](mailto:ausra.ciuladiene@chgf.vu.lt) (A. Čiuladienė)

red pigment (red ochre, red bolus, hematite) and three binding media (gum Arabic, fish glue, parchment glue) were fabricated in this study. The reconstructed paints before and after artificial aging were then characterized by SEM/EDX, FTIR, XRD, TG/DTG/DSC analysis methods.

## 2. EXPERIMENTAL

### 2.1. Materials

Three different red pigments (red ochre (Fe<sub>2</sub>O<sub>3</sub>), (11274), red bolus (Fe<sub>2</sub>O<sub>3</sub>·SiO<sub>2</sub>·Al<sub>2</sub>O<sub>3</sub>), (40503), and hematite (Fe<sub>2</sub>O<sub>3</sub>), (48651)) and three binding media (gum Arabic (63320), fish glue (63080), and parchment glue (63035)) were purchased from Kremer Pigmente and used for the preparation of red paints. These samples were characterized at first by XRD, SEM/EDX, FTIR, and TG/DTG/DSC analysis. The results of this characterization are already published elsewhere [18].

### 2.2. Paints preparation

A set of pigment-binding media combinations were prepared in the following way. For the preparation of binding media slightly different procedures were used. The parchment and fish glue were washed with distilled water, cut into small pieces and covered with water for 24 h. Next, the glue gently heated (40–50 °C) and stirred for 4 h till became liquid. Then, 9 % acetic acid (*Eurochemicals Reachem*) solution was added to the prepared binding media with ratio 1:4. Gum Arabic was fine-cut, covered with distilled water and was left to swell. Then was stirred and filtered through linen fabric. Finally, the glue was mixed with the same concentration solution of acetic acid with ratio (4:1). The red iron pigments were first ground in an agate mortar with a drop of distilled water and then mixed with the binders resulting in ~85 wt.% of binding media on a dry-paint composition. Nine different analogous to ancient red paints were fabricated using the compositions of each iron pigment with each binding material. A set of pigment-binding media combinations were coated on microscope glass slides and dried in the dark. The prepared samples were artificially aged at intervals of 1, 4, 7, 14, 21, 28 and 35 days in a chamber with a constant intensity of UV irradiation of 14887 mW/m<sup>2</sup>. Measurements were made using a versatile lux-hygrometer ELSEC 764 UV. The UV source in the aging chamber was the 10-luminescent Osram Eversun L40W/79K fluorescent lamp with a power output of 40 W (400 W total). Lamps disseminated a wavelength of

310–400 nm and are hung 50 cm above the samples. The temperature in the chamber did not exceed 35 °C and the relative humidity was 21 % RH [19].

### 2.3. Characterization

The colour change of the paint was measured with a FLAME-S-VIS-NIR-ES spectrometer with light source HL-2000-FHSA 20 W, resolution ~1.5 nm, measuring time – 2 s, measuring range 350–1000 nm, used the standard – WS-1 Reflectance Standard. The surface morphology of the samples and elemental analysis was studied by the scanning electron microscope coupled with energy dispersive X-ray spectroscopy (SEM/EDX) using Hitachi TM3000 and with

the scanning electron microscope (SEM) SU70, 5 kV. IR spectroscopy was used for the identification and characterization of functional groups of pigments and binding media in the paint. Infrared spectra were obtained by an FTIR spectrophotometer Perkin Elmer Spectrum TWO with ATR accessory. All spectra were recorded at 4 cm<sup>-1</sup> resolution in an interval of 450–4000 cm<sup>-1</sup> and 24 scans were accumulated before Fourier transformation. The

X-ray diffraction (XRD) analysis was performed using Benchtop XRD MiniFlex II, Rigaku in the range of 10 to 80° 2θ, 5°/min speed, using CuKα<sub>1</sub> radiation. The thermal analysis (TG/DTG/DSC) was recorded using a Perkin Elmer pyris TGA instrument. The heating rate was 10 °C/min in air flow from 30 to 900 °C.

## 3. RESULTS AND DISCUSSION

### 3.1. Colorimetric measurements

To investigate the colour stability, the accelerated aging was initially performed on the fabricated red paints [20]. The colour difference ΔE in the CIE(Lab)\* system of paints was calculated according to the formula [19, 21, 22]:

$$\Delta E = [(\Delta L^*)^2 + (\Delta a^*)^2 + (\Delta b^*)^2]^{1/2}, \quad (1)$$

where ΔL\* (lightness-darkness difference) = L\*<sub>aged</sub> – L\*<sub>unaged</sub>; Δa\* (redness-greenness difference) = a\*<sub>aged</sub> – a\*<sub>unaged</sub>; and Δb\* (yellowness-blueness difference) = b\*<sub>aged</sub> – b\*<sub>unaged</sub>.

Each sample was photographed under the same lighting and at the same height from the sample to capture the appropriate colour. Since the binding media are transparent their photos were made using a white sheet of the paper base. The colour changes of red paints and binding medias before and after accelerated aging are represented in Fig. 1. Visually, the paints fabricated using red ochre exhibit deep red colour independent on the used binding media. However, the paints produced from red bolus and parchment or fish glue have slightly yellowish tint. Red-brownish colour was observed for the paints prepared using hematite pigment. Evidently, the colours of most of the paints have changed after artificial aging.

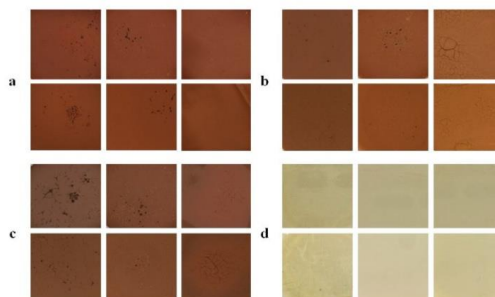


**Fig. 1.** The digital images of paints fabricated from mixtures: a – red ochre; b – red bolus; c – hematite; with gum Arabic, fish glue and parchment glue (from left to right); d – binding medias, gum Arabic, fish glue and parchment glue before (top) and after 35 days accelerated aging (bottom)

The paint having the composition of red bolus and parchment glue, probably, had least changes during accelerated aging of paints. The dependence of colour difference  $\Delta E$  on accelerated aging time for the parchment glue was mostly affected by artificial aging, while determined  $\Delta E$  for the fish glue and gum Arabic are negligible. The results of dependences of colour differences  $\Delta E$  for different fabricated paints on accelerated aging time, however, were distributed very widely. The results show that the colour changes during artificial aging are not distributed evenly and are dependent very much on individual composition. All paints, except red bolus with parchment glue, ( $\Delta E = 0.2$ ), were affected by accelerated light temperature and relative humidity. For instance, the red ochre with gum Arabic changed colour at about 11 times, with fish and parchment glue about 2 times. Red bolus with gum Arabic and fish glue changed colour a bit less ( $\sim 6-7$  times), with parchment glue the colour difference was almost unnoticeable. The colour difference was the same for hematite with all binding media, at about two times higher than the baseline. Note, that a colour difference of  $\Delta E \geq 3$  is perceptible to the human eye [23].

### 3.2. Scanning electron microscopy (SEM/EDX)

According to the SEM images, the surface morphology of red paints has changed significantly after 35 days of accelerated aging. The gum Arabic is a complex polysaccharide found as a mixed calcium salt of a polysaccharide acid (Arabic acid) [24]. However, the microstructure of three red paints containing the gum Arabic is quite different. Red bolus and hematite gum Arabic paints are composed of different shape particles of about  $50-60 \mu\text{m}$  in size. However, the particles of red bolus show evident tendency to form agglomerates. On the other hand red ochre paint with gum Arabic is composed of smaller mostly spherical particles. It is clearly, that the particle size of all red paints with gum Arabic decreased to  $3-20 \mu\text{m}$  after aging for 35 days. The microstructure of red paints fabricated with fish glue is also mostly determined by used pigment but not by binding media, which like parchment glue is a proteinaceous substance consisting of collagen. The SEM micrograph of composition of hematite and fish glue shows the presence of large microsized particles. When red bolus was used for the preparation of red paints with fish glue the distribution of smaller particles around the large ones is clearly seen. Again, the red ochre paint with fish glue is composed of smaller mostly spherical particles. After artificial aging the particle sizes reduced to approximately of  $10 \mu\text{m}$  for all red paints obtained with fish glue. The similar microstructure before and after aging was observed for the red paint samples fabricated with parchment glue. In conclusion, the microstructure of red paints is mostly influenced by the nature of red pigment. In most of the cases the decreasing of particle size of paint components was observed during the artificial aging.

### 3.3. FTIR spectroscopy

FTIR spectra of binding media before and after accelerated aging did not change after artificial aging for 35 days. These results confirm that artificial aging does not destroy chemical composition of gum Arabic, fish glue and

parchment glue. The main vibrations attributable to the functional groups of binding media and acetic acid [25] were determined in all three FTIR spectra. In the FTIR spectrum of gum Arabic, the intensive absorption bands at  $3300 \text{ cm}^{-1}$  and  $1008 \text{ cm}^{-1}$  are characteristic stretching vibrations of the O-H bond [26]. The band at  $2929 \text{ cm}^{-1}$  is due to characteristic vibrations of C-H. The absorption band at  $1600 \text{ cm}^{-1}$  could be attributed to vibration of the double bond in C=O. The new absorption band of low intensity was observed at  $1727 \text{ cm}^{-1}$  after aging. The FTIR spectra of fish glue and parchment glue are almost identical since the collagen is the main component of these materials. The assignment of absorption bands visible at  $3286$  and  $3266 \text{ cm}^{-1}$  is the same as for gum Arabic. The bands detected at  $2945$  and  $2930 \text{ cm}^{-1}$ , from  $1480$  to  $1300 \text{ cm}^{-1}$  could be attributed to C-H vibrations. Absorption bands of amides coupled to C=O are seen at  $1634 \text{ cm}^{-1}$  (amide I), at  $1525$  and  $1535 \text{ cm}^{-1}$  (amide II) and at  $1229$ ,  $1235 \text{ cm}^{-1}$  (amide III) [27]. Thus, the FTIR spectra of binding media samples qualitatively are the same before and after artificial aging. Just the intensity of some absorption bands is slightly different upon the aging of the specimens. The representative FTIR spectra of red paints with various compositions are depicted in Fig. 2.

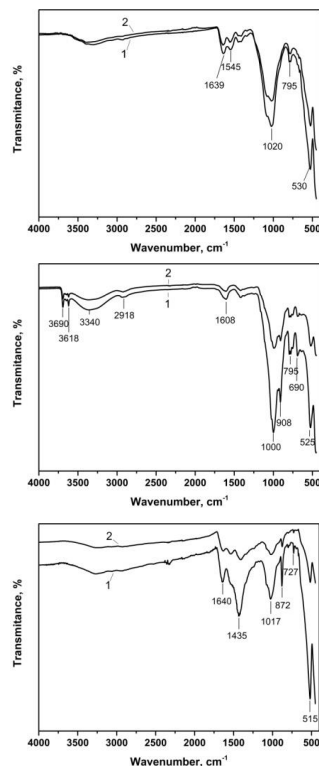


Fig. 2. FTIR spectra of red paint before (1) and after (2) accelerated aging: red ochre with parchment glue (top), red bolus with gum Arabic (middle) and hematite with fish glue (bottom)

In the FTIR spectrum of paint obtained from pigment red ochre with parchment glue the absorption band at

1020  $\text{cm}^{-1}$  can be identified as asymmetric Si–O–Si stretching band from silica which is present in commercial red ochre. The band at 795  $\text{cm}^{-1}$  could be attributed to the stretching vibrations of Si–O–Al. The intensive absorption band at 530  $\text{cm}^{-1}$  is characteristic Fe–O vibration in iron oxide. Absorption bands attributable to the parchment glue are also seen just with decreased intensity. The FTIR spectrum of the red paint fabricated from pigment red bolus and gum Arabic represents all absorption bands characteristic to gum Arabic and additional bands for kaolin ( $\text{Al}_2\text{Si}_2\text{O}_5(\text{OH})_4$ ). The O–H stretching bands are located at 3690 and 3618  $\text{cm}^{-1}$ , and asymmetric Si–O–Si stretching band and Si–O stretching bands are visible at 1000  $\text{cm}^{-1}$  and 908  $\text{cm}^{-1}$ , respectively. The absorption bands determined at 690 and 795  $\text{cm}^{-1}$  are due to Si–O–Al vibrations, and the origin of absorption at 525  $\text{cm}^{-1}$  is Fe–O vibrations. The FTIR spectrum of the mixture of hematite and fish glue also shows the characteristic absorption bands of iron oxide at the wavenumbers of 515  $\text{cm}^{-1}$ . The absorption bands at 1435  $\text{cm}^{-1}$  and 872  $\text{cm}^{-1}$  are due to vibrations in ionic carbonate ( $\text{CO}_3^{2-}$ ). Again, the absorption band at 1017  $\text{cm}^{-1}$  could be identified as asymmetric Si–O–Si stretching band [28, 29]. According to the FTIR spectroscopy results, the artificial aging had no any deleterious effect on the fabricated red paints.

### 3.4. XRD analysis

XRD patterns of gum Arabic, fish glue, and parchment glue as was expected, these materials are amorphous and no any crystalline phases could be detected [30–32]. The only one diffraction peak of low intensity at around  $2\theta \approx 23.5^\circ$  could be detected in the XRD pattern of fish glue. The exact origin of this diffraction line is unknown. Interestingly, this peak disappeared after artificial aging of material for 35 days. The XRD patterns of binding media samples before and after 35 days of accelerated aging are just slightly different with small shifts of amorphous bumps to various directions.

The XRD patterns of all compositions of red iron paints were without any big differences after aging. The main crystalline phase of the red ochre paint is  $\text{Fe}_2\text{O}_3$  (PDF 00-033-0664), but additional crystalline  $\text{Al}_2\text{Si}_2\text{O}_5(\text{OH})_4$  phase (at  $2\theta = 12.33^\circ, 20.98^\circ, 68.29^\circ$ ) and an impurity of  $\text{SiO}_2$  phase (at  $2\theta = 26.60^\circ, 36.37^\circ, 37.68^\circ, 45.68^\circ, 59.84^\circ$ ) are also present in the paint. The XRD patterns of all compositions of red bolus paints were also almost identical before and after aging. Additionally, the paints of red bolus contain three  $\text{Fe}_2\text{O}_3$ ,  $\text{SiO}_2$ , and  $\text{Al}_2\text{Si}_2\text{O}_5(\text{OH})_4$  crystalline phases. The XRD patterns recorded for the hematite paint with and parchment glue before and after aging were almost identical. However, the phase compositions of hematite with fish glue and gum Arabic were slightly different after artificial aging (see Fig. 3). As seen, the paints of hematite also contain diffraction peaks attributable to the impurity  $\text{SiO}_2$  phase (at  $2\theta = 30.74^\circ$ ). Moreover, the diffraction peak at around  $2\theta \approx 23.5^\circ$  visible in the XRD pattern of hematite paint with fish glue is not detectable already after artificial aging. This peak probably originates from fish glue. Also, small diffraction line located at about  $2\theta \approx 34.5^\circ$  in the XRD

pattern of hematite paint with fish glue is not visible anymore after aging.

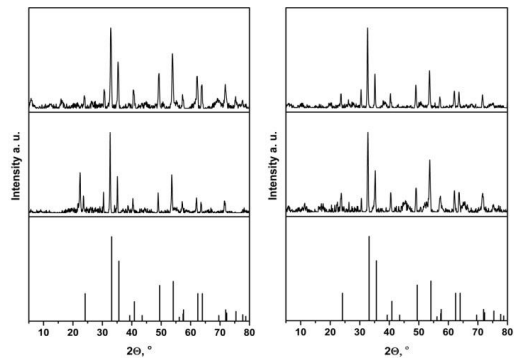


**Fig. 3.** XRD patterns of hematite paint with fish glue (left) and with gum Arabic (right) before (middle) and after accelerated aging (top) for 35 days. The standard XRD pattern of  $\text{Fe}_2\text{O}_3$  is presented as vertical lines at the bottom

Small changes in the XRD patterns upon aging could be determined in the range of  $2\theta \approx 44 - 46^\circ$  for the hematite and gum Arabic system.

### 3.5. Thermal analysis

Thermal analysis is suitable for the investigation of stability of biological macromolecules presented gum Arabic, fish and parchment glue (polysaccharide and collagen). It was reported, that this method is useful to detect the changes in the biomaterials, such as protein denaturing and aggregation, and degradation during thermal treatment [33]. Fig. 4 shows the TG/DTG/DSC curves of binding media affected by artificial aging for 35 days.

Thermal behaviour of parchment and fish glues is very similar and proceeds via three main decomposition steps. The total mass loss of 100 % was determined for both specimens, however, the full combustion of the fish glue reaches at about 680  $^\circ\text{C}$  and the full decomposition of parchment glue could be achieved at lower temperature ( $\sim 630^\circ\text{C}$ ). The initial mass loss of these glues (up to 200  $^\circ\text{C}$ ) is associated with broad endotherms and could be attributed to the evaporation of moisture, so-called structurally bound water and decomposition of hydroxyl groups present in the collagen molecule. The main exothermic decomposition proceeds in two steps very similarly for both samples [17, 18, 34–38]. Multistep decomposition with several mass losses could be determined from the TG curve of the gum Arabic. The first mass loss ( $\sim 9\%$ ) observed in the temperature range of 30–250  $^\circ\text{C}$  is due to the loss of adsorbed and structural water of gums. The next mass losses of about 89 % at the temperatures 250–450  $^\circ\text{C}$ , 450–480  $^\circ\text{C}$ , 480–560  $^\circ\text{C}$ , 560–660  $^\circ\text{C}$  is related to the decomposition of polysaccharide and could be also associated with thermal decomposition of intermediate residues formed in carboxymethylated samples with inorganic compounds [18, 39–41]. As seen, the total mass loss for gum Arabic aged for 35 days is about 98 %.

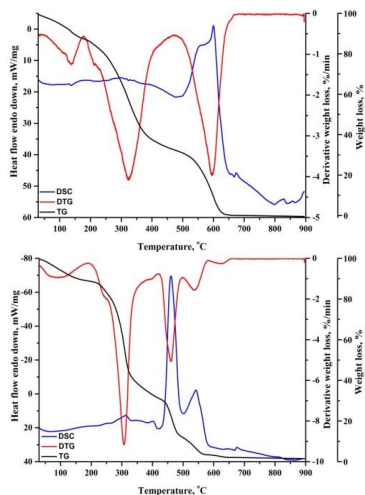


**Fig. 4.** TG/DTG/DSC curves of binding media affected by artificial aging for 35 days: parchment glue (top) and gum Arabic (bottom).

The TG/DTG/DSC curves of fabricated red ochre, red bolus and hematite paints with selected binding media are presented in Fig. 5.

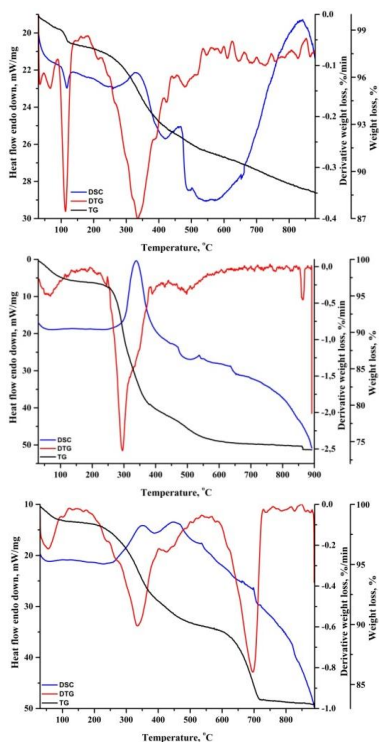


**Fig. 5.** TG/DTG/DSC curves of different red paints after artificial aging for 35 days: red ochre with parchment glue (top), red bolus with gum Arabic (middle) and hematite with fish glue (bottom)

The main thermal events in these curves correlate very well with those determined for the individual binding media samples. The differences observed in thermal analysis curves for different paints are mainly caused by the presence of different impurities. The red ochre and bolus pigments contain  $\text{Al}_2\text{Si}_2\text{O}_5(\text{OH})_4$  as impurity phase which decomposes monotonically by heating the sample up to 700–800 °C. Moreover, according to FTIR results the hematite contains also calcium carbonate which decomposes between 600 and 700 °C [18]. The determined total mass loss varied in the range of 13–26 % depending on the composition of red paints.

#### 4. CONCLUSIONS

In this study the red iron paints used in ancient manuscripts were fabricated by combining three different iron pigments (red ochre ( $\text{Fe}_2\text{O}_3$ ), red bolus ( $\text{Fe}_2\text{O}_3 \cdot x\text{SiO}_2 \cdot y\text{Al}_2\text{O}_3$ ) and hematite ( $\text{Fe}_2\text{O}_3$ )) with three binding media (gum Arabic, fish glue and parchment glue). The obtained model red iron paints before and after accelerating aging for 35 days have been investigated. Visually, the paints fabricated using red ochre exhibit deep red colour independent on the used binding media. However, the paints produced from red bolus and parchment or fish glue have slightly yellowish tint. Red-brownish colour was observed for the paints prepared using hematite pigment. It was determined that the colours the paints have changed slightly after artificial aging. The composition of red bolus and gum Arabic had least changes during accelerated aging of paints. According to the SEM micrographs, the surface morphology of red paints has changed significantly after 35 days of accelerated aging depending on the nature of red pigment. In most of the cases the decreasing of particle size of paints was observed during the artificial aging. According to the FTIR spectroscopy results, the artificial aging had no any deleterious effect on the fabricated red paints. Thus, the characterization of historical red paints by FTIR spectroscopy along with XRD analysis data would serve valuable information on the initial composition of samples. The thermal analysis of red paints before and after accelerating aging showed that the most thermal events observed in the TG/DTG/DSC curves are related with changes of chemical composition of binding media. In conclusion, it should be emphasized that the most effective identification of historical paints could be done using combination of several characterization methods, including FTIR spectroscopy, X-ray diffraction, SEM/EDX, thermal analyses and specific characterization of colour. Finally, these analytical data can be successfully used to identify iron pigments and corresponding red paints in the ancient manuscripts.

#### Acknowledgements

This research was funded by a grant SINALAN (No. S-LU-18-13) from the Research Council of Lithuania.

#### REFERENCES

1. **Clark, R.J.H.** Pigment Identification by Spectroscopic means: an Arts/Science Interface *Comptes Rendus Chimie* 5 2002: pp. 7–20. [https://doi.org/10.1016/S1631-0748\(02\)01341-3](https://doi.org/10.1016/S1631-0748(02)01341-3)



2. **Clark, R.J.H.** The Application of Diffuse Reflectance Spectroscopy to Inorganic Chemistry *Journal of Chemical Education* 41 1964: pp. 488–492.  
<https://doi.org/10.1021/ed041p488>
3. **Senvaitienė, J., Pakutinskiėnė, I., Beganskiėnė, A., Tautkus, A., Kazlauskas, R., Kareiva, A.** Destructive Effects of Paper Conservation Procedure on the Writing Iron Gall Ink – Evidence from Transmetalation Reaction *Polish Journal of Chemistry* 79 2005: pp. 1575–1583.
4. **Vanmeert, F., de Keyser, N., van Loon, A., Klaassen, L., Noble, P., Janssens, K.** Transmission and Reflection Mode Macroscopic X-ray Powder Diffraction Imaging for the Noninvasive Visualization of Paint Degradation in Still Life Paintings by Jan Davidsz. DeHeem *Analytical Chemistry* 91 2019: pp. 7153–7161.  
<https://doi.org/10.1021/acs.analchem.9b00328>
5. **Opuchovič, O., Kareiva, A.** Historical Hematite Pigment: Synthesis by an Aqueous Sol-gel Method, Characterization and Application for the Colouration of Ceramic Glazes *Ceramics International* 41 2015: pp. 4504–4513.  
<https://doi.org/10.1016/j.ceramint.2014.11.145>
6. **Kokins, A., Kostjukovs, J., Zarina, L.** Natural Iron Oxide (Earth Colour) Deposits in Latvia: an Assessment of the Possibilities for Their Use in Inorganic Pigment Manufacturing *Coloration Technology* 134 2018: pp. 491–500.  
<https://doi.org/10.1111/cote.12367>
7. **Lopes, M.M.S., Alvarenga, R.D.S.S., Pedroti, L.G., Ribeiro, J.C.L., de Carvalho, A.F., Cardoso, F.D., Mendes, B.C.** Influence of the Incorporation of Granite Waste on the Hiding Power and Abrasion Resistance of Soil Pigment-based Paints *Construction and Building Material* 205 2019: pp. 463–474.  
<https://doi.org/10.1016/j.conbuildmat.2019.02.046>
8. **Pottier, F., Gerardin, M., Michelin, A., Hebert, M., Andraud, C.** Simulating the Composition and Structuration of Coloring Layers in Historical Painting from Non-invasive Spectral Reflectance Measurements *Comptes Rendus Physique* 19 2018: pp. 599–611.  
<https://doi.org/10.1016/j.cryh.2018.09.007>
9. **Lomax, S.Q., Lomax, J.F., Graham, T.K., Moore, T.J. T., Knapp, C.G.** Historical Azo Pigments: Synthesis and Characterization *Journal of Culture Heritage* 35 2019: pp. 218–224.  
<https://doi.org/10.1016/j.culher.2018.03.022>
10. **Nicolopoulos, S., Das, P.P., Perez, A.G., Zacharias, N., Cuapa, S.T., Alatorre, J.A.A., Mugnaioli, E., Gemmi, M., Rauch, E.F.** Novel TEM Microscopy and Electron Diffraction Techniques to Characterize Cultural Heritage Materials: From Ancient Greek Artefacts to Maya Mural Paintings *Scanning* 2019 Art. ID.4870695.  
<https://doi.org/10.1155/2019/4870695>
11. **Amano, K., Linhares, J.M.M., Nascimento, S.M.C.** Color Constancy of Color Reproductions in Art Paintings *Journal of the Optical Society of America A: Optics, Image Science & Vision* 35 2018: pp. B324–B333.  
<https://doi.org/10.1364/JOSAA.35.00B324>
12. **Phan, H.Q., Fu, H.B., Chan, A.B.** Color Orchestra: Ordering Color Palettes for Interpolation and Prediction *IEEE Transactions on Visualization and Computer Graphics* 24 2018: pp. 1942–1955.  
<https://doi.org/10.1109/TVCG.2017.2697948>
13. **Perez-Arantegui, J., Ruperez, D., Almazan, D., Diez-de-Pinos, N.** Colours and Pigments in Late Ukiyo-e Art Works: A Preliminary Non-invasive Study of Japanese Woodblock Prints to Interpret Hyperspectral Images Using In-situ Point-by-point Diffuse Reflectance Spectroscopy *Microchemical Journal* 139 2018: pp. 94–109.  
<https://doi.org/10.1016/j.microc.2018.02.015>
14. **Hradil, D., Grygar, T., Hradilova, J., Bezdička, P.** Clay and Iron Oxide Pigments in the History of Painting *Applied Clay Science* 22 2003: pp. 223–236.  
[https://doi.org/10.1016/S0169-1317\(03\)00076-0](https://doi.org/10.1016/S0169-1317(03)00076-0)
15. **Clarke, M.** The Analysis of Medieval European Manuscripts *Studies in Conservation* 46 2001: pp. 3–17.  
<https://doi.org/10.1179/sic.2001.46.Supplement-1.3>
16. **Ghezzi, L., Duce, C., Bernazzani, L., Bramanti, E., Colombini, M.P., Tine, M.R., Bonaduce, I.** Interactions between Inorganic Pigments and Rabbit Skin Glue in Reference Paint Reconstructions *Journal of Thermal Analysis and Calorimetry* 122 2015: pp. 315–322.  
<https://doi.org/10.1007/s10973-015-4759-x>
17. **Vieira, M., Nabais, P., Angelin, E.M., Araujo, R., Lopes, J.A., Martin, L., Sameno, M., Melo, M.J.** Organic Red Colorants in Islamic Manuscripts (12th–15th c.) Produced in al-Andalus, part 1 *Dyes and Pigments* 166 2019: pp. 451–459.  
<https://doi.org/10.1016/j.dyepig.2019.03.061>
18. **Čiuladienė, A., Luckutė, A., Kiuberis, J., Kareiva, A.** Investigation of the Chemical Composition of Red Pigments and Binding Media *Chemija* 29 2018: pp. 243–256.  
<https://doi.org/10.6001/chemija.v29i4.3840>
19. **Ragauskienė, D., Makuška, R.** Consolidation and Ageing Features of Vinylneodecanoatecontaining in Adhesive Films Used as a Support for Museum Textiles *Chemija* 17 2006: pp. 52–59.
20. **Feller, R.L.** Accelerated Aging: Photochemical and Thermal Aspects. Marina del Rey, CA: Getty Conservation Institute, 1994.
21. **Opuchovič, O., Kreiza, G., Senvaitienė, J., Kazlauskas, K., Beganskiėnė, A., Kareiva, A.** Sol-gel Synthesis, Characterization and Application of Selected Sub-microsized Lanthanide (Ce, Pr, Nd, Tb) Ferrites *Dyes and Pigments* 118 2015: pp. 176–182.  
<https://doi.org/10.1016/j.dyepig.2015.03.017>
22. **Gražėnaitė, E., Jasulaitienė, V., Senvaitienė, J., Ramanauskas, R., Kareiva, A.** Sol-gel Synthesis, Characterization and Application of Lanthanide-doped Cobalt Chromites (CoCr<sub>2-x</sub>Ln<sub>x</sub>O<sub>4</sub>; Ln=Tm<sup>3+</sup> and Yb<sup>3+</sup>) *Journal of the European Ceramic Society* 38 2018: pp. 3361–3368.  
<https://doi.org/10.1016/j.jeurceramsoc.2018.03.038>
23. **Elert, K., Herrera, A., Cardell, C.** Pigment-Binder Interactions in Calcium-based Tempera Paints *Dyes and Pigments* 148 2018: pp. 236–248.  
<https://doi.org/10.1016/j.dyepig.2017.09.013>
24. **Sanchez, C., Nigen, M., Tamayo, V.M., Doco, T., Williams, P., Amine, C., Renard, D.** Acacia Gum: History of the Future *Food Hydrocolloids* 78 2018: pp. 140–160.  
<https://doi.org/10.1016/j.foodhyd.2017.04.008>
25. **Kroustallis, S.** Binding Media in Medieval Manuscript Illumination: a Source Research *Revista de História da Arte, Serie W* 1 2011: pp. 105–117.
26. **Don, Y., Sørensen, K.M., He, S., Balling Engelsen, S.** Gum Arabic Authentication and Mixture Quantification by Near Infrared Spectroscopy *Food Control* 78 2017: pp. 144–149.  
<https://doi.org/10.1016/j.foodcont.2017.02.002>

27. **de Campos Vidal, B., Mello, M.L.S.** Collagen Type I Amide I Band Infrared Spectroscopy *Micron* 42 2011; pp. 283–289.  
<https://doi.org/10.1016/j.micron.2010.09.010>
28. **Jonynaitė, D., Senvaitienė, J., Beganskienė, A., Kareiva, A.** Spectroscopic Analysis of Blue Cobalt Smalt Pigment *Vibrational Spectroscopy* 52 2010; pp. 158–162.  
<https://doi.org/10.1016/j.vibspec.2009.12.005>
29. **Vila, A., Garcia, J.F.** Analysis of the Chemical Composition of Red Pigments and Inks for the Characterization and Differentiation of Contemporary Prints *Analytical Letters* 45 2012; pp. 1274–1285.  
<https://doi.org/10.1080/00032719.2012.673100>
30. **Niu, F., Kou, M., Fan, J., Pan, W., Feng, Z., Su, Y., Yang, Y., Zhou, W.** Structural Characteristics and Rheological Properties of Ovalbumin-gum Arabic Complex Coacervates *Food Chemistry* 260 2018; pp. 1–6.  
<https://doi.org/10.1016/j.foodchem.2018.03.141>
31. **Davidenko, N., Campbell, J.J., Thian, E.S., Watson, C.J., Cameron, R.E.** Collagen-hyaluronic Acid Scaffolds for Adipose Tissue Engineering *Acta Biomaterialia* 6 2010; pp. 3957–3968.  
<https://doi.org/10.1016/j.actbio.2010.05.005>
32. **Wang, K., Wang, W., Ye, R., Liu, A., Xiao, J., Liu, Y., Zhao, Y.** Mechanical Properties and Solubility in Water of Corn Starch-collagen Composite Films: Effect of Starch Type and Concentrations *Food Chemistry* 216 2017; pp. 2009–2016.  
<https://doi.org/10.1016/j.foodchem.2016.08.048>
33. **Fessas, D., Signorelli, M., Schiraldi, A., Kennedy, C.J., Wess, T.J., Hassel, B., Nielsen, K.** Thermal Analysis on Parchments I: DSC and TGA Combined Approach for Heat Damage Assessment *Thermochemica Acta* 447 2006; pp. 30–35.  
<https://doi.org/10.1016/j.tca.2006.04.007>
34. **Sebestyén, Z., Czégény, Z., Badea, E., Carsote, C., Şendrea, C., Barta-Rajnai, E., Bozi, J., Miu, L., Jakab, E.** Thermal Characterization of New, Artificially Aged and Historical Leather and Parchment *Journal of Analytical and Applied Pyrolysis* 115 2015; pp. 419–427.  
<https://doi.org/10.1016/j.jaap.2015.08.022>
35. **Tomassetti, M., Marini, F., Campanella, L., Coppa, A.** Study of Modern or Ancient Collagen and Human Fossil Bones from an Archaeological Site of Middle Nile by Thermal Analysis and Chemometrics *Microchemical Journal* 108 2013; pp. 7–13.  
<https://doi.org/10.1016/j.micro.2012.11.006>
36. **Axelsson, K.M., Larsen, R., Sommer, D.V.P.** Dimensional Studies of Specific Microscopic Fibre Structures in Deteriorated Parchment Before and During Shrinkage *Journal of Culture Heritage* 13 2012; pp. 128–136.  
<https://doi.org/10.1016/j.culher.2011.08.001>
37. **Budrugać, P., Badea, E., Della Gatta, G., Miu, L., Comănescu, A.** A DSC Study of Deterioration Caused by Environmental Chemical Pollutants to Parchment, a Collagen-based Material *Thermochemica Acta* 500 2010; pp. 51–62.  
<https://doi.org/10.1016/j.tca.2009.12.010>
38. **Riccardi, A., Mercuri, F., Paoloni, S., Zammit, U., Marinelli, M., Scudieri, F.** Parchment Ageing Study: New Methods Based on Thermal Transport and Shrinkage Analysis *e-PS* 7 2010; pp. 87–95.
39. **Jamaludin, J., Adam, F., Rasid, R.A., Hassan, Z.** Thermal Studies on Arabic Gum – Carrageenan Polysaccharides Film *Chemical Engineering Research Bulletin* 19 2017; pp. 80–86.  
<https://doi.org/10.3329/ceb.v19i0.33800>
40. **Daoub, R.M.A., Elmubarak, A.H., Misran, M., Hassan, E.A., Osman, M.E.** Characterization and Functional Properties of Some Natural Acacia Gums *Journal of the Saudi Society of Agricultural Sciences* 17 2018; pp. 241–249.  
<https://doi.org/10.1016/j.jssas.2016.05.002>
41. **Silva, D.A., Feitosa, J.P.A., Maciel, J.S., Paula, H.C.B., de Paula, R.C.M.** Characterization of Cross Linked Cashew Gum Derivatives *Carbohydrate Polymers* 66 2006; pp. 16–26.  
<https://doi.org/10.1016/j.carbpol.2006.02.021>



© Ciuladiene et al. 2021 Open Access This article is distributed under the terms of the Creative Commons Attribution 4.0 International License (<http://creativecommons.org/licenses/by/4.0/>), which permits unrestricted use, distribution, and reproduction in any medium, provided you give appropriate credit to the original author(s) and the source, provide a link to the Creative Commons license, and indicate if changes were made.

### 3

## From model to artefact: Versatile characterization of cinnabar, red lead and realgar red paints for rubrics and miniatures

Aušra Čiuladienė, Aivaras Kareiva, Rimantas Raudonis

## 4

# Investigation of the chemical composition of red pigments and binding media

Aušra Čiuladienė, Austėja Luckutė, Jonas Kiuberis, Aivaras Kareiva





Vilnius University Press  
9 Saulėtekio Ave., Building III, LT-10222 Vilnius  
Email: [info@leidykla.vu.lt](mailto:info@leidykla.vu.lt), [www.leidykla.vu.lt](http://www.leidykla.vu.lt)  
Print run copies 17